Verifiable Adaptive Control Solutions for Flight Control Applications

Jiang Wang

Dissertation submitted to the Faculty of the
Virginia Polytechnic Institute and State University
in partial fulfillment of the requirements for the degree of

Doctor of Philosophy
in
Aerospace and Ocean Engineering

Naira Hovakimyan, Co-chair
Craig A. Woolsey, Co-chair
Andrew Kurdila
Daniel J. Stilwell

February 05, 2009
Blacksburg, Virginia

Keywords: Adaptive Control, Flight Control, Nonlinear Systems, Time-varying Systems

Errata List for the dissertation

Verifiable Adaptive Control Solutions for Flight Control Applications

authored by Jiang Wang

Last updated on May 06, 2009

- On Page 16, Lemma 5: change the text to:

  Suppose that for the linear state equation

  $$\dot{x}(t) = A(t)x(t), \quad x(t_0) = x_0\,,$$

  *with $A(t)$ continuously differentiable, there exist positive constants μ_A, μ_λ such that, for all $t \geq 0$, $\|A(t)\|_\infty \leq \mu_A$, and at each time t, the eigenvalues of $A(t)$ (*point-wise eigenvalue*) satisfy* $\mathrm{Re}[\lambda(t)] \leq -\mu_\lambda$. *Then there exists a positive constant ζ such that if the time-derivative of $A(t)$ satisfies $\|\dot{A}(t)\|_\infty \leq \zeta$ for all $t \geq 0$, then the state equation is uniformly exponentially stable and $\|\dot{P}(t)\|_\infty < 1$ where $P(t)$ is the solution of*

  $$A^\top(t)P(t) + P(t)A(t) = -\mathbb{I}\,.$$

- On page 101, Assumption 8: change the text to:

  There exists ζ such that $\|\dot{A}_m(t)\|_\infty \leq \zeta$ for all $t \geq 0$ where ζ is defined in Lemma 5.

Verifiable Adaptive Control Solutions for Flight Control Applications

Jiang Wang

(ABSTRACT)

This dissertation addresses fundamental theoretical problems relevant to flight control for aerial vehicles and weapons in highly uncertain dynamical environment. The approach taken in this dissertation is the $\mathcal{L}_1$ adaptive control, which is elaborated from its design perspective for output feedback solution and is extended to time-varying reference systems to support augmentation of gain-scheduled baseline controllers. Compared to conventional adaptive controllers, $\mathcal{L}_1$ control has the following advantages: i) it has guaranteed uniformly bounded transient response for system's both signals, input and output; ii) it enables fast adaptation while maintains a bounded away from zero time-delay margin. The proposed adaptive control approach can recover the nominal performance of the flight control systems in the presence of rapid variation of uncertainties. Furthermore, the benefit of $\mathcal{L}_1$ adaptive control is its promise for development of theoretically justified tools for Verification and Validation (V&V) of adaptive systems.

Adaptive control for uncertain systems usually needs to handle two types of uncertainties: matched and unmatched uncertainties. Both of these two uncertainties will appear in practical flight control problems. In this dissertation, adaptive approaches which can compensate for these two types of uncertainties will be discussed respectively. Two architectures of $\mathcal{L}_1$ adaptive control, namely $\mathcal{L}_1$ state feedback adaptive control and $\mathcal{L}_1$ output feedback adaptive control, are studied. The state feedback adaptive control is applied for compensation of matched uncertainties. Although the state feedback scheme is capable of handling certain type of unmatched uncertainties, such approach is not explored in this dissertation. On the

other hand, the output feedback approach is mainly aimed to solve problems in the presence of unmatched uncertainties.

The dissertation first discusses the state feedback $\mathcal{L}_1$ adaptive control for time-invariant reference systems. The adaptive controller is designed to augment an existing baseline controller. The closed loop system of the plant and the baseline controller is time-invariant. This closed loop system, which is a Linear Time Invariant (LTI) system, determines the dynamics of the reference system. The adaptive feedback can compensate for nonlinear state- and time-dependent uncertainty with uniformly bounded transient response. In this dissertation we discuss the Multi-Input Multi-Output (MIMO) extension of the method. Two flight control examples, Unmanned Combat Aerial Vehicle (UCAV) and Aerial Refueling Autopilot, are considered in the presence of nonlinear uncertainties and control surface failures. The $\mathcal{L}_1$ adaptive controller without any redesign leads to scaled response for system's both signals, input and output, dependent upon changes in the initial conditions, system parameters and uncertainties. The time-delay margin analysis for these two examples verifies the theoretical claims.

Next, the output feedback approach is studied. The adaptive output feedback controller can be applied to reference systems that do not verify the Strict Positive Real (SPR) condition for their input-output transfer function. In this dissertation, specific design guidelines are presented that render the approach suitable for practical applications. A missile autopilot design example is given to demonstrate the benefits of the design approach.

Finally, the $\mathcal{L}_1$ state feedback adaptive controller is extended to time-varying reference systems. The adaptive controller intends to augment a gain-scheduled baseline controller. The reference system, which is determined by the closed loop system of the plant and the baseline gain-scheduled controller, is time-varying. The adaptive controller with time-varying reference system is proved to have guaranteed performance bounds similar to those obtained for the case of linear time-invariant reference systems. With this result, the aerial refueling application can be extended to a complete scenario, which includes a racetrack maneuver

for an aircraft.

The concluding chapter discusses the challenging issues for future research.

Acknowledgments

First and foremost, my great appreciation goes to my dissertation advisor, Dr. Naira Hovakimyan. For the past several years, her excellent guidance, her vision and insightful suggestions, continuous encouragement and enormous help, both to my study and my life, have contributed greatly to my achievements in this dissertation. Undoubtedly, she was the most influential person during my PhD studies. She is more than an excellent mentor. Her friendship made my busy life in past years more colorful. She challenged me to explore open problems and new directions beyond the existing boundaries of control theory. What I have learned from her will have plenty of beneficial influences on my future career path. My special thanks go to Dr. Chengyu Cao. His outstanding research work inspired me in my research and study. He was always willing to guide me to find solutions to my problems, and his creative way of finding solutions and critical insights to engineering problems broadened my horizon. Without his help, I could not have had the confidence to attack the challenging problems. I thank both of them for giving me huge support.

I also want to express my gratitude to my co-chair, Dr. Craig Woolsey, and committee members: Dr. Andrew Kurdila and Dr. Daniel Stilwell. Their insightful suggestions and kind support are precious to me. Their help is extremely important in shaping the final stage of my dissertation. One person who gave me a lot of guidance during my work is Dr. Eugene Lavretsky. He could not serve as my committee member due to the University policy, however, he was guiding me as if he was one of my committee members. My great appreciation goes to him.

Dr. Darrell Ridgely and Dr. Richard Hindman from Raytheon helped me to develop solutions of practical problems. Their kind support and guidance are greatly appreciated. Dr. Kevin Wise from Boeing shared his invaluable insights on flight control, while working on a joint paper. My appreciation goes to him. Dr. Irene Gregory from NASA gave me plenty of suggestions on my work, and I would like to thank her for the help. Dr. Vijay Patel was an influential person in my PhD studies. He is an excellent engineer and researcher. He helped me with plenty of issues in my research. I would also show my appreciation to Dr. Thomas Alberts, my Master thesis advisor from Old Dominion University, for his great guidance and help. My thanks also go to Dr. Brett Newman from Old Dominion University for his support to me. My colleague and office-mate, Dr. Vahram Stepanyam, always provided the first help. The discussions with him were always inspirational. My thanks further go to my colleagues, Dr. Lili Ma, Dr. Konda Reddy Chevva, Mr. Dapeng Li, Ms. Amanda Young, Mr. Zhiyuan Li, Mr. Enric Xargay, Mr. Evgeny Kharisov, Mr. Yu Lei, Mr. Aditya Paranjape.

Besides the people who work with me closely, I would like to show my great appreciations to my family, which is the most important part in my life. My parents provided me with endless love and support all the time. Finally, special thanks go to Pengbo, who has been encouraging and supporting me for a long time.

Jiang Wang

February 01, 2009
Blacksburg, Virignia

This work is based upon work supported by the United States Air Force under Contract No. F33615-00-D-3052, AFOSR under Contract FA9550-08-1-0135, FA9550-05-1-0157, and by NASA under contracts NNX08AB97A, NNX08AC81A.

Contents

Nomenclature

X_V	Drag derivative due to velocity
X_q	Drag derivative due to pitch rate
X_α	Drag derivative due to angle of attack
M_q	Pitch moment derivative due to pitch angle
M_α	Pitch moment derivative due to angle of attack
Z_α	Vertical force derivative due to angle of attack
Y_β	Lateral force derivative due to side slip angle
L_β	Roll moment derivative due to side slip angle
L_p	Roll moment derivative due to roll rate
L_r	Roll moment derivative due to yaw rate
N_r	Yaw moment derivative due to yaw rate
N_β	Yaw moment derivative due to side slip
N_p	Yaw moment derivative due to roll rate
M_{δ_e}	Pitch moment derivative due to elevator deflection
X_{δ_T}	Thrust derivative
L_{δ_a}	Roll moment derivative due to aileron deflection
N_{δ_r}	Yaw moment derivative due to rudder deflection
N_{δ_a}	Yaw moment derivative due to aileron deflection
$\bar{c}$	Wing mean aerodynamic chord
M_p	Mach number
m_p	Mass

q_p	Pitch rate
p_p	Roll rate
S	Wing reference area
V_t	Velocity
g	Gravity coefficient
α_p	Angle of attack rad
β_p	Side slip angle rad
γ_p	Flight-path angle rad
δ_T	Throttle setting
δ_e	Elevator deflection, degree
δ_a	Aileron deflection, degree
δ_r	Rudder deflection, degree
ρ_p	Density of air, slugs/ft^3
θ_p	Pitch angle, rad
ϕ_p	Roll angle, rad
l_s	Change of the relative horizontal separation, positive forward
z_s	Vertical separation from the tanker, positive down
y_s	Lateral separation relative to the tanker, positive right
l_p	Horizontal position, relative to the inertial frame
s_p	Lateral position, relative to the inertial frame
h_p	Vertical position, relative to the inertial frame
D_p	Drag
T_p	Thrust
S_p	Side force
L_f	Lift force
$I_{(\cdot)(\cdot)}$	Moment or product of inertial relative to the body axis
$\mathcal{L}_p$	Rolling moment
$\mathcal{M}_p$	Pitching moment
$\mathcal{N}_p$	Yawing moment

List of Figures

List of Tables

Chapter 1

Introduction

1.1 Overview and Motivation

Aerospace applications define challenging nonlinear control design problems. Although gain-scheduling is partially simplifying the nonlinear control design problem, it cannot completely address the uncertainties throughout the entire flight envelope. Adaptive control has been effectively used to partially address these challenges. Since the early 1990's, Air Force, Navy and NASA, in collaboration with industry and academia have made significant progress towards maturing the adaptive control theory for application to reconfigurable/damage adaptive flight control for aircraft and weapon systems. Reconfigurable flight control refers to the ability of a flight control system to adapt to unknown failures, damage, and uncertain aerodynamics. Flight control systems that are adaptive and reconfigurable constitute an important element in the design of mission effective unmanned combat systems. These properties of the control system can increase the reliability of unmanned systems.

Both indirect and direct adaptive control methods have been investigated, and several approaches have been successfully flown on manned and unmanned aircraft, and also on advanced weapon systems. Indirect adaptive based approaches include Self-Repairing Flight

Control Systems (SRFCS), Self Designing Controller (SDC) and Intelligent Flight Control System (IFCS) Generation I. Direct adaptive control based approaches have been successfully used in Reconfigurable Control for Tailless Fighters (RESTORE) program. The application of those technologies under the RESTORE program led to the flight testing of the approach on the Boeing/NASA X-36 Agility Research Test Aircraft. Success in the RESTORE dynamic inversion based adaptive neural-network control of aircraft and missiles offered the potential to develop flight control systems without precise knowledge of the aerodynamics.

In spite of demonstrated progress of the applications of adaptive methods to flight control, some practical challenges still need to be addressed [1, 2]. Those include:

1. ensuring stability, robustness and uniform performance, despite the wide range of flight control inputs, initial conditions, and nonlinear dynamics;
2. providing sufficient design insights to allow tuning of control laws to meet a full set of qualitative and quantitative design criteria, especially transient performance criteria;
3. suppressing excitation of aircraft structural modes;
4. maintaining acceptable pilot handling qualities.

The recently developed $\mathcal{L}_1$ adaptive control successfully addressed some of these challenges. The method establishes a new paradigm for design of adaptive control systems. Compared to conventional adaptive controllers, $\mathcal{L}_1$ adaptive controller has the following advantages [3, 4, 5, 6, 7, 8, 9, 10]:

1. Guaranteed fast adaptation, limited only by available hardware (CPU);
2. Decoupling between adaptation and robustness;
3. Guaranteed transient performance for system's input and output signals;
4. Guaranteed and bounded away from zero time-delay margin in the presence of fast adaptation;

5. Uniform scaled transient response dependent on changes in initial conditions, value of the unknown parameters, and reference commands.

These characteristics of $\mathcal{L}_1$ adaptive controller help to successfully solve some of above posed challenges. Its guaranteed performance bounds and systematic design procedure can significantly reduce the tuning effort required for achieving desired closed-loop performance, while operating in the presence of uncertainties. Its ability of fast adaptation allows for control of systems in the presence of time and state dependent nonlinearities. This, in particularly, eliminates the need for selecting and tuning neural network basis functions, and with that significantly reduces the control design efforts. The performance limitations of $\mathcal{L}_1$ adaptive controller are shown to be consistent with hardware limitations. With $\mathcal{L}_1$ adaptive control architectures, adaptation and robustness are decoupled, which means that the speed of adaptation can be increased dependent upon the CPU, while the robustness can be resolved via conventional robust control methods. These features lay foundation for development of theoretically justified tools for Validation and Verification (V&V) of adaptive systems.

The motivation for this dissertation stems from practical challenges of flight control applications. In Autonomous Aerial Refueling problem (AAR), the receiver aircraft experiences unknown aerodynamic forces and moments caused by wing tip vortices of the lead aircraft. The vortex effects can be described by a nonlinear function, which depends on relative separation between the two aircraft. This poses the problem of compensating for matched uncertainties, which are nonlinear functions of time and system states. By saying "matched" uncertainties, we mean a system which has the following form:

$$\dot{x}(t) = A_m x(t) + B(u(t) + f(t, x)),$$

where A_m is known and Hurwitz, while $f(t, x)$ is an unknown nonlinear function that is within the span of control input $u(t)$. The conventional adaptive approaches are not suitable for addressing state- and time-dependent unknown nonlinearities, while $\mathcal{L}_1$ state feedback adaptive control can solve it with semi-global domain of attraction and with uniform, guaranteed, transient performance. Furthermore, $\mathcal{L}_1$ adaptive controller can handle the case,

when the control effectiveness reduction is unknown, as in

$$\dot{x}(t) = A_m x(t) + B(\Lambda u(t) + f(t, x)), \tag{1.1}$$

where Λ is an unknown matrix with known sign.

In another benchmark flight control example, the X-45A Unmanned Combat Aerial Vehicle, the $\mathcal{L}_1$ adaptive controller is designed to augment the baseline controller in the presence of pitching moment uncertainty, which is a nonlinear function of system state (angle of attack). It can recover the nominal performance of the closed loop system controlled by baseline controller, in the presence of uncertainties.

For aircraft, flying a full flight envelope, the nominal performance is obtained by applying a gain-scheduled controller to a linear time-varying system. Such scenario requires inclusion of a time varying reference system in the $\mathcal{L}_1$ adaptive controller, and this motivates the study of adaptive control with time-varying reference system in this dissertation. It is shown that under certain conditions, the $\mathcal{L}_1$ adaptive controller for time-varying reference system has stability and performance properties similar to those for the time invariant reference system. This result is applied to the design of an autopilot for a complete Autonomous Aerial Refueling scenario, which includes a racetrack maneuver of the aircraft.

In flight control applications, unmatched uncertainties are very common. "Unmatched" means that the uncertainties appear in $[A, B, C, D]$ matrices of the linear system

$$\begin{aligned} \dot{x}(t) &= Ax(t) + Bu(t) \\ y(t) &= Cx(t) + Du(t) \end{aligned} \tag{1.2}$$

and cannot be expressed in the form of (1.1). If the linear system is expressed in transfer function form, the uncertainties correspond to unknown coefficients of the transfer function. Although the state feedback scheme is capable of handling certain type of unmatched uncertainties, like systems in strict feedback form, such approach is not explored in this dissertation. The $\mathcal{L}_1$ output feedback adaptive control is explored to compensate for unmatched uncertainties. One example of unmatched uncertainty is the unknown change of

aerodynamic coefficients in the dynamics of aerial vehicles and weapons. A missile longitudinal autopilot design example demonstrates the application of $\mathcal{L}_1$ adaptive output feedback controller for compensation of unmatched uncertainties.

1.2 State of the Art in Adaptive Control Theory

Adaptive control theory has been developed for decades, see books [13, 14, 15, 16, 17, 18] and references therein. Conventional MRAC defines sufficient conditions for stable performance, but does not provide effective ways to characterize the system's input/output performance during the transient phase. Application of adaptive controllers was therefore largely restricted due to the fact that the system uncertainties during the transient, or changes of reference inputs and initial conditions, have led to unpredictable/undesirebale situations. Those situations include generation of control signals of high-frequency or large amplitudes, large transient errors or slow convergence rate of tracking errors, to name a few. Extensive tuning of adaptive gains and Monte-Carlo runs have been the primary methods up today enabling the transition of adaptive control solutions to real world applications.

Improvement of the transient performance of adaptive controllers has been addressed from various perspectives in numerous publications [14, 19, 20, 21, 22, 23, 24, 25, 26, 27, 28, 29, 30, 32], to name a few. As compared to the linear systems theory, several important aspects of the transient performance analysis seem to be missing in these papers. First, all the bounds in these papers are computed for tracking errors only, and not for control signals. Second, changes in reference input and unknown parameters due to possible faults or unexpected uncertainties should not lead to unacceptable transient deviations or oscillatory control signals, implying that a re-tuning of adaptive parameters is required. Finally, one needs to ensure that whatever modifications or solutions are suggested for performance improvement of adaptive controllers, they are not achieved via high-gain feedback. The new type of model following adaptive controller, $\mathcal{L}_1$ adaptive control, addresses those issues

satisfactorily.

Adaptive control of nonlinear systems with time varying parameters was investigated in [33]. The results in [33] improved upon [34, 35, 36], by extending the class of system beyond the slow time variation of the unknown parameters and guaranteeing performance improvement to an arbitrary degree. In [37, 38, 39], local robustness to time variations and unmodeled dynamics was obtained in the presence of persistent excitation. However, these results did not provide means for regulating the frequency spectrum of the control signal during the transient, and hence did not provide any guarantees for robustness. Moreover, although the above papers consider control of time-varying plants, their control objective is not defined in terms of a time-varying reference system. Time-varying reference system has been considered in [40] in the framework of model reference adaptive control, albeit without transient performance guarantees and robustness analysis.

In this dissertation, we consider linear time-varying reference system and develop the $\mathcal{L}_1$ adaptive augmentation of baseline gain-scheduled controller with performance guarantees with respect to that reference system. In the same spirit of the earlier $\mathcal{L}_1$-results, we prove that with fast adaptation of $\mathcal{L}_1$ adaptive controller, one can recover the the nominal performance of the gain-scheduled controlled system at different operating points, without overruling the performance of the baseline controller.

In this dissertation we only focus on the applications of adaptive control to reconfigurable or damage flight control for aircraft and weapon systems.

1.3 State of the Art in Adaptive Flight Control

In the 1990s, with the development in computer technology and advances in adaptive control theory, adaptive control methods for flight control reconfiguration were intensively explored.

Direct Model Reference Adaptive Control was applied to both aircraft systems [41] and

weapons [42]. The Self-Repairing Flight Control System [43] performed on-line damage isolation and estimation to achieve tolerance to failure and damage. Maybeck looked at multiple model adaptive control [44]. Ahmed-Zaid et al. investigated a Linear Quadratic Regulator (LQR) based indirect adaptive control approach [45].

The Self Designing Controller program [46] was successfully flight tested on the VISTA/F-16 aircraft, which applied least square system identification to estimate parameters required for the solution of a receding horizon optimal control problem. Steinberg [47] studied neural network and fuzzy logic based approaches for flight control. Some important advances were made in development of adaptive neural-network flight control laws in Calise and Kim [48]. They used two neural networks to invert the nonlinearities in a dynamic inversion control law. One neural network was trained off-line and remained static during flight, the other adapted on-line to handle uncertainties. This approach was later modified and used in the Reconfigurable Control for Tailless Fighters (RESTORE) program [49]. The application of those technologies under the RESTORE program led to the flight testing of the approach on the Boeing/NASA X-36 Agility Research Test Aircraft. Success in the RESTORE dynamic inversion based adaptive neural-network control of aircraft and missiles offered the potential to develop flight control systems without knowledge of the aerodynamics. These technological advances paved the road to successful transition of adaptive flight control methods into two Boeing / USAF production programs [50, 51, 52, 53, 54, 55].

Two application examples where adaptive flight control can be applied are discussed next. These two examples are: autonomous aerial refueling and adaptive augmentation to gain scheduled baseline controller. In autonomous aerial refueling case, satisfactory performance of the receiver aircraft in the presence of uncertain airflow field is highly desired. Adaptive flight control can play a critical role for compensation of the unknown aerodynamic effects. In full flight envelope, both the plant and the gain-scheduled controllers are essentially time-varying. For the augmentation purpose, the adaptive controller should include the time-varying dynamics as a part of its feedback. The $\mathcal{L}_1$ adaptive controller is developed for time-varying reference systems and is used to augment the baseline gain-scheduled controller.

1.3.1 Autonomous Aerial Refueling

With the advent of unmanned flight vehicles, safe and reliable Autonomous Aerial Refueling (AAR) capabilities become a necessity. Reference [56] presents a good overview of the challenges involved in Autonomous Aerial Refueling. Two aerial refueling procedures, probe-and-drogue method and boom-receptacle method, are being employed by US Navy/North Atlantic Treaty Organization and US Air Force respectively. The boom-receptacle refueling procedure requires special tanker and human operator onboard, and the workload of the receiver aircraft is less, compared to that of the probe-and-drogue approach. On the contrary, the probe-and-drogue refueling procedure does not need a special tanker and/or human operator in the loop, but it requires a good autonomous tracking controller. This has proven to be extremely difficult due to the aerodynamic coupling among the two aircraft and the drogue. The autopilot has to compensate for the uncertainties due to the trailing vortices of the tanker, when the receiver is flying from the observation point to the contact point. The method proposed in this dissertation achieves this control objective with uniformly bounded transient response. It can be also equally applied for the boom-receptacle method employed for aerial refueling.

Aerial refueling has been intensively addressed over the past decade from various perspectives [56, 57, 58, 59, 60, 61, 62, 63, 64, 65, 66, 67, 68, 69, 70, 71, 72, 73, 74, 75]. Several methods, combined with various sensors, have been practiced for obtaining accurate measurements of the drogue, like use of global positioning system (GPS) [57, 64], visual servoing with pattern recognition [58, 59, 66] and vision-based navigation systems [68, 69]. GPS based sensor has been used with machine vision-based sensors to achieve accurate positioning and capturing [63]. In Ref. [61], a new set of nonlinear equations of motion, including the relative motion of the receiver and the tanker and the aerodynamic coupling due to the trailing vortex of the tanker, are derived. Vortex effect modeling is developed in Refs. [70, 60]. Proportional-Integral-Derivative (PID) control laws for each of the three position separation axis are used in Ref. [71] without considering the effect of the trailing vortex

in the simulation. Quantitative feedback theory was applied to take care of the wind gust and fuel transferring disturbances [65]. In Ref. [73], the authors studied the applicability of proportional navigation guidance and line-of-sight angle control in aerial refueling, using a turbulence model instead of modeling the vortex induced effect. An optimal nonzero set point with control rate weighting controller was applied to track and dock with a stationary drogue under the influence of Dryden light turbulence [68]. Reference [69] developed a reference-observer-based tracking controller.

The trailing vortex induced wind field presents a significant challenge from control design perspective. The situation is also complicated by the fact that the modeling of vortex effect is far from satisfactory. This brings up the idea of implementing Model Reference Adaptive Control (MRAC) architecture with neural networks [67], which requires less *a priori* knowledge of the trailing vortex effect. However in such uncertain dynamic environment the transient performance of MRAC can be unpredictable [28]. $\mathcal{L}_1$ adaptive control was considered for solving the AAR problem in [83, 84, 79].

1.3.2 Augmentation of Baseline Gain-Scheduled Controller

In this dissertation, adaptive augmentation of a baseline gain-scheduled controller is studied. The literature is rich on gain-scheduled control design methods. A more-or-less complete survey of gain scheduled control design methods is presented in [94, 95]. There are two major categories of gain scheduling control approaches: linearization-based gain scheduling approach and Linear Parameter-Varying (LPV) approach. In this dissertation, linearization-based design method is considered to be the baseline controller. One commonly used design method is that one interpolates on point design controllers. Theoretically justified interpolation methods were reported in [89, 90, 91, 92, 93, 94, 95, 96, 97, 98]. Since the study in this dissertation is focusing on how to augment the existing baseline controller, it is assumed that a well-designed gain-scheduled controller is available. For details on the design of the gain-scheduled controllers, refer to the above mentioned papers.

One rule-of-thumb stability requirement of gain-scheduled controllers is the "slow time-variation" of scheduling variables. In the context of the conventional adaptive methods that are limited to constant unknown parameters, the adaptive augmentation of baseline gain-scheduled controllers raises a natural question: when the baseline controller is augmented by an adaptive controller, does the combined controller require a smaller rate of variation of the scheduling variables than that required by the baseline controller? In this dissertation we prove that the stability condition of $\mathcal{L}_1$ adaptive controller with time-varying reference system does not impose more conservative condition regarding the rate of time-variation for the scheduling variables. The explicit study of this stability condition is absent in some previous work, e.g., in [40]. Furthermore, the $\mathcal{L}_1$ adaptive controller with time-varying reference system has similar characteristics and performance bounds as for linear time-invariant reference systems, i.e. with fast adaptation one can ensure that the state and the control input of the closed-loop system remain arbitrarily close to the same signals of the linear time-varying reference system for all $t \geq 0$.

1.4 Research Contributions and Key Results

The theoretical contributions and key results of this dissertation are the following.

The results in [10] are extended to Multi-input Multi-output (MIMO) case with particular flight control examples in mind. For example, in Autonomous Aerial Refueling scenario, the receiver aircraft needs to compensate for vortex induced uncertainties in horizonal, vertical and lateral directions. The control objective is achieved by using thrust, elevator and aileron at the same time. This brings up the challenge of controlling the aircraft with three input signals to recover the nominal flight performance of three outputs in the presence of uncertainties in multiple directions. The results in [10] only consider Single-input Single-output case. Hence, the work in this dissertation extends that of [10] to more general multi-input multi-output flight control problems.

The $\mathcal{L}_1$ output feedback adaptive controller in [11, 12] relaxes the condition that the reference system needs to verify the Strict Positive Real (SPR) requirement, which is a significant extension upon the existing solutions. However, one of the sufficient conditions for stability in this approach poses challenging design issues for unstable and/or non-minimum phase plants, while for the dynamics of missiles the "instability" and "non-minimum phase property" are very common. This dissertation gives practical design methods to overcome the design challenges of this new approach.

In this dissertation, time-varying reference system is considered for application of $\mathcal{L}_1$ adaptive controller. The adaptive controller intends to augment a time-varying baseline controller. The application considered in this dissertation is augmentation of baseline gain-scheduled controller. The reference system, which is determined by the closed-loop system of the plant and the baseline controller, is essentially time-varying. The adaptive controller with time-varying reference system is proved to have guaranteed performance bounds similar to those obtained for the case of time-invariant reference systems. With this result, the aerial refueling application can be extended to a complete racetrack scenario for the aircraft. Since the theoretical framework changes to that of time-varying reference system, novel mathematical tools, definitions and proofs are developed and presented in this dissertation. This constitutes the main contribution of this dissertation.

The contributions related to flight control applications are: i) problem formulations are given for several benchmark flight control examples, and the modeling of system dynamics is tailored to the structure of the adaptive control problem; ii) practical design issues are addressed in addition to theoretical developments; iii) compensation for uncertainties that are commonly present in aerospace applications, i.e., matched and unmatched uncertainties, is studied, and satisfactory simulation results are demonstrated; iv) the problem of augmentation of a baseline gain-scheduled controller is given.

The work in this dissertation demonstrates the benefit of $\mathcal{L}_1$ adaptive controller in terms of *verifiable flight control applications*.

1.5 Dissertation Layout

The dissertation has five chapters.

Chapter 2 gives mathematical preliminaries that are necessary for theoretical results in this dissertation.

Chapter 3 presents the state feedback solution for multi-input multi-output nonlinear time-varying system with time-invariant reference system. The uncertainties considered are state-dependent, time-varying unknown nonlinear functions which satisfy "matched" form, in addition to unknown control effectiveness. Two flight control examples are studied: unmanned combat aerial vehicle and autonomous aerial refueling.

Chapter 4 considers uncertainties in "unmatched" form by exploring the $\mathcal{L}_1$ adaptive output feedback architecture. The "unmatched" uncertainty is common in flight control problems, for example, unknown changes in aerodynamic coefficients cause unknown changes of transfer function coefficients. Specific design issues are addressed. A missile autopilot design is shown.

Chapter 5 presents state feedback $\mathcal{L}_1$ adaptive controller for time-varying reference systems. This is motivated by the problem of adaptively augmenting gain-scheduled baseline controllers. The main challenge is that for time-varying reference systems is that the performance specifications cannot be stated in the form of standard $\mathcal{L}_1$ norms, commonly used for LTI systems. New mathematical preliminaries other than those of Chapter 3 are introduced. A racetrack maneuver of aerial refueling is simulated for the application of this newly developed $\mathcal{L}_1$ adaptive controller, which is the main contribution of this dissertation.

Chapter 6 concludes the results of the above chapters, discusses some issues of the application of proposed adaptive methods, and gives future direction of research with respect to adaptive flight control.

Chapter 2

Mathematical Preliminaries

Recall some definitions and facts from linear systems theory, [24, 81, 82, 104].

Definition 1 *For a signal* $\xi(t)$, $\xi \in \mathbb{R}^n$, *its truncated* $\mathcal{L}_\infty$ *norm and* $\mathcal{L}_\infty$ *norm are defined as* $\|\xi_t\|_{\mathcal{L}_\infty} = \max\limits_{i=1,..,n} \left(\sup\limits_{0\leq\tau\leq t} |\xi_i(\tau)| \right)$, $\|\xi\|_{\mathcal{L}_\infty} = \max\limits_{i=1,..,n} \left(\sup\limits_{\tau\geq 0} |\xi_i(\tau)| \right)$, *where* ξ_i *is the* i^{th} *component of* ξ.

Definition 2 *The* $\mathcal{L}_1$ *norm of a stable proper single–input single–output system* $H(s)$ *is defined to be* $||H(s)||_{\mathcal{L}_1} = \int_0^\infty |h(t)|dt$, *where* $h(t)$ *is the impulse response of* $H(s)$.

Definition 3 *For a stable proper* m *input* n *output system* $H(s)$ *its* $\mathcal{L}_1$ *norm is defined as* $\|H(s)\|_{\mathcal{L}_1} = \max_{i=1,\cdots,n} \left(\sum_{j=1}^m \|H_{ij}(s)\|_{\mathcal{L}_1} \right)$, *where* $H_{ij}(s)$ *is the* i^{th} *row* j^{th} *column element of* $H(s)$.

Lemma 1 *For a stable proper multi-input multi-output (MIMO) system* $H(s)$ *with input* $r(t) \in \mathbb{R}^m$ *and output* $x(t) \in \mathbb{R}^n$, *we have* $\|x_t\|_{\mathcal{L}_\infty} \leq \|H(s)\|_{\mathcal{L}_1} \|r_t\|_{\mathcal{L}_\infty}$, $\forall\ t \geq 0$.

Corollary 1 *For a stable proper MIMO system* $H(s)$, *if the input* $r(t) \in \mathbb{R}^m$ *is bounded, then the output* $x(t) \in \mathbb{R}^n$ *is also bounded:* $\|x\|_{\mathcal{L}_\infty} \leq \|H(s)\|_{\mathcal{L}_1} \|r\|_{\mathcal{L}_\infty}$.

Lemma 2 *For a cascaded system $H(s) = H_2(s)H_1(s)$, where $H_1(s)$ is a stable proper system with m inputs and l outputs and $H_2(s)$ is a stable proper system with l inputs and n outputs, we have $\|H(s)\|_{\mathcal{L}_1} \leq \|H_2(s)\|_{\mathcal{L}_1}\|H_1(s)\|_{\mathcal{L}_1}$.*

Consider a linear time invariant system $\dot{x}(t) = Ax(t) + bu(t)$, where $x \in \mathbb{R}^n$, $u \in \mathbb{R}$, $b \in \mathbb{R}^n$, $A \in \mathbb{R}^{n\times n}$ is Hurwitz, and assume that the transfer function $(s\mathbb{I}-A)^{-1}b$ is strictly proper and stable. Notice that it can be expressed as $(s\mathbb{I}-A)^{-1}b = n(s)/d(s)$, where $d(s) = \det(s\mathbb{I}-A)$ is a n^{th} order stable polynomial, and $n(s)$ is a $n \times 1$ vector with its i^{th} element being a polynomial function: $n_i(s) = \sum_{j=1}^{n} n_{ij}s^{j-1}$.

Lemma 3 *If $(A \in \mathbb{R}^{n\times n}, b \in \mathbb{R}^n)$ is controllable, the matrix N with its i^{th} row j^{th} column entry n_{ij} is full rank.*

The proof can be found in [3].

Lemma 4 *If (A, b) is controllable and $(s\mathbb{I} - A)^{-1}b$ is strictly proper and stable, there exists $c \in \mathbb{R}^n$ such that the transfer function $c^\top(s\mathbb{I} - A)^{-1}b$ is minimum phase with relative degree one, i.e. all its zeros are located in the left half plane, and its denominator is one order larger than its numerator.*

The proof can be found in [3].

Definition 4 *The $\|\cdot\|_\infty$ of an $m \times n$ matrix A is defined as*

$$\|A\|_\infty = \max_i \sum_{j=1}^{n} |a_{ij}|.$$

Next we will introduce some preliminaries for linear time varying systems.

Definition 5 *Given a linear time-varying (LTV) system*

$$\begin{aligned} \dot{x}(t) &= A(t)x(t) + B(t)u(t) \\ y(t) &= C(t)x(t), \quad x(t_0) = 0, \end{aligned} \tag{2.1}$$

where $x(t) \in \mathbb{R}^N$, $y(t) \in \mathbb{R}^n$ and $u(t) \in \mathbb{R}^m$, the impulse response, which specifies the input-output behavior of (2.1), is given by

$$G(t,\sigma) = C(t)\Phi(t,\sigma)B(\sigma), \quad t \geq \sigma\,, \tag{2.2}$$

where $\Phi(t,\sigma)$ is the transition matrix of the system (2.1).

Let $H : \mathbb{R}^m \to \mathbb{R}^n$ be the input-output map of the system (2.1) from $u(t)$ to $y(t)$ and write $y = Hu$.

Definition 6 *The $\mathcal{L}_1$-norm of the single-input single-output (SISO) LTV system H_0 is defined as*

$$\|H_0\|_{\mathcal{L}_1} = \sup_{\forall t,\tau,\, t\geq\tau} \int_\tau^t |g(t,\sigma)|d\sigma\,,$$

where $g(t,\sigma)$ is the impulse response of the SISO system H_0.

Remark 1 *For linear time-invariant (LTI) system $H_0(s)$, the definition of $\mathcal{L}_1$-norm reduces to conventional one:*

$$\|H_0(s)\|_{\mathcal{L}_1} = \int_0^\infty |g(\sigma)|d\sigma\,.$$

Definition 7 *The $\mathcal{L}_1$-norm of the m input n output LTV system H as in (2.1) is defined as*

$$||H||_{\mathcal{L}_1} = \max_{i=1,\cdots,n} \Big(\sum_{j=1}^m \|H_{ij}\|_{\mathcal{L}_1} \Big),$$

where

$$\|H_{ij}\|_{\mathcal{L}_1} = \sup_{\forall t,\tau,\, t\geq\tau} \int_\tau^t |G_{ij}(t,\sigma)|d\sigma\,.$$

Definition 8 *The linear unforced system $\dot{x}(t) = A(t)x(t)$, $x(t_0) = x_0$, is called* uniformly exponentially stable *if there exist finite positive constants γ, λ such that for any t_0 and x_0 the corresponding solution satisfies*

$$\|x(t)\|_\infty \leq \gamma e^{-\lambda(t-t_0)}\|x_0\|_\infty, \quad t \geq t_0\,.$$

Lemma 5 *([104], Theorem 8.7) Suppose that for the linear state equation*

$$\dot{x}(t) = A(t)x(t), \quad x(t_0) = x_0\,,$$

*with $A(t)$ continuously differentiable, there exist positive constants μ_A, μ_λ such that, for all $t \geq 0$, $\|A(t)\|_\infty \leq \mu_A$, and at each time t, the eigenvalues of $A(t)$ (*point-wise eigenvalue*) satisfy* $\mathrm{Re}[\lambda(t)] \leq -\mu_\lambda$. *Then there exists a positive constant ζ such that if the time-derivative of $A(t)$ satisfies $\|\dot{A}(t)\|_\infty \leq \zeta$ for all $t \geq 0$, then the state equation is uniformly exponentially stable.*

This lemma proves only the existence of ζ such that if $\|\dot{A}(t)\|_\infty \leq \zeta$, then the point-wise eigenvalue condition can lead to uniform exponential stability. However, it does not provide a constructive solution for determining ζ. For the purposes of practical design, one would like to have an idea of the smallest possible value for the upper bound of $\|\dot{A}(t)\|_\infty$. In the analysis below, this is important for quantification of the performance bounds that depend upon the max $\|\dot{A}(t)\|_\infty$. The proof of this lemma reveals an important property needed for stability analysis of the adaptive controller shown later. Hence, we analyze that part of the proof. For details of this proof refer to [104] (Theorem 8.7).

Sketch of the proof: For each fixed t, the point-wise eigenvalue condition implies there exists a positive definite $P(t)$ which is the unique solution of

$$A^\top(t)P(t) + P(t)A(t) = -\mathbb{I}\,.$$

This solution has the form $P(t) = \int_0^\infty e^{A^\top(t)\sigma} e^{A(t)\sigma} d\sigma$. The strategy of the proof is to show that for all t, $P(t)$ is symmetric, continuously differentiable and such that

$$\eta\mathbb{I} \leq P(t) \leq \rho\mathbb{I} \tag{2.3}$$

$$A^\top(t)P(t) + P(t)A(t) + \dot{P}(t) \leq -\upsilon\mathbb{I} \tag{2.4}$$

where η, ρ and υ are finite positive constants. The uniform exponential stability then follows.

The first part of the proof shows that there exists ρ such that $P(t) \leq \rho\mathbb{I}$ for all t. Then it is shown that there exists η such that $P(t) \geq \eta\mathbb{I}$. This part is omitted here.

We need to show that there exists a $\upsilon > 0$ such that

$$A^\top(t)P(t) + P(t)A(t) + \dot{P}(t) \leq -\upsilon\mathbb{I}$$

for all $t \geq 0$. Recall that $P(t)$ is the solution of $A^\top(t)P(t) + P(t)A(t) = -\mathbb{I}$. Then (2.4) can be written as

$$\dot{P}(t) \leq (1-\upsilon)\mathbb{I}. \tag{2.5}$$

Next we need to look at the norm of $\dot{P}(t)$. Differentiation of (2.4) with respect to t yields

$$A^\top(t)\dot{P}(t) + \dot{P}(t)A(t) = -\dot{A}^\top(t)P(t) - P(t)\dot{A}(t).$$

At each t this Lyapunov equation has a unique solution

$$\dot{P}(t) = \int_0^\infty e^{A^\top(t)\sigma}\left[\dot{A}^\top(t)P(t) + P(t)\dot{A}(t)\right]e^{A(t)\sigma}d\sigma$$

To derive a bound on $\|\dot{P}(t)\|_\infty$, we use the boundedness of $\|P(t)\|_\infty$. For any $n \times 1$ vector x and any $t \geq 0$,

$$\begin{aligned}&\left|x^\top e^{A^\top(t)\sigma}\left[\dot{A}^\top(t)P(t) + P(t)\dot{A}(t)\right]e^{A(t)\sigma}\right| \\ &\leq \|\dot{A}^\top(t)P(t) + P(t)\dot{A}(t)\|_\infty x^\top e^{A^\top(t)\sigma}e^{A(t)\sigma}x.\end{aligned} \tag{2.6}$$

Thus

$$\begin{aligned}\left|x^\top\dot{P}(t)x\right| &= \left|\int_0^\infty x^\top e^{A^\top(t)\sigma}\left[\dot{A}^\top(t)P(t) + P(t)\dot{A}(t)\right]e^{A(t)\sigma}xd\sigma\right| \\ &\leq \|\dot{A}^\top(t)P(t) + P(t)\dot{A}(t)\|_\infty x^\top P(t)x \\ &\leq 2\|\dot{A}(t)\|_\infty\|P(t)\|_\infty x^\top P(t)x.\end{aligned} \tag{2.7}$$

For all $\|x\|_2 = 1$, the maximum of the right hand side leads to the following upper bound

$$\left|x^\top\dot{P}(t)x\right| \leq 2\|\dot{A}(t)\|_\infty\|P(t)\|_\infty^2. \tag{2.8}$$

Since the bound on the right hand side is uniform, it holds uniformly for the maximum of the left hand side for the same $\|x\|_2 = 1$:

$$\|\dot{P}(t)\|_\infty \leq 2\|\dot{A}(t)\|_\infty\|P(t)\|_\infty^2$$

Next we will study the conditions on $\|\dot{A}(t)\|_\infty$ and $\|P(t)\|_\infty$, which can ensure that (2.5) can hold. It is obvious to see that if $\|\dot{P}(t)\|_\infty < 1$ then (2.5) can hold. Although there are other possible values of $\dot{P}(t)$ that can satisfy (2.5), restricting the norm of $\dot{P}(t)$ to less than one can ensure that (2.5) holds.

Considering

$$\|\dot{P}(t)\|_\infty \leq 2\|\dot{A}(t)\|_\infty \|P(t)\|_\infty^2,$$

we want to make sure that $2\|\dot{A}(t)\|_\infty \|P(t)\|_\infty^2 < 1$, which will lead to (2.5). Since we have shown that there exist finite bounds on $\|P(t)\|_\infty$, it is straightforward to show the existence of a finite positive constant ζ, such that if $\|\dot{A}(t)\|_\infty \leq \zeta$ for all $t \geq 0$, then $2\|\dot{A}(t)\|_\infty \|P(t)\|_\infty^2 < 1$, and the uniform exponential stability follows.

Notice that one important implication of this lemma is that if $\|\dot{A}(t)\|_\infty \leq \zeta$ for all $t \geq 0$ and the point-wise eigenvalue condition holds, we have

$$\|\dot{P}(t)\|_\infty < 1. \tag{2.9}$$

This property will be used in the proof of stability of the adaptive controller, detailed later in the dissertation.

Definition 9 *The linear system in (2.1) is called* uniformly bounded-input, bounded-output stable*, if there exists a finite constant η such that for any t_0 and any input signal $u(t)$ the corresponding zero-state response satisfies*

$$\sup_{t \geq t_0} \|y(t)\|_\infty \leq \eta \sup_{t \geq t_0} \|u(t)\|_\infty .$$

Lemma 6 *([104], Lemma 12.4) Suppose the linear state equation (2.1) is uniformly exponentially stable; i.e. there exist finite constants μ_B and μ_C such that for all $t \geq t_0$*

$$\|B(t)\|_\infty \leq \mu_B, \quad \|C(t)\|_\infty \leq \mu_C.$$

Then the state equation is uniformly bounded-input, bounded-output stable:

$$\|x_t\|_{\mathcal{L}_\infty} \leq \|H\|_{\mathcal{L}_1} \|u_t\|_{\mathcal{L}_\infty}.$$

Further, if the input $u(t)$ is bounded, then $\|x\|_{\mathcal{L}_\infty} \leq \|H\|_{\mathcal{L}_1}\|u\|_{\mathcal{L}_\infty}$.

Lemma 7 *For a cascaded system $H = H_2H_1$, where H_1 and H_2 are stable systems, we have $\|H\|_{\mathcal{L}_1} \leq \|H_2\|_{\mathcal{L}_1}\|H_1\|_{\mathcal{L}_1}$.*

Proof: Let $(u_1(t), y_1(t))$ and $(u_2(t), y_2(t))$ be the input-output pairs of the systems H_1 and H_2 respectively, and $u_2(t) = y_1(t)$. Further, let $u_1(t)$ be bounded. From Lemma 6 we have

$$\begin{aligned} \|y_1\|_{\mathcal{L}_\infty} &\leq \|H_1\|_{\mathcal{L}_1}\|u_1\|_{\mathcal{L}_\infty}, \\ \|y_2\|_{\mathcal{L}_\infty} &\leq \|H_2\|_{\mathcal{L}_1}\|u_2\|_{\mathcal{L}_\infty}. \end{aligned} \tag{2.10}$$

Since $H = H_1H_2$, then

$$y_2(t) = Hu_1(t) = H_2(H_1u_1(t)) = H_2y_1(t).$$

Hence we have

$$\|y_2\|_{\mathcal{L}_\infty} \leq \|H_2\|_{\mathcal{L}_1}\|y_1\|_{\mathcal{L}_\infty} \leq \|H_2\|_{\mathcal{L}_1}\|H_1\|_{\mathcal{L}_1}\|u_1\|_{\mathcal{L}_\infty}. \tag{2.11}$$

Recalling the input-output relationship of linear time-varying systems, we can write

$$\begin{aligned} \|y_2(t)\|_\infty &= \Big\| \int_{t_0}^t C(t)\Phi(t,\sigma)B(\sigma)u_1(\sigma)d\sigma \Big\|_\infty \\ &= \Big\| \Big[\sum_{j=1}^m \int_{t_0}^t G_{1j}(t,\sigma)(u_1)_j(\sigma)d\sigma, \cdots, \sum_{j=1}^m \int_{t_0}^t G_{nj}(t,\sigma)(u_1)_j(\sigma)d\sigma \Big]^\top \Big\|_\infty \\ &= \max_{i=1,\cdots,n} \Big(\Big| \sum_{j=1}^m \int_{t_0}^t G_{ij}(t,\sigma)(u_1)_j(\sigma)d\sigma \Big| \Big) \\ &\leq \max_{i=1,\cdots,n} \Big(\sum_{j=1}^m \int_{t_0}^t \Big| G_{ij}(t,\sigma) \Big| \Big| (u_1)_j(\sigma) \Big| d\sigma \Big) \\ &\leq \max_{i=1,\cdots,n} \Big(\sum_{j=1}^m \sup_{\forall t,t_0,\, t\geq t_0} \int_{t_0}^t \Big| G_{ij}(t,\sigma) \Big| d\sigma \Big) \sup_{\forall \sigma \geq t_0} \|u_1(\sigma)\|_\infty, \end{aligned} \tag{2.12}$$

where $G(t,\sigma)$ is the impulse response of H. Hence from (2.12) we can write

$$\sup_{t\geq 0} \|y_2(t)\|_\infty \leq \|H\|_{\mathcal{L}_1} \sup_{\sigma \geq 0} \|u_1(\sigma)\|_\infty. \tag{2.13}$$

Thus, when $\|u_1\|_{\mathcal{L}_\infty} \leq 1$, we have $\sup_{\tau \geq 0} \|y_2(\tau)\|_\infty \leq \|H\|_{\mathcal{L}_1}$, or $\|y_2\|_{\mathcal{L}_\infty} \leq \|H\|_{\mathcal{L}_1}$.

Next we show that $\|H\|_{\mathcal{L}_1}$ is the least upper bound of $\|y_2\|_{\mathcal{L}_\infty}$, when $\|u_1\|_{\mathcal{L}_\infty} \leq 1$. This can be done by contradiction. Let $\|u_1\|_{\mathcal{L}_\infty} \leq 1$, and let $\|y_2\|_{\mathcal{L}_\infty} \leq \eta_y < \|H\|_{\mathcal{L}_1}$. This implies that

$$\sup_{t \geq 0} \|y_2(t)\|_\infty \leq \eta_y < \|H\|_{\mathcal{L}_1}.$$

Then there exist t_1 and t_2, $t_1 > t_2$, and index k such that

$$\sum_{j=1}^{m} \int_{t_2}^{t_1} \Big| G_{kj}(t_1, \sigma) \Big| d\sigma > \eta_y.$$

We can choose the control signal as

$$u_1(\sigma) = [\text{sign}(G_{k1}(t_1, \sigma)), \cdots, \text{sign}(G_{km}(t_1, \sigma))]^\top, \quad \sigma \in [t_2,\ t_1],$$

and

$$u_1(\sigma) = 0 \ \text{ for } \ \sigma > t_1.$$

Notice that for this control signal $\|(u_1)_t\|_{\mathcal{L}_\infty} \leq 1$. Then we have

$$\begin{aligned} (y_2)_k(t_1) &= \sum_{j=1}^{m} \int_{t_2}^{t_1} G_{kj}(t_1, \sigma)(u_1)_j(\sigma) d\sigma \\ &= \sum_{j=1}^{m} \int_{t_2}^{t_1} \Big| G_{kj}(t_1, \sigma) \Big| d\sigma > \eta_y. \end{aligned} \tag{2.14}$$

This implies $\sup_{t \geq 0} \|y_2(t)\|_\infty > \eta_y$, which contradicts the fact that η_y is an upper bound for $\|y_2\|_{\mathcal{L}_\infty}$. Hence $\|H\|_{\mathcal{L}_1}$ is the least upper bound for $\|y_2\|_{\mathcal{L}_\infty}$ for $\|u_1\|_{\mathcal{L}_\infty} \leq 1$. To complete the proof, in (2.11) we consider $\|u_1\|_{\mathcal{L}_\infty} \leq 1$, which gives

$$\|y_2\|_{\mathcal{L}_\infty} \leq \|H_2\|_{\mathcal{L}_1} \|H_1\|_{\mathcal{L}_1}. \tag{2.15}$$

Since $\|H\|_{\mathcal{L}_1}$ is the least upper bound, the proof is complete.

□

Theorem 1 *([81], Theorem 5.6) ($\mathcal{L}_1$* **Small Gain Theorem**) *The interconnected system $w_2(t) = \Delta(w_1(t) - M w_2(t))$ with input $w_1(t)$ and output $w_2(t)$ is stable if $\|M\|_{\mathcal{L}_1} \|\Delta\|_{\mathcal{L}_1} < 1$.*

Next we introduce some facts, which help to prove the performance bounds of $\mathcal{L}_1$ adaptive controller for time-varying reference systems.

Definition 10 *[107] The state-space representation* $[A(t), B(t)]$ *with* $\dim[A] = n \times n$ *is said to be* uniformly controllable*, if the controllability matrix*

$$Q_c(t) = [p_0(t),\, p_1(t), \cdots, p_{n-1}(t)]\,, \tag{2.16}$$

where $p_{k+1} = -A(t)p_k + \dot{p}_k$ *with* $p_0 = B(t)$*, is nonsingular for all* t*. The representation is* strongly controllable *if the controllability matrix of it is strongly nonsingular, i.e. there exists a finite constant* $c > 0$ *such that*

$$\Big|\det[Q_c(t)]\Big| \geq c, \qquad \forall\ t \geq 0.$$

Lemma 8 *[108],[109],[110] For the single input system* $\dot{x}(t) = A(t)x(t) + B(t)u(t)$ *there exists a nonsingular continuously differentiable transformation* $T(t)$ *reducing the system to its controllable (phase-variable) canonical form, given by*

$$\dot{\hat{x}}(t) = \hat{A}(t)\hat{x}(t) + \hat{B}(t)\hat{u}(t)$$

where $\hat{A}(t) = (T(t)A(t) + \dot{T}(t))^{-1}$*,* $\hat{B}(t) = T(t)B(t)$ *with*

$$\hat{A}(t) = \begin{bmatrix} 0 & 1 & 0 & \cdots & 0 \\ 0 & 0 & 1 & \cdots & 0 \\ \vdots & \vdots & \vdots & \ddots & \vdots \\ 0 & 0 & 0 & \cdots & 1 \\ -a_1(t) & -a_2(t) & -a_3(t) & \cdots & -a_n(t) \end{bmatrix}, \qquad \hat{B}(t) = \begin{bmatrix} 0 \\ 0 \\ \vdots \\ 0 \\ 1 \end{bmatrix},$$

if and only if $[A(t), B(t)]$ *is uniformly controllable. If* $A(t)$ *and* $B(t)$ *are uniformly bounded and smooth, and if* $[A(t), B(t)]$ *is strongly controllable, then the transformation* $T(t)$ *is uniformly bounded, and the resulting entries* $a_i(t)$ *in* $\hat{A}(t)$ *are also uniformly bounded.*

We now introduce the definition of the projection operator and some of its properties, which will be used in the derivation of the adaptive laws in the following sections. The smooth projection operator defined in [99] ensures boundedness of the parameter estimates by definition.

Definition 11 *Consider a convex compact set with a smooth boundary given by:*

$$\Omega_c \triangleq \{\boldsymbol{\theta} \in \mathbb{R}^n \mid f(\boldsymbol{\theta}) \leq c\}, \quad 0 \leq c \leq 1, \tag{2.17}$$

where $f : \mathbb{R}^n \to \mathbb{R}$ *is the following smooth convex function:*

$$f(\boldsymbol{\theta}) = \frac{\boldsymbol{\theta}^\top \boldsymbol{\theta} - \theta_{\max}^2}{\epsilon_\theta}, \tag{2.18}$$

where $\theta_{\max} > 0$ *is the norm bound imposed on the parameter vector* $\boldsymbol{\theta}$*, and* $0 < \epsilon_\theta < 1$ *denotes the convergence tolerance of our choice. For any given* $\boldsymbol{y} \in \mathbb{R}^n$ *the projection operator, denoted by* $\mathrm{Proj}(\cdot, \cdot)$*, is defined as:*

$$\mathrm{Proj}(\boldsymbol{\theta}, \boldsymbol{y}) = \begin{cases} \boldsymbol{y}, & \text{if } f(\boldsymbol{\theta}) < 0 \\ \boldsymbol{y}, & \text{if } f(\boldsymbol{\theta}) \geq 0,\ \nabla f^\top \boldsymbol{y} \leq 0 \\ \boldsymbol{y} - \frac{\nabla f \nabla f^\top \boldsymbol{y}}{\|\nabla f\|^2} f(\boldsymbol{\theta}), & \text{if } f(\boldsymbol{\theta}) \geq 0,\ \nabla f^\top \boldsymbol{y} > 0. \end{cases}$$

The properties of the Projection operator are given by the following lemma:

Lemma 9 *Let* $\boldsymbol{\theta}^* \in \Omega_0 = \{\boldsymbol{\theta} \in \mathbb{R}^n \mid f(\boldsymbol{\theta}) \leq 0\}$*, and let the parameter* $\boldsymbol{\theta}(t)$ *evolve according to the following dynamics*

$$\dot{\boldsymbol{\theta}}(t) = \mathrm{Proj}(\boldsymbol{\theta}(t), \boldsymbol{y}), \quad \boldsymbol{\theta}(t_0) \in \Omega_c\,. \tag{2.19}$$

Then

$$\boldsymbol{\theta}(t) \in \Omega_c \tag{2.20}$$

for all $t \geq t_0$*, and*

$$h_{\boldsymbol{\theta},\boldsymbol{y}} \triangleq (\boldsymbol{\theta}(t) - \boldsymbol{\theta}^*)^\top [\mathrm{Proj}(\boldsymbol{\theta}(t), \boldsymbol{y}) - \boldsymbol{y}] \leq 0\,. \tag{2.21}$$

From Definition 11 it follows that $\boldsymbol{y}$ is not altered if $\boldsymbol{\theta}$ belongs to the set Ω_0. In the set $\{0 \leq f(\boldsymbol{\theta}) \leq 1\}$, $\text{Proj}(\boldsymbol{\theta}, \boldsymbol{y})$ subtracts a vector normal to the boundary of Ω_c so that we get a smooth transformation from the original vector field $\boldsymbol{y}$ to an inward or tangent vector field for $c = 1$. Therefore, on the boundary of Ω_c, $\dot{\boldsymbol{\theta}}(t)$ always points toward the inside of Ω_c and $\boldsymbol{\theta}(t)$ never leaves the set Ω_c, which is the first property.

From the convexity of $f(\boldsymbol{\theta})$ it follows that for any $\boldsymbol{\theta}^* \in \Omega_0$ and $\boldsymbol{\theta} \in \Omega_c$, the inequality $l_{\boldsymbol{\theta}} \triangleq (\boldsymbol{\theta} - \boldsymbol{\theta}^*)^\top \nabla f(\boldsymbol{\theta}) \leq 0$ holds. Consequently, from Definition 11 it follows that

$$h_{\boldsymbol{\theta},\boldsymbol{y}} = \begin{cases} 0, & \text{if } f < 0 \\ 0, & \text{if } f \geq 0,\ \nabla f^\top \boldsymbol{y} \leq 0 \\ \dfrac{\underbrace{l_{\boldsymbol{\theta}}}_{\leq 0}\ \underbrace{\nabla f^T \boldsymbol{y}}_{\geq 0}\ \underbrace{f(\boldsymbol{\theta})}_{\geq 0}}{\|\nabla f\|^2}, & \text{if } f \geq 0,\ \nabla f^\top \boldsymbol{y} > 0 \end{cases}$$

The second property follows.

Chapter 3

$\mathcal{L}_1$ State Feedback Adaptive Control: Time Invariant Reference Systems

3.1 Problem Formulation

The adaptive control architecture considered in this chapter includes a fixed robust baseline controller and an augmentation of it by an adaptive controller. The baseline controller is designed to yield consistent nominal system performance in the absence of uncertainties and failures, while the adaptive element provides adaptation and reconfiguration in the presence of system uncertainties (e.g., battle damage), control failures and unknown aerodynamics. The linearized open-loop plant dynamics can be generalized and written in the form:

$$\begin{cases} \dot{x}_p(t) = A_p x_p(t) + B_p \Lambda \left[u(t) + K_0(t, x_p(t)) \right], & x_p(0) = x_{p_0} \\ y(t) = C_p x_p(t) + D_p \Lambda \left[u(t) + K_0(t, x_p(t)) \right] \\ z_p(t) = F y(t) \end{cases} \tag{3.1}$$

where $A_p \in \mathbb{R}^{n_1 \times n_1}$, $B_p \in \mathbb{R}^{n_1 \times m}$, $C_p \in \mathbb{R}^{l \times n_1}$, $D_p \in \mathbb{R}^{l \times m}$ and $F \in \mathbb{R}^{p \times l}$ are known matrices, $u(t) \in \mathbb{R}^m$ is the virtual control input, the diagonal matrix $\Lambda \in \mathbb{R}^{m \times m}$ is unknown with strictly positive diagonal elements Λ_i, $i = 1, 2, \cdots, m$, and represents the uncertainties in

control effectiveness, $K_0(t, x_p) \in \mathbb{R}^m$ is an unknown nonlinear function of system states. The output $y(t)$ represents the sensor measurements, and $z_p(t)$ is the subset of the plant outputs that are to be controlled.

The dynamics of the baseline controller can be generalized and written in the form:

$$\begin{cases} \dot{x}_c(t) = A_c x_c(t) + B_{1c} z_c(t) + B_{2c} z_p(t) \\ u(t) = C_c x_c(t) + D_{1c} z_c(t) + D_{2c} z_p(t) \end{cases} \tag{3.2}$$

where $z_c(t) \in \mathbb{R}^q$ is the vector of outer-loop commands from guidance, and $x_c \in \mathbb{R}^{n_2}$. Substituting $z_p(t)$ from (3.1) into (3.2), yields:

$$\begin{cases} \dot{x}_c(t) = A_c x_c(t) + B_{1c} z_c(t) + B_{2c} F \left[C_p x_p(t) + D_p \Lambda \left(u(t) + K_0(t, x_p(t)) \right) \right] \\ u(t) = C_c x_c(t) + D_{1c} z_c(t) + D_{2c} F \left[C_p x_p(t) + D_p \Lambda \left(u(t) + K_0(t, x_p(t)) \right) \right] \end{cases} \tag{3.3}$$

Consequently, the second equation in (3.3) can be solved explicitly for $u(t)$:

$$\begin{aligned} u(t) &= \left(\mathbb{I} - D_{2c} F D_p \Lambda \right)^{-1} \left[C_c x_c(t) + D_{1c} z_c(t) + D_{2_c} F C_p x_p(t) + D_{2c} F D_p \Lambda K_0(t, x_p(t)) \right] \\ &= \left(\mathbb{I} - D_{2c} F D_p \Lambda \right)^{-1} \left[D_{2c} F C_p \quad C_c \right] \underbrace{\begin{bmatrix} x_p(t) \\ x_c(t) \end{bmatrix}}_{x(t)} + \left(\mathbb{I} - D_{2c} F D_p \Lambda \right)^{-1} D_{1c} z_c(t) \\ &\quad + \left(\mathbb{I} - D_{2c} F D_p \Lambda \right)^{-1} D_{2c} F D_p \Lambda K_0(t, x_p(t)). \end{aligned} \tag{3.4}$$

The baseline controller $u_L(t)$, assuming no uncertainties, $\Lambda = \mathbb{I}$, $K_0(t, x_p(t)) = \mathbf{0}$, can be written as:

$$u_L(t) = K_x^\top x(t) + K_z^\top z_c(t) \tag{3.5}$$

where

$$K_x^\top = \left(\mathbb{I} - D_{2c} F D_p \right)^{-1} \left[D_{2c} F C_p \quad C_c \right], \qquad K_z^\top = \left(\mathbb{I} - D_{2c} F D_p \right)^{-1} D_{1c}.$$

The extended system dynamics are

$$\begin{aligned} \underbrace{\begin{bmatrix} \dot{x}_p(t) \\ \dot{x}_c(t) \end{bmatrix}}_{\dot{x}(t)} &= \underbrace{\begin{bmatrix} A_p & 0 \\ B_{2c} F C_p & A_c \end{bmatrix}}_{A} \underbrace{\begin{bmatrix} x_p(t) \\ x_c(t) \end{bmatrix}}_{x(t)} + \underbrace{\begin{bmatrix} B_p \\ B_{2c} F D_p \end{bmatrix}}_{B_1} \Lambda \left[u(t) + K_0(t, x_p(t)) \right] + \underbrace{\begin{bmatrix} 0 \\ B_{1c} \end{bmatrix}}_{B_2} z_c(t) \\ y(t) &= \underbrace{\begin{bmatrix} C_p & [0] \end{bmatrix}}_{C} x(t) + D_p \Lambda \left[u(t) + K_0(t, x_p(t)) \right], \end{aligned} \tag{3.6}$$

or equivalently,

$$\begin{aligned} \dot{x}(t) &= Ax(t) + B_1\Lambda\left[u(t) + K_0(t, x_p(t))\right] + B_2 z_c(t) \\ y(t) &= Cx(t) + D_p\Lambda\left[u(t) + K_0(t, x_p(t))\right], \end{aligned} \tag{3.7}$$

where $x \in \mathbb{R}^n$, $n = n_1 + n_2$.

In the absence of uncertainties, the linear closed-loop dynamics take the form:

$$\begin{aligned} \dot{x}_m(t) &= \underbrace{(A + B_1 K_x^\top)}_{A_m} x_m(t) + \underbrace{(B_1 K_z^\top + B_2)}_{B_m} z_c(t) \\ y_m(t) &= \underbrace{(C + D_p K_x^\top)}_{C_m} x_m(t) + \underbrace{D_p K_z^\top}_{D_m} z_c(t) \end{aligned} \tag{3.8}$$

The closed-loop system (3.8) defines the desired nominal response, with A_m being Hurwitz. The control design relies on the following assumptions.

Assumption 1

$$\Lambda_i \in [\Lambda_l, \ \Lambda_u], \qquad i = 1, 2, \cdots, m, \tag{3.9}$$

where $\Lambda_u > \Lambda_l > 0$ are known.

Let $f(t, x(t)) = \Lambda K_0(t, x_p(t))$, where $f : \mathbb{R} \times \mathbb{R}^n \to \mathbb{R}^m$ is an unknown nonlinear function. Notice that

$$\begin{aligned} \|x_p\|_\infty &\leq \|x\|_\infty \\ \|x_{p1} - x_{p2}\|_\infty &\leq \|x_1 - x_2\|_\infty . \end{aligned}$$

Assumption 2 *[Semiglobal Lipschitz Condition]*

For any $\delta > 0$, there exist positive L_δ and B such that

$$\|f(t, x_1) - f(t, x_2)\|_\infty \leq L_\delta \|x_1 - x_2\|_\infty . \tag{3.10}$$

$$\|f(t, 0)\|_\infty \leq B, \tag{3.11}$$

for all $\|x_1\|_\infty \leq \delta$ and $\|x_2\|_\infty \leq \delta$ uniformly in $t \geq 0$.

Assumption 3 (Semiglobal uniform boundedness of partial derivatives) *For any $\delta > 0$, there exist $d_{f_x}(\delta) > 0$, and $d_{f_t}(\delta) > 0$ such that for any $\|x\|_\infty \leq \delta$, the partial derivatives of $f(t,x)$ are piece-wise continuous and bounded*

$$\left\|\frac{\partial f(t,x)}{\partial x}\right\|_\infty \leq d_{f_x}(\delta), \quad \left\|\frac{\partial f(t,x)}{\partial t}\right\|_\infty \leq d_{f_t}(\delta). \tag{3.12}$$

The control objective is to design a state feedback controller $u(t)$ to ensure that the system state $x(t)$ tracks the desired model state $x_m(t)$ in the presence of system uncertainties Λ and $K_0(t, x_p(t))$. Next we present the $\mathcal{L}_1$ adaptive controller that achieves this objective without the need for any retuning.

3.2 $\mathcal{L}_1$ Adaptive Control

Consider the following control law

$$u(t) = u_L(t) + u_{ad}(t), \tag{3.13}$$

where $u_L(t)$ is the component of the baseline linear controller, and $u_{ad}(t)$ is the adaptive increment. The baseline controller is defined in (3.5), which is repeated here:

$$u_L(t) = K_x^\top x(t) + K_z^\top z_c(t)\,, \tag{3.14}$$

where K_x and K_z denote the $(n \times m)$ and $(q \times m)$ nominal feedback and feedforward gain matrices, correspondingly. Using these stabilizing gains for the system in (3.6), it takes the form:

$$\dot{x}(t) = (A + B_1 \Lambda K_x^T)x(t) + B_1\Lambda(u_{ad} + K_0(t, x_p(t))) + (B_2 + B_1\Lambda K_z^T)z_c(t)\,. \tag{3.15}$$

From (3.8) and (3.15), we have

$$\dot{x}(t) \;=\; A_m x(t) + B_m z_c(t) + B_1\Big(\Lambda u_{ad}(t) + \Lambda K_0(t, x_p(t)) + k_x^\top x(t) + k_z^\top z_c(t)\Big)\,, \tag{3.16}$$

where

$$k_x^\top = (\Lambda - \mathbb{I})K_x^\top, \quad k_z^\top = (\Lambda - \mathbb{I})K_z^\top . \tag{3.17}$$

Remark 2 *In the absence of actuator failures, i.e. when* $\Lambda = \mathbb{I}_m$*, there is* $k_x(t) = 0_{n\times m}$ *and* $k_z(t) = 0_{q\times m}$*. This implies that the adaptive system augments the baseline inner-loop controller, and therefore the* incremental *adaptive feedback gains can be initialized at zero.*

The design of $\mathcal{L}_1$ adaptive controller involves a diagonal transfer function matrix $D(s)$ with strictly proper transfer function elements and a positive diagonal feedback gain matrix $k \in \mathbb{R}^{m\times m}$

$$D(s) = \begin{bmatrix} D_1(s) & 0 & 0 & \cdots & 0 \\ 0 & D_2(s) & 0 & \cdots & 0 \\ 0 & 0 & \ddots & \cdots & 0 \\ \vdots & \vdots & \vdots & \ddots & \vdots \\ 0 & 0 & 0 & \cdots & D_m(s) \end{bmatrix} \tag{3.18}$$

$$k = \begin{bmatrix} k_1 & 0 & 0 & \cdots & 0 \\ 0 & k_2 & 0 & \cdots & 0 \\ 0 & 0 & \ddots & \cdots & 0 \\ \vdots & \vdots & \vdots & \ddots & \vdots \\ 0 & 0 & 0 & \cdots & k_m \end{bmatrix}. \tag{3.19}$$

Furthermore, $D(s)$ and k lead to a strictly proper stable matrix transfer function

$$\begin{aligned} C(s) &= \begin{bmatrix} C_1(s) & 0 & 0 & \cdots & 0 \\ 0 & C_2(s) & 0 & \cdots & 0 \\ 0 & 0 & \ddots & \cdots & 0 \\ \vdots & \vdots & \vdots & \ddots & \vdots \\ 0 & 0 & 0 & \cdots & C_m(s) \end{bmatrix}, \\ C_i(s) &= \frac{\Lambda_i k_i D_i(s)}{1 + \Lambda_i k_i D(s)}, \quad i = 1, 2, \cdots, m \end{aligned} \tag{3.20}$$

with low-pass gain $C_i(0) = 1$ for all i. One simple choice is

$$D_i(s) = \frac{1}{s}\,, \tag{3.21}$$

which yields a first order strictly proper $C(s)$ in the following form

$$C(s) = \begin{bmatrix} \frac{\Lambda_1 k_1}{s+\Lambda_1 k_1} & 0 & 0 & \cdots & 0 \\ 0 & \frac{\Lambda_2 k_2}{s+\Lambda_2 k_2} & 0 & \cdots & 0 \\ 0 & 0 & \ddots & \cdots & 0 \\ \vdots & \vdots & \vdots & \cdots & \vdots \\ 0 & 0 & 0 & \cdots & \frac{\Lambda_m k_m}{s+\Lambda_m k_m} \end{bmatrix}. \tag{3.22}$$

Further, let

$$\begin{aligned} L_x &= \max\{|\Lambda_l - 1|, |\Lambda_u - 1|\}\|K_x^\top\|_{\mathcal{L}_1} = \max\{|\Lambda_l - 1|, |\Lambda_u - 1|\} \max_{i=1,2,\cdots,m} (\sum_{j=1}^{n} |K_{x_{ji}}|)\,, \\ L_z &= \max\{|\Lambda_l - 1|, |\Lambda_u - 1|\}\|K_z^\top\|_{\mathcal{L}_1} = \max\{|\Lambda_l - 1|, |\Lambda_u - 1|\} \max_{i=1,2,\cdots,m} (\sum_{j=1}^{n} |K_{z_{ji}}|)\,, \end{aligned}$$

where $K_{x_{ji}}(t)$ are the j^{th} row i^{th} column element of K_x. The $\mathcal{L}_1$-norm upper bound that ensures stability of the entire system and desired transient performance is stated [10], which we repeat here.

Let

$$H(s) = (s\mathbb{I} - A_m)^{-1}B_1\,, \tag{3.23}$$

$$H_m(s) = (s\mathbb{I} - A_m)^{-1}B_m, \tag{3.24}$$

and $r_0(t)$ be the signal with its Laplace transformation $(s\mathbb{I} - A_m)^{-1}x_0$. Since A_m is Hurwitz and x_0 is finite, $\|r_0\|_{\mathcal{L}_\infty}$ is finite.

$\mathcal{L}_1$-norm upper bound: The choice of $D(s)$ and k needs to ensure that there exists ρ_r such that:

$$\|G(s)\|_{\mathcal{L}_1} < \frac{\left(\rho_r - (\|G(s)\|_{\mathcal{L}_1} L_z + \|H_m(s)\|_{\mathcal{L}_1})\,\|z_c\|_{\mathcal{L}_\infty} - \|r_0\|_{\mathcal{L}_\infty}\right)}{(\rho_r L_{\rho_r} + \rho_r L_x + B)}\,, \tag{3.25}$$

where

$$G(s) = H(s)(\mathbb{I}_{m\times m} - C(s))\,.$$

Remark 3 *Notice that the $\mathcal{L}_1$-norm upper bound in (3.25) is a consequence of the* semiglobal *Lipschitz property of $f(t,x)$, stated in Assumption 1. If $f(t,x)$ is globally Lipschitz with uniform Lipschitz constant L_g, then*

$$\begin{aligned}&\lim_{\rho_r\to\infty}\Big(\rho_r - (\|G(s)\|_{\mathcal{L}_1}L_z + \|H_m(s)\|_{\mathcal{L}_1})\,\|z_c\|_{\mathcal{L}_\infty} - \|r_0\|_{\mathcal{L}_\infty}\Big)/(\rho_r L_g + \rho_r L_x + B)\\ &= \frac{1}{L_g + L_x} = \frac{1}{L}\,,\end{aligned}$$

where $L = L_g + L_x$, and the $\mathcal{L}_1$-norm upper bound in (3.25) degenerates into

$$\|G(s)\|_{\mathcal{L}_1} < 1/L\,,$$

which is the same as the one derived in [3] for systems with constant unknown parameters. Notice that (3.25) is a sufficient condition for stability.

The elements of $\mathcal{L}_1$ adaptive controller are introduced next:

State Predictor: For derivation of the adaptive laws we have the following state predictor:

$$\begin{aligned}\dot{\hat{x}}(t) &= A_m\hat{x}(t) + B_m z_c(t) + B_1\Big(\hat{\Lambda}(t)u_{ad}(t) + \hat{\theta}^\top(t)\|x(t)\|_\infty + \hat{\sigma}^\top(t) + \hat{k}_x^\top(t)x(t) + \hat{k}_z^\top(t)z_c(t)\Big)\\ \hat{y}(t) &= c^\top\hat{x}(t)\,,\quad \hat{x}(0) = x_0\,,\end{aligned}\tag{3.26}$$

where $\hat{\theta}(t)\in\mathbb{R}^{1\times m}$ and $\hat{\sigma}(t)\in\mathbb{R}^{1\times m}$.

Adaptive Laws: Adaptive estimates $\hat{\Lambda}(t), \hat{\theta}(t), \hat{\sigma}(t), \hat{k}_x(t), \hat{k}_z(t)$ are governed by the following adaptation laws:

$$\begin{aligned}\dot{\hat{\theta}}(t) &= \Gamma_\theta\text{Proj}(\hat{\theta}(t), -\|x(t)\|_\infty\tilde{x}^\top(t)PB_1),\ \hat{\theta}(0) = \hat{\theta}_0\\ \dot{\hat{\sigma}}(t) &= \Gamma_\sigma\text{Proj}(\hat{\sigma}(t), -\tilde{x}^\top(t)PB_1),\qquad \hat{\sigma}(0) = \hat{\sigma}_0\\ \dot{\hat{\Lambda}}(t) &= \Gamma_\Lambda\text{Proj}(\hat{\Lambda}(t), -u_{ad}(t)\tilde{x}^\top(t)PB_1),\ \hat{\Lambda}(0) = \hat{\Lambda}_0\\ \dot{\hat{k}}_x(t) &= \Gamma_{kx}\text{Proj}(\hat{k}_x(t), -x(t)\tilde{x}^\top(t)PB_1)\,,\ \hat{k}_x(0) = 0\\ \dot{\hat{k}}_z(t) &= \Gamma_{kz}\text{Proj}(\hat{k}_z(t), -z_c(t)\tilde{x}^\top(t)PB_1)\,,\ \hat{k}_z(0) = 0,\end{aligned}$$

where $\tilde{x}(t) = \hat{x}(t) - x(t)$, $\Gamma_\theta = \Gamma_c \mathbb{I}_{1\times 1}$, $\Gamma_\sigma = \Gamma_c \mathbb{I}_{1\times 1}$, $\Gamma_\Lambda = \Gamma_c \mathbb{I}_{m\times m}$, $\Gamma_{kx} = \Gamma_c \mathbb{I}_{n\times n}$, $\Gamma_{kz} = \Gamma_c \mathbb{I}_{q\times q}$ are the adaptation gain matrices, P is the solution of the algebraic equation $A_m^\top P + P A_m = -Q$, $Q > 0$, and the projection operator ensures that the adaptive estimates $\hat{\Lambda}(t)$, $\hat{\theta}(t)$, $\hat{\sigma}(t)$,$\hat{k}_x(t)$,$\hat{k}_z(t)$ remain inside the compact sets $[\Lambda_l,\ \Lambda_u]$, $[-\theta_b,\ \theta_b]$, $[-\sigma_b,\ \sigma_b]$, $[-L_x,\ L_x]$, $[-L_z,\ L_z]$ respectively, with θ_b, σ_b defined as follows

$$\theta_b = L_\rho, \qquad \sigma_b = B + \epsilon\,, \tag{3.27}$$

where ϵ is an arbitrary positive constant and

$$\rho \;=\; \rho_r + \beta\,, \tag{3.28}$$

with β being an arbitrary positive constant as well.

Control Law: The control signal is generated through gain feedback of the following system:

$$\chi(s) \;=\; D(s)\bar{r}(s)\,, \quad u_{ad}(s) = -k\chi(s)\,, \tag{3.29}$$

where $\bar{r}(s)$ is the Laplace transformation of

$$\bar{r}(t) = \hat{\Lambda}(t)u_{ad}(t) + \hat{\theta}^\top(t)\|x(t)\|_\infty + \hat{\sigma}^\top(t) + \hat{k}_x^\top(t)x(t) + \hat{k}_z^\top(t)z_c(t). \tag{3.30}$$

The complete $\mathcal{L}_1$ adaptive controller consists of (3.26), (3.27) and (3.29) subject to the $\mathcal{L}_1$-norm supper bound in (3.25).

3.3 Analysis of $\mathcal{L}_1$ Adaptive Controller

3.3.1 Reference System

The following closed-loop reference system is considered, with its control signal and system response being defined as follows:

$$\begin{aligned} \dot{x}_{ref}(t) &= A_m x_{ref}(t) + B_m z_c(t) + \\ &\quad B_1\Big(f(t, x_{ref}(t)) + \Lambda u_{ref}(t) + k_x^\top x_{ref} + k_z^\top z_c(t)\Big) \qquad (3.31) \\ u_{ref}(s) &= -\Lambda^{-1} C(s)\bar{r}_{ref}(s) \qquad (3.32) \\ y_{ref}(t) &= c^\top x_{ref}(t)\,, \quad x_{ref}(0) = x_0\,, \qquad (3.33) \end{aligned}$$

where $\bar{r}_{ref}(s)$ is the Laplace transformation of the signal $\bar{r}_{ref}(t) = f(t, x_{ref}(t)) + k_x^\top x_{ref}(t) + k_z^\top z_c(t)$. The next lemma establishes the stability of the closed-loop system in (3.31)-(3.33).

Lemma 10 *For the closed-loop reference system in (3.31)-(3.33) subject to the $\mathcal{L}_1$-norm upper bound in (3.25), we have*

$$\begin{aligned} \|x_{ref}\|_{\mathcal{L}_\infty} &< \rho_r\,, \qquad (3.34) \\ \|u_{ref}\|_{\mathcal{L}_\infty} &< \rho_{u_r}\,, \qquad (3.35) \end{aligned}$$

where ρ_r is defined in (3.25) and

$$\rho_{u_r} = \|\Lambda^{-1}C(s)\|_{\mathcal{L}_1}(L_{\rho_r}\rho_r + L_x\rho_r + B + L_z\|z_c\|_{\mathcal{L}_\infty}).$$

The proof is similar to that of [10] and is therefore omitted.

3.3.2 Equivalent Linear Time-Varying System

In this section it is demonstrated that the nonlinear system in (3.16) can be transformed into a linear system with unknown time varying parameters. Several notations need to be

introduced first. Choose γ_0 to satisfy

$$\gamma_1 \triangleq \frac{\|C(s)\|_{\mathcal{L}_1}}{1-\|G(s)\|_{\mathcal{L}_1}(L_\rho+L_x)}\gamma_0+\beta_1<\beta\,, \tag{3.36}$$

where $0<\beta_1<\beta$ is an arbitrary positive constant. Notice that γ_0 can be arbitrarily small since β and β_1 can be set arbitrarily. It will be proved that by increasing the adaptive gain, γ_0 can serve as an upper bound for the prediction error signal $\tilde{x}(t)$. Define

$$\begin{aligned} B_r &\triangleq \begin{bmatrix} B_1 & \bar{B}_1 \end{bmatrix}, \\ H_r(s) &\triangleq (s\mathbb{I}-A_m)^{-1}B_r\,, \\ C_r(s) &\triangleq \begin{bmatrix} \Lambda^{-1}C(s) & 0 \\ 0 & \bar{C}(s) \end{bmatrix}, \end{aligned} \tag{3.37}$$

where the choice of $\bar{B}_1$ renders $B_r \in \mathbb{R}^{n\times n}$ full rank, and $\bar{C}(s)$ is an arbitrary diagonal strictly proper stable transfer function that yields a $C_r(s)\in\mathbb{R}^{n\times n}$ of appropriate dimension. Further, let

$$\rho_u = \rho_{u_r}+\gamma_2\,, \tag{3.38}$$

$$\gamma_2 = \left\|\Lambda^{-1}C(s)\right\|_{\mathcal{L}_1}(L_\rho+L_x)\gamma_1+\|C_r(s)H_r^{-1}(s)\|_{\mathcal{L}_1}\gamma_0\,. \tag{3.39}$$

It will be shown that the scalar function $f_i(t,x)$, $i=1,\cdots,m$ is equal to a linear structure $\theta_i(t)\|x(t)\|_\infty+\sigma_i(t)$. Hence, the vector of function $f(t,x)$ will be equal to $\theta(t)^\top\|x(t)\|_\infty+\sigma^\top(t)$, where $\theta(t)=[\theta_1(t),\theta_2(t),\cdots,\theta_m(t)]$, $\sigma(t)=[\sigma_1(t),\sigma_2(t),\cdots,\sigma_m(t)]$.

Lemma 11 *If*

$$\|x_t\|_{\mathcal{L}_\infty} \leq \rho\,, \tag{3.40}$$

$$\|u_t\|_{\mathcal{L}_\infty} \leq \rho_u\,, \tag{3.41}$$

where $\|(\cdot)_t\|_{\mathcal{L}_\infty}$ denotes the truncated $\mathcal{L}_\infty$ norm, there exist differentiable $\theta(\tau)$ and $\sigma(\tau)$ with bounded $\dot{\theta}(\tau)$ and $\dot{\sigma}(t)$ over $\tau\in[0,\ t]$ such that

$$\|\theta(\tau)\|_\infty < \theta_b\,, \tag{3.42}$$

$$\|\sigma(\tau)\|_\infty < \sigma_b\,, \tag{3.43}$$

$$f_i(\tau,x(\tau)) = \theta_i(\tau)\|x(\tau)\|_\infty+\sigma_i(\tau) \quad i=1,\cdots,m. \tag{3.44}$$

The proof is similar to that of [10] and is therefore omitted.

Since

$$\|x_0\|_\infty \leq \rho_r \leq \rho\,, \quad u(0) = 0\,, \tag{3.45}$$

and $x(t)$, $u(t)$ are continuous, there always exists t such that

$$\|x_t\|_{\mathcal{L}_\infty} \leq \rho\,, \quad \|u_t\|_{\mathcal{L}_\infty} \leq \rho_u\,. \tag{3.46}$$

It follows from (3.46) and Lemma 11 that the system in (3.16) can be rewritten over $[0, t]$ as:

$$\begin{aligned} \dot{x}(\tau) &= A_m x(\tau) + B_m z_c(\tau) + B_1\left(\theta^\top(\tau)\|x(\tau)\|_\infty + \Lambda u_{ad}(\tau) + \sigma^\top(\tau) + k_x^\top x(\tau) + k_z^\top z_c(\tau)\right)\,, \\ y(\tau) &= c^\top x(\tau), \quad x(0) = x_0\,, \end{aligned} \tag{3.47}$$

where $\theta(\tau)$, $\sigma(\tau)$ are unknown time-varying signals subject to:

$$\|\theta(\tau)\|_\infty < \theta_b\,, \quad \|\sigma(\tau)\|_\infty < \sigma_b\,, \quad \forall\ \tau \in [0, t]\,. \tag{3.48}$$

$$\|\dot{\theta}(\tau)\|_\infty \leq d_\theta(\rho, \rho_u)\,, \quad \|\dot{\sigma}(\tau)\|_\infty \leq d_\sigma(\rho, \rho_u)\,, \quad \forall\ \tau \in [0, t]. \tag{3.49}$$

3.3.3 Transient and Steady-State Performance

Before the main theorem, we prove the following lemma.

Lemma 12 *For the system in (3.16) and the $\mathcal{L}_1$ adaptive controller in (3.26), (3.27) and (3.29), if*

$$\|x_t\|_{\mathcal{L}_\infty} \leq \rho\,, \quad \|u_t\|_{\mathcal{L}_\infty} \leq \rho_u\,, \tag{3.50}$$

then

$$\|\tilde{x}_t\|_{\mathcal{L}_\infty} \leq \sqrt{\frac{\theta_m(\rho, \rho_u)}{\lambda_{\min}(P)\Gamma_c}}\,, \tag{3.51}$$

where

$$\begin{aligned} \theta_m(\rho, \rho_u) \triangleq\ & 4m^2\theta_b^2 + 4m^2\sigma_b^2 + m^2\left(\Lambda_u - \Lambda_l\right)^2 + 4m^2 L_x^2 + 4m^2 L_z^2 \\ & + 4\frac{\lambda_{\max}(P)}{\lambda_{\min}(Q)}\left(\theta_b d_\theta(\rho, \rho_u) + \sigma_b d_\sigma(\rho, \rho_u)\right)\,. \end{aligned} \tag{3.52}$$

Proof: It follows from (3.49) and (3.50) that

$$|\dot{\theta}(\tau)| \leq d_\theta(\rho, \rho_u)\,, \quad |\dot{\sigma}(\tau)| \leq d_\sigma(\rho, \rho_u) \tag{3.53}$$

for any $\tau \in [0, t]$. Consider the following Lyapunov function candidate:

$$\begin{aligned} & V(\tilde{x}(\tau), \tilde{\Lambda}(\tau), \tilde{\theta}(\tau), \tilde{\sigma}(\tau)) \\ = \;& \tilde{x}^\top(\tau) P \tilde{x}(\tau) + \text{trace}(\tilde{\Lambda}^\top(\tau)\Gamma_\Lambda^{-1}\tilde{\Lambda}(\tau)) + \text{trace}(\tilde{\theta}^\top(\tau)\Gamma_\theta^{-1}\tilde{\theta}(\tau)) + \\ & \text{trace}(\tilde{\sigma}^\top(\tau)\Gamma_\sigma^{-1}\tilde{\sigma}(\tau)) + \text{trace}(\tilde{k_x}^\top(\tau)\Gamma_{kx}^{-1}\tilde{k_x}(\tau)) + \text{trace}(\tilde{k_z}^\top(\tau)\Gamma_{kz}^{-1}\tilde{k_z}(\tau))\,, \end{aligned} \tag{3.54}$$

where

$$\begin{aligned} \tilde{\Lambda}(\tau) \triangleq \hat{\Lambda}(\tau) - \Lambda, \tilde{\theta}(\tau) \triangleq \hat{\theta}(\tau) - \theta(\tau), \tilde{\sigma}(\tau) \triangleq \hat{\sigma}(\tau) - \sigma(\tau), \\ \tilde{k}_x(\tau) \triangleq \hat{k}_x(\tau) - k_x, \tilde{k}_z(\tau) \triangleq \hat{k}_z(\tau) - k_z. \end{aligned} \tag{3.55}$$

It follows from (3.26) and (3.47) that over $[0, t]$

$$\dot{\tilde{x}}(\tau) = A_m\tilde{x}(\tau) + B_1\left(\tilde{\Lambda}(\tau)u(\tau) + \tilde{\theta}^\top(\tau)\|x(\tau)\|_\infty + \tilde{\sigma}(\tau) + \tilde{k}_x^\top(\tau)x(\tau) + \tilde{k}_z^\top(\tau)z_c(\tau)\right), \tag{3.56}$$

where $\tilde{x}(0) = 0$. We can verify straightforwardly that

$$V(0) \leq \frac{\left(m^2(\Lambda_u - \Lambda_l)^2 + 4m^2\theta_b^2 + 4m^2\sigma_b^2 + 4m^2L_x^2 + 4m^2L_z^2\right)}{\Gamma_c} \leq \frac{\theta_m(\rho, \rho_u)}{\Gamma_c}\,.$$

Let $t_1 \in (0, t]$ be the first time-instant of the discontinuity of either of the derivatives of $\dot{\hat{\theta}}(t)$, $\dot{\hat{\sigma}}(t)$, $\dot{\theta}(t)$, $\dot{\sigma}(t)$.

The projection algorithm ensures that for all $\tau \in [0, t_1)$

$$\Lambda_l \leq \hat{\Lambda}(t) \leq \Lambda_u\,, \quad |\hat{\theta}(\tau)| \leq \theta_b, \quad |\hat{\sigma}(\tau)| \leq \sigma_b\,, |\hat{k}_x| \leq L_x\,, |\hat{k}_z| \leq L_z, \tag{3.57}$$

and therefore

$$\begin{aligned} & \max_{\tau\in[0,t_1)} \Big(\text{trace}(\tilde{\Lambda}^\top(\tau)\Gamma_\Lambda^{-1}\tilde{\Lambda}(\tau)) + \text{trace}(\tilde{\theta}^\top(\tau)\Gamma_\theta^{-1}\tilde{\theta}(\tau)) + \\ & \text{trace}(\tilde{\sigma}^\top(\tau)\Gamma_\sigma^{-1}\tilde{\sigma}(\tau)) + \text{trace}(\tilde{k_x}^\top(\tau)\Gamma_{kx}^{-1}\tilde{k_x}(\tau)) + \text{trace}(\tilde{k_z}^\top(\tau)\Gamma_{kz}^{-1}\tilde{k_z}(\tau))\Big) \\ & \leq \left(m^2(\Lambda_u - \Lambda_l)^2 + 4m^2\theta_b^2 + 4m^2\sigma_b^2 + 4m^2L_x^2 + 4m^2L_z^2\right)/\Gamma_c \end{aligned} \tag{3.58}$$

for any $\tau \in [0, t_1)$.

In what follows, we need to prove that

$$V(\tau) \leq \frac{\theta_m(\rho, \rho_u)}{\Gamma_c}, \quad \forall\, \tau \in [0, t]\,. \tag{3.59}$$

Using the projection based adaptation laws from (3.27), the following upper bound for $\dot{V}(\tau)$ can be obtained:

$$\dot{V}(\tau) \leq -\tilde{x}^\top(\tau) Q \tilde{x}(\tau) + 2\Gamma_c^{-1} \left| \tilde{\theta}(\tau)\dot{\theta}(\tau) + \tilde{\sigma}(\tau)\dot{\sigma}(\tau) \right| \tag{3.60}$$

for any $\tau \in [0, t_1)$. The projection algorithm ensures that for all $\tau \in [0, t_1)$

$$\Lambda_l \leq \hat{\Lambda}(t) \leq \Lambda_u\,, \quad |\hat{\theta}(\tau)| \leq \theta_b, \quad |\hat{\sigma}(\tau)| \leq \sigma_b\,, \tag{3.61}$$

and therefore

$$\begin{aligned}
&\max_{\tau \in [0, t_1)} \Big(\mathrm{trace}(\tilde{\Lambda}^\top(\tau)\Gamma_\Lambda^{-1}\tilde{\Lambda}(\tau)) + \mathrm{trace}(\tilde{\theta}^\top(\tau)\Gamma_\theta^{-1}\tilde{\theta}(\tau)) + \\
&\mathrm{trace}(\tilde{\sigma}^\top(\tau)\Gamma_\sigma^{-1}\tilde{\sigma}(\tau)) + \mathrm{trace}(\tilde{k_x}^\top(\tau)\Gamma_{kx}^{-1}\tilde{k_x}(\tau)) + \mathrm{trace}(\tilde{k_z}^\top(\tau)\Gamma_{kz}^{-1}\tilde{k_z}(\tau)) \Big) \\
&\leq \left(m^2(\Lambda_u - \Lambda_l)^2 + 4m^2\theta_b^2 + 4m^2\sigma_b^2 + 4m^2 L_x^2 + 4m^2 L_z^2 \right) / \Gamma_c
\end{aligned} \tag{3.62}$$

for any $\tau \in [0, t_1)$. If at any $\tau \in [0, t_1)$

$$V(\tau) \geq \frac{\theta_m(\rho, \rho_u)}{\Gamma_c}\,, \tag{3.63}$$

where $\theta_m(\rho, \rho_u)$ is defined in (3.52), then it follows from (3.62) that

$$\tilde{x}^\top(\tau) P \tilde{x}(\tau) \geq \frac{4\lambda_{\max}(P)}{\Gamma_c \lambda_{\min}(Q)} \left(\theta_b d_\theta(\rho, \rho_u) + \sigma_b d_\sigma(\rho, \rho_u) \right), \tag{3.64}$$

and hence

$$\tilde{x}^\top(\tau) Q \tilde{x}(\tau) \geq \frac{\lambda_{\min}(Q)}{\lambda_{\max}(P)} \tilde{x}^\top(\tau) P \tilde{x}(\tau) \geq 4 \frac{\theta_b d_\theta(\rho, \rho_u) + \sigma_b d_\sigma(\rho, \rho_u)}{\Gamma_c}\,. \tag{3.65}$$

It follows from (3.42), (3.43) and (3.61) that

$$|\tilde{\theta}(\tau)| \leq 2\theta_b, \quad |\tilde{\sigma}(\tau)| \leq 2\sigma_b \tag{3.66}$$

for all $\tau \in [0, t_1)$. Since $\dot{\theta}(\tau)$ and $\dot{\sigma}(\tau)$ are continuous over $[0, t_1)$, the upper bounds in (3.53) and (3.66) lead to the following upper bound:

$$\frac{|\tilde{\theta}(\tau)\dot{\theta}(\tau) + \tilde{\sigma}(\tau)\dot{\sigma}(\tau)|}{\Gamma_c} \leq 2\frac{\theta_b d_\theta(\rho, \rho_u) + \sigma_b d_\sigma(\rho, \rho_u)}{\Gamma_c}\,. \tag{3.67}$$

Hence, if $V(\tau) \geq \dfrac{\theta_m(\rho, \rho_u)}{\Gamma_c}$, then from (3.60) and (3.65) we have

$$\dot{V}(\tau) \leq 0\,. \tag{3.68}$$

It follows from (3.68) that $V(\tau) \leq \dfrac{\theta_m(\rho, \rho_u)}{\Gamma_c}$ for any $\tau \in [0, t_1)$.

Since $\lambda_{\min}(P)\|\tilde{x}(\tau)\|^2 \leq \tilde{x}^\top(\tau)P\tilde{x}(\tau) \leq V(\tau)$, then for any $\tau \in [0, t_1)$

$$||\tilde{x}(\tau)||^2 \leq \frac{\theta_m(\rho, \rho_u)}{\lambda_{\min}(P)\Gamma_c}\,.$$

Since $V(\tau)$ is continuous, we further have

$$\|\tilde{x}(\tau)\|_\infty \leq \sqrt{\frac{\theta_m(\rho, \rho_u)}{\lambda_{\min}(P)\Gamma_c}}\,, \quad \tau \in [0, t_1]\,. \tag{3.69}$$

Given $t_1 \in [0, t]$ such that

$$V(t_1) \leq \frac{\theta_m(\rho, \rho_u)}{\Gamma_c}\,,$$

let $t_2 \in (t_1, t]$ be the next time-instant such that discontinuity of any of the derivatives $\dot{\hat{\theta}}(t)$, $\dot{\hat{\sigma}}(t)$, $\dot{\theta}(t)$, and $\dot{\sigma}(t)$ occurs. Using similar derivations as above, we can prove that

$$\|\tilde{x}(\tau)\|_\infty \leq \sqrt{\frac{\theta_m(\rho, \rho_u)}{\lambda_{\min}(P)\Gamma_c}}\,, \quad \tau \in [t_1, t_2]\,. \tag{3.70}$$

Iterating the process until the time instant t, we get

$$\|\tilde{x}_t\|_{\mathcal{L}_\infty} \leq \sqrt{\frac{\theta_m(\rho, \rho_u)}{\lambda_{\min}(P)\Gamma_c}}, \tag{3.71}$$

which concludes the proof. □

Theorem 2 *Consider the reference system in (3.31)-(3.33) and the closed-loop $\mathcal{L}_1$ adaptive controller in (3.16), (3.26), (3.27), (3.29) subject to (3.25). If the adaptive gain is chosen to verify the lower bound:*

$$\Gamma_c > \frac{\theta_m(\rho, \rho_u)}{\lambda_{\min}(P)\gamma_0^2}\,, \tag{3.72}$$

where

$$\begin{aligned}\theta_m(\rho, \rho_u) \triangleq\ & 4m^2\theta_b^2 + 4m^2\sigma_b^2 + m^2\left(\Lambda_u - \Lambda_l\right)^2 + 4m^2L_x^2 + 4m^2L_z^2 \\ & + 4\frac{\lambda_{\max}(P)}{\lambda_{\min}(Q)}\left(\theta_b d_\theta(\rho, \rho_u) + \sigma_b d_\sigma(\rho, \rho_u)\right)\,,\end{aligned} \tag{3.73}$$

we have:

$$\|\tilde{x}\|_{\mathcal{L}_\infty} \leq \gamma_0\,, \tag{3.74}$$

$$\|x - x_{ref}\|_{\mathcal{L}_\infty} < \gamma_1\,, \tag{3.75}$$

$$\|u - u_{ref}\|_{\mathcal{L}_\infty} < \gamma_2\,, \tag{3.76}$$

where γ_1 and γ_2 are defined in (3.36) and (3.39).

Proof: The proof is done by contradiction. Assume that (3.75)-(3.76) are not true. Then, since $\|x(0) - x_{ref}(0)\|_\infty = 0 \leq \gamma_1$, $u(0) - u_{ref}(0) = 0$, and $x(\tau)$, $x_{ref}(\tau)$, $u(\tau)$, $u_{ref}(\tau)$ are continuous, there exists $t \geq 0$ such that

$$\begin{aligned}\|x(t) - x_{ref}(t)\|_\infty &= \gamma_1\,, \text{ or} \\ \|u(t) - u_{ref}(t)\|_\infty &= \gamma_2\,,\end{aligned} \tag{3.77}$$

while

$$\|(x - x_{ref})_t\|_{\mathcal{L}_\infty} \leq \gamma_1,\ \|(u - u_{ref})_t\|_{\mathcal{L}_\infty} \leq \gamma_2\,. \tag{3.78}$$

Taking into consideration the relationships in (3.28),(3.36), (3.38) and (3.78), it follows from Lemma 10 that

$$\|x_t\|_{\mathcal{L}_\infty} \leq \rho\,, \quad \|u_t\|_{\mathcal{L}_\infty} \leq \rho_u\,. \tag{3.79}$$

Hence, it follows from (3.72), (3.79), and Lemma 12 that

$$\|\tilde{x}_t\|_{\mathcal{L}_\infty} \leq \gamma_0\,. \tag{3.80}$$

Let $\tilde{r}(\tau) = \tilde{\Lambda}(\tau)u(\tau)+\tilde{\theta}(\tau)\|x(\tau)\|_\infty+\tilde{\sigma}(\tau)+\tilde{k}_x(\tau)x(\tau)+\tilde{k}_z(\tau)z_c(\tau)$, $r_2(\tau) = \theta^\top(\tau)\|x(\tau)\|_\infty+\sigma(\tau)+k_x x(\tau)+k_z z_c(\tau)$. It follows from (3.29) that $\chi(s) = D(s)(\Lambda u(s)+r_2(s)+\tilde{r}(s))$, where $\tilde{r}(s)$ and $r_2(s)$ are the Laplace transformations of signals $\tilde{r}(\tau)$ and $r_2(\tau)$. Consequently

$$\begin{aligned}\chi(s) &= \frac{D(s)}{1+k\Lambda D(s)}(r_2(s)+\tilde{r}(s)),\\ u(s) &= -\frac{kD(s)}{1+k\Lambda D(s)}(r_2(s)+\tilde{r}(s)).\end{aligned} \tag{3.81}$$

Using the definition of $C(s)$ from (3.20), we can write

$$\Lambda u(s) = -C(s)(r_2(s)+\tilde{r}(s)), \tag{3.82}$$

and the system in (3.16) consequently takes the form:

$$x(s) = H(s)\Big((1-C(s))r_2(s) - C(s)\tilde{r}(s)\Big) + (s\mathbb{I}-A_m)^{-1}x_0. \tag{3.83}$$

It follows from (3.31)-(3.32) that $x_{ref}(s) = H(s)(1-C(s))\bar{r}_{ref}(s) + (s\mathbb{I}-A_m)^{-1}x_0$. Let $e(\tau) = x(\tau) - x_{ref}(\tau)$. Then using (3.83) one gets

$$e(s) = H(s)\left((1-C(s))r_3(s) - C(s)\tilde{r}(s)\right), \quad e(0) = 0, \tag{3.84}$$

where $r_3(s)$ is the Laplace transformation of the signal

$$r_3(\tau) = r_2(\tau) - \bar{r}_{ref}(\tau). \tag{3.85}$$

Lemma 12 gives the following upper bound:

$$\|e_t\|_{\mathcal{L}_\infty} \le \|H(s)(1-C(s))\|_{\mathcal{L}_1}\|r_{3_t}\|_{\mathcal{L}_\infty} + \|r_{4_t}\|_{\mathcal{L}_\infty}, \tag{3.86}$$

where $r_4(\tau)$ is the signal with its Laplace transformation being $r_4(s) = C(s)H(s)\tilde{r}(s)$. From the relationship in (3.56) we have $\tilde{x}(s) = H(s)\tilde{r}(s)$, which leads to $r_4(s) = C(s)\tilde{x}(s)$, and hence $\|r_{4_t}\|_{\mathcal{L}_\infty} \le \|C(s)\|_{\mathcal{L}_1}\|\tilde{x}_t\|_{\mathcal{L}_\infty}$.

Since

$$r_3(\tau) = f(\tau,x) - f(\tau,x_{ref}) + k_x\Big(x(\tau) - x_{ref}(\tau)\Big),$$

it follows that

$$\|r_{3_t}\|_{\mathcal{L}_\infty} \leq \|(f(\tau,x) - f(\tau,x_{ref}))_t\|_{\mathcal{L}_\infty} + \|k_x(x-x_{ref})_t\|_{\mathcal{L}_\infty}.$$

Since $\|x(\tau)\|_\infty \leq \rho$, $\|x_{ref}(\tau)\|_\infty \leq \rho$ for all $\tau \in [0,t]$, from Assumption 2 we have

$$\|f(\tau,x) - f(\tau,x_{ref})\|_\infty \;\; \leq \;\; L_\rho \|x - x_{ref}\|_\infty \tag{3.87}$$

for all $\tau \in [0,t]$. Hence,

$$\|r_{3_t}\|_{\mathcal{L}_\infty} \leq L_\rho \|(x-x_{ref})_t\|_{\mathcal{L}_\infty} + L_x \|(x-x_{ref})_t\|_{\mathcal{L}_\infty} \leq (L_\rho + L_x)\|e_t\|_{\mathcal{L}_\infty}$$

From (3.86) we have $\|e_t\|_{\mathcal{L}_\infty} \leq \|H(s)(1-C(s))\|_{\mathcal{L}_1}(L_\rho + L_x)\|e_t\|_{\mathcal{L}_\infty} + \|C(s)\|_{\mathcal{L}_1}\|\tilde{x}_t\|_{\mathcal{L}_\infty}$. Eq. (3.80) and the $\mathcal{L}_1$-norm upper bound from (3.25) lead to the following upper bound $\|e_t\|_{\mathcal{L}_\infty} \leq \frac{\|C(s)\|_{\mathcal{L}_1}}{1-\|H(s)(1-C(s))\|_{\mathcal{L}_1}(L_\rho+L_x)}\gamma_0$, which along with (3.36) leads to

$$\|e_t\|_{\mathcal{L}_\infty} \leq \gamma_1 - \beta_1 < \gamma_1\,. \tag{3.88}$$

We notice that from (3.32) and (3.82) one can derive $u(s) - u_{ref}(s) = -\Lambda^{-1}C(s)\Big(\theta^\top(\tau)(x(s) - x_{ref}(s)) + k_x(x(s) - x_{ref}(s))\Big) - r_5(s)$, where $r_5(s) = \Lambda^{-1}C(s)\tilde{r}(s)$. Therefore, it follows from Lemma 12 that

$$\|(u-u_{ref})_t\|_{\mathcal{L}_\infty} \leq (L_\rho + L_x)\|\Lambda^{-1}\|_{\mathcal{L}_1}\|C(s)\|_{\mathcal{L}_1}\|(x-x_{ref})_t\|_{\mathcal{L}_\infty} + \|r_{5_t}\|_{\mathcal{L}_\infty}\,. \tag{3.89}$$

Let

$$r_{5_e}(\tau) \;\triangleq\; [r_5^\top(\tau) \quad \mathbf{0}]^\top \tag{3.90}$$

$$\tilde{r}_e(\tau) \;\triangleq\; [\tilde{r}^\top(\tau) \quad \mathbf{0}]^\top \tag{3.91}$$

where $\mathbf{0}$ renders $r_{5_e}(\tau) \in \mathbb{R}^{m\times 1}$, $\tilde{r}_e(\tau) \in \mathbb{R}^{m\times 1}$. It is straightforward to show

$$r_{5_e}(s) = C_r(s)\tilde{r}_e(s),$$

while the definitions in (3.90) and (3.91) lead to

$$\|r_{5_e}\|_{\mathcal{L}_\infty} = \|r_5\|_{\mathcal{L}_\infty}, \quad \|\tilde{r}_e\|_{\mathcal{L}_\infty} = \|\tilde{r}\|_{\mathcal{L}_\infty}.$$

Recalling (3.37), (3.91) and that $\tilde{x}(s) = H(s)\tilde{r}(s)$, we have

$$\tilde{x}(s) = H_r(s)\tilde{r}_e(s),$$

which leads to

$$r_{5_e}(s) = C_r(s)H_r^{-1}(s)H_r(s)\tilde{r}_e(s) = C_r(s)H_r^{-1}(s)\tilde{x}(s).$$

The non-singularity of the matrix B_r implies that

$$C_r(s)H_r^{-1}(s) = C_r(s)B_r(s\mathbb{I} - A_m).$$

Since $C_r(s)$ is a diagonal matrix with all the elements strictly proper, it can be verified easily that $C_r(s)B_r(s\mathbb{I} - A_m)$ is proper and hence the $\mathcal{L}_1$ norm

$$\|C_r(s)H_r^{-1}(s)\|_{\mathcal{L}_1}$$

is finite. Hence,

$$\|r_{5_t}\|_{\mathcal{L}_\infty} = \|(r_{5_e})_t\|_{\mathcal{L}_\infty} \leq \|C_r(s)H_r^{-1}(s)\|_{\mathcal{L}_1}\|\tilde{x}_t\|_{\mathcal{L}_\infty}\,.$$

The upper bound in (3.80) leads to the following upper bound:

$$\|r_{5_t}\|_{\mathcal{L}_\infty} \leq \|C_r(s)H_r^{-1}(s)\|_{\mathcal{L}_1}\gamma_0\,. \tag{3.92}$$

It follows from (3.88), (3.89), and (3.92) and the definition of γ_2 in (3.39) that

$$\begin{aligned}\|(u - u_{ref})_t\|_{\mathcal{L}_\infty} &\leq (L_\rho + L_x)\|\Lambda^{-1}\|_{\mathcal{L}_1}\|C(s)\|_{\mathcal{L}_1}(\gamma_1 - \beta_1) + \|C_r(s)H_r^{-1}(s)\|_{\mathcal{L}_1}\gamma_0 \\ &< \gamma_2\,. \end{aligned} \tag{3.93}$$

We note that the upper bounds in (3.88) and (3.93) contradict the equality in (3.77), which proves (3.75)-(3.76). Eq. (3.74) follows from (3.75)-(3.76) and (3.80) directly. □

It follows from (3.72) that arbitrarily small γ_0 can be obtained by increasing the adaptive gain.

3.3.4 Time-Delay Margin

In the case, when the nonlinearity permits the following representation

$$f(t, x(t)) = \theta^\top x(t) + \sigma(t)\,,$$

where θ is a constant vector, the time-delay margin of $\mathcal{L}_1$ adaptive controller can be computed analytically [9]. The dynamics in (3.16) can be re-written as

$$\dot{x}(t) \;=\; A_m x(t) + B_m z_c(t) + B_1\Big(\Lambda u_{ad}(t) + \theta^\top x(t) + k_x^\top x(t) + \sigma(t) + k_z^\top z_c(t)\Big). \quad (3.94)$$

Define

$$\bar{H}(s) = (s\mathbb{I} - A_m - B_1\theta^\top - B_1 k_x^\top)^{-1} B_1.$$

Following the results in [9], when $\Gamma_c \to \infty$, the time-delay margin of the closed loop $\mathcal{L}_1$ adaptive control system has a conservative lower-bound, which is given by the time-delay margin of the following open-loop LTI system:

$$H_o(s) = \frac{C(s)}{1 - C(s)}\Big(1 + (\theta^\top + k_x^\top)\bar{H}(s)\Big)\,. \quad (3.95)$$

Since in this structure $C(s)$ is decoupled from $\bar{H}(s)$, it is obvious that one can choose $C(s)$ judiciously to maximize the phase-margin of the open-loop transfer function $H_o(s)$ and minimize its cross-over frequency to obtain larger time-delay margin. Although analytical derivation of the time-delay margin for multi-input multi-output systems with more general unknown nonlinear function $f(t, x(t))$ is not available[1], insights from this analysis can be used for the selection of $C(s)$ to tune the time-delay margin in the applications discussed in this dissertation.

[1]The fact that this analytical derivation is somewhat complicated, follows from the fact that for open-loop nonlinear systems there are no general results for computing the time-delay margin, as one has for linear systems, expressed via the phase margin and the crossover frequency.

3.3.5 Design Guidelines

Note that the control law $u_{ref}(t)$ in the closed-loop reference system, which is used in the analysis of $\mathcal{L}_\infty$ norm bounds, is not implementable since its definition involves the unknown parameters. Theorem 2 ensures that the $\mathcal{L}_1$ adaptive controller approximates $u_{ref}(t)$ both in transient and steady state. So, it is important to understand how these bounds can be used for ensuring uniform transient response with *desired* specifications. Notice that the following *ideal* control signal

$$u_{id}(t) = \Lambda^{-1}\Big(- f(t, x_{id}(t)) + k_x^\top x_{id}(t) + k_z^\top z_c(t)\Big) \tag{3.96}$$

is the one that leads to desired system response:

$$\dot{x}_{id}(t) = A_m x_{id}(t) + B_m z_c(t), \quad y_{id}(t) = c^\top x_{id}(t) \tag{3.97}$$

by canceling the uncertainties exactly. In the closed-loop reference system (3.31)-(3.33), $u_{id}(t)$ is further low-pass filtered by $C(s)$ to have guaranteed low-frequency range. Thus, the reference system in (3.31)-(3.33) has a different response as compared to (3.97) achieved with (3.96). The reader can refer to [3] for specific design guidelines on selection of $C(s)$ to ensure that the response of $x_{ref}(t)$ and $u_{ref}(t)$ can be made as close as possible to (3.97). Moreover, for systems linearly dependent upon unknown parameters, the (nonlinear) $\mathcal{L}_1$ adaptive controller has analytically computable time-delay margin [9]. The trade-off between the time-delay margin and the performance of the $\mathcal{L}_1$ adaptive controller depends solely upon the bandwidth of $C(s)$. Increasing the bandwidth of $C(s)$ leads to improved performance at the price of reduced time-delay margin. In [78], constrained optimization of the performance and/or the robustness of $\mathcal{L}_1$ adaptive controller is considered by resorting to appropriate Linear Matrix Inequality (LMI) type conditions. If the corresponding LMI has a solution, then arbitrary desired performance bound can be achieved, while retaining a prespecified lower-bound on the time-delay margin.

3.4 Flight Control Examples

3.4.1 Unmanned Combat Aerial Vehicle

The $\mathcal{L}_1$ adaptive controller is applied to a model of the aerodynamically unstable X-45A Unmanned Combat Aerial Vehicle (UCAV) in the presence of control effectiveness reduction and pitch break uncertainty (unknown nonlinear in Angle of Attack (AOA) pitching moment increment). This uncertainty is introduced in pitch dynamics in order to model unknown changes in the aircraft pitching moment that can drive the aircraft into an uncontrollable (in AOA) region.

Recall the aircraft dynamics from (3.7):

$$\begin{aligned} \dot{x}(t) &= Ax(t) + B_1\Lambda\left(u(t) + K_0(t, x_p(t))\right) + B_2 z_c(t)\,, \\ x(0) &= x_0 = 0\,, \end{aligned} \tag{3.98}$$

where $x(t) \in \mathbb{R}^9, u(t) \in \mathbb{R}^3$ (virtual control input), $z_c(t) \in \mathbb{R}^4$ are the measured system states, control signals and reference inputs, respectively, $A \in \mathbb{R}^{9\times 9}$, $B_2 \in \mathbb{R}^{9\times 4}$, $B_1 \in \mathbb{R}^{9\times 3}$ are known matrices where the three columns of B_1 are linearly independent,

$$\Lambda = \begin{bmatrix} \Lambda_1 & 0 & 0 \\ 0 & \Lambda_2 & 0 \\ 0 & 0 & \Lambda_3 \end{bmatrix} \tag{3.99}$$

is an unknown diagonal matrix with strictly positive diagonal elements. The state vector $x = (\alpha_p, \beta_p, p_p, q_p, r_p, q_I, p_I, r_I, r_w)^\top$ comprises five plant states (x_p), which include angle of attack α_p, angle of sideslip β_p, body roll rate p_p, body pitch rate q_p, body yaw rate r_p and four baseline controller (x_c) states, which include pitch, roll and yaw (q_I, p_I and r_I) integrator states and yaw rate washout filter signal r_w. The vector $z_c = (a_z^{cmd}, \beta^{cmd}, p^{cmd}, r^{cmd})^\top$ consists of four inner loop commands that include vertical acceleration, sideslip, roll rate and yaw rate, while $u(t)$ is the vector of virtual controls (roll, pitch and yaw control). Considering the control signal $u(t) = u_L(t) + u_{ad}(t)$, where $u_L(t)$ is defined in (3.5), the partially closed

loop system from (3.16) is repeated here:

$$\dot{x}(t) = A_m x(t) + B_m z_c(t) + B_1\Big(\Lambda u_{ad}(t) + \Lambda K_0(t, x_p(t)) + k_x^\top x(t) + k_z^\top z_c(t)\Big) \quad (3.100)$$

where the adaptive control signal $u_{ad}(t)$ is defined according to $\mathcal{L}_1$ adaptive controller (3.26), (3.27) and (3.29), subject to the $\mathcal{L}_1$-norm upper bound in (3.25). This is different from the approach, presented in [76], where RBF approximation was employed for approximation of the nonlinearity. This significantly reduces the design effort by eliminating the need for RBF distributions and centers/widths tuning.

Note that the vector-function $K_0(t, x_p)$ represents the matched unknown nonlinearities. In addition to unknown $K_0(t, x_p)$, Λ models the loss of control effectiveness caused by actuator failure(s), damage(s) or combinations of them. The matrix Λ models the uncertainties in virtual control $u(t)$, and is defined in a way that each diagonal element of Λ represents a scaling factor for control effectiveness in particular input channel. Thus, Λ is diagonal and is different from the control allocation matrix, which has already been incorporated in B_1 in (3.98). When some of the control surfaces fail or are damaged, the scaling factor for each virtual control will change. In simulations below it is assumed that the failure/damage situations will not cause change of sign in the diagonal elements of Λ. This may exclude certain types of actuator failures, for example, complete loss of controllability of some control surfaces. However, as shown in our simulations, control effectiveness reduction, even a small amount of reduction, can degrade the output performance significantly. The $\mathcal{L}_1$ adaptive controller is shown to recover the nominal performance in the presence of the uncertain control effectiveness subject to Assumption 1[2].

The inner-loop control objective is to design a full state-feedback controller $u_{ad}(t)$ for (3.100) such that all closed-loop signals remain bounded, and the system state tracks the state of a desired reference model in the presence of uncertainties and control effectiveness reduction.

[2]Note that in [76] a broader class of uncertainties has been considered, which violate Assumption 1, and the performance of $\mathcal{L}_1$ adaptive controller has been verified for that class of uncertainties as well. This was pursued for the purpose of comparison with the results from [55].

The performance of the nominal plant in the presence of pitch break and control effectiveness reduction is compared with the performance of the closed-loop system with $\mathcal{L}_1$ adaptive controller. For the $\mathcal{L}_1$ adaptive controller we set $k_i = 20$, where $i = 1, 2, 3$, and $D(s) = \frac{1}{s}$ which verifies the $\mathcal{L}_1$ norm upper bound, and we set $\Gamma_c = 100000$. The results are shown in Figures 3.1 and 3.2. For comparison purposes, simulation data are obtained from the following three closed-inner-loop systems: a) adaptation OFF, uncertainties OFF, b) adaptation OFF, uncertainties ON, c) $\mathcal{L}_1$ adaptation ON, uncertainties ON.

Figures 3.1-3.2 demonstrate the benefits of adaptation, when the control effectiveness reduction of each control surface occurs at 1 second and the pitch break phenomenon is active throughout the entire maneuver. The reduction up to (30%) of control effectiveness for each actuator channel causes changes the Λ matrix to the following:

$$\Lambda = \begin{bmatrix} 0.7 & 0 & 0 \\ 0 & 0.7 & 0 \\ 0 & 0 & 0.7 \end{bmatrix}.$$

Figure 3.1 indicates that in spite of the control effectiveness reduction and pitch break uncertainty, the $\mathcal{L}_1$ adaptive system is able to quickly reconfigure and track the commanded vertical acceleration, sideslip angle, roll rate, and yaw rate signals, simultaneously. In fact, Figure 3.1 shows that with the adaptation turned on the desired/nominal system tracking behavior has been recovered. In addition, Figure 3.2 compares the three virtual control feedback signals, and confirms that the level of control activity is reasonable. In Figure 3.3, the subplot of Figure 3.1 is re-plotted to show the perfect tracking achieved by $\mathcal{L}_1$ for vertical acceleration.

When the reference commands change, the system output and input have scaled responses similar to those of linear systems. These are shown in Figures 3.4, 3.5.

Next robustness of the scheme is discussed. The time-delay margin for the inner loop (without adaptive feedback) can be computed from the phase margin of the open loop transfer functions. The open loop transfer functions are calculated by breaking the virtual control

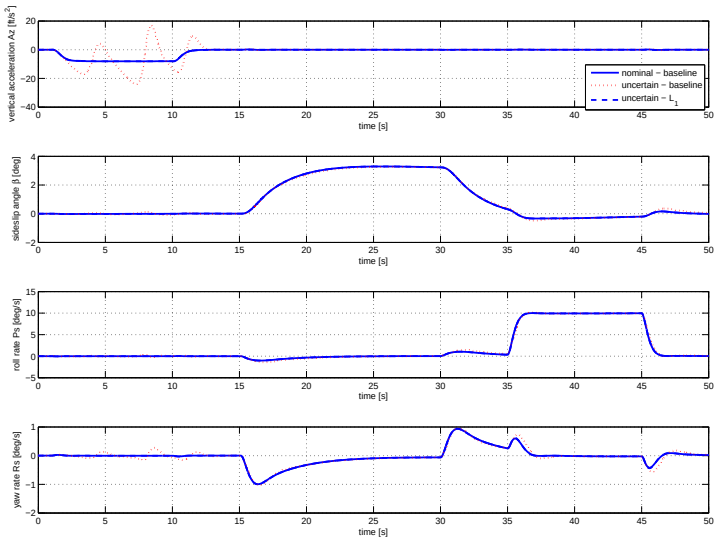

Figure 3.1: Inner-loop adaptation with control effectiveness reduction and pitch break phenomenon: command tracking

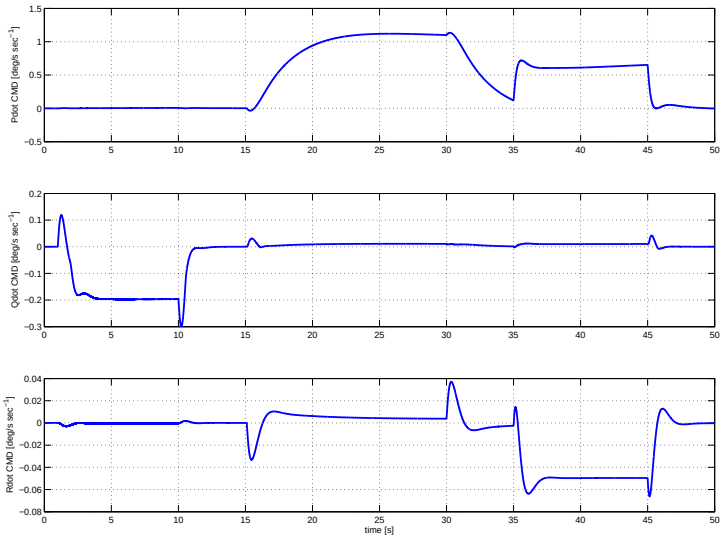

Figure 3.2: Inner-loop adaptation with control effectiveness reduction and pitch break phenomenon: virtual controls

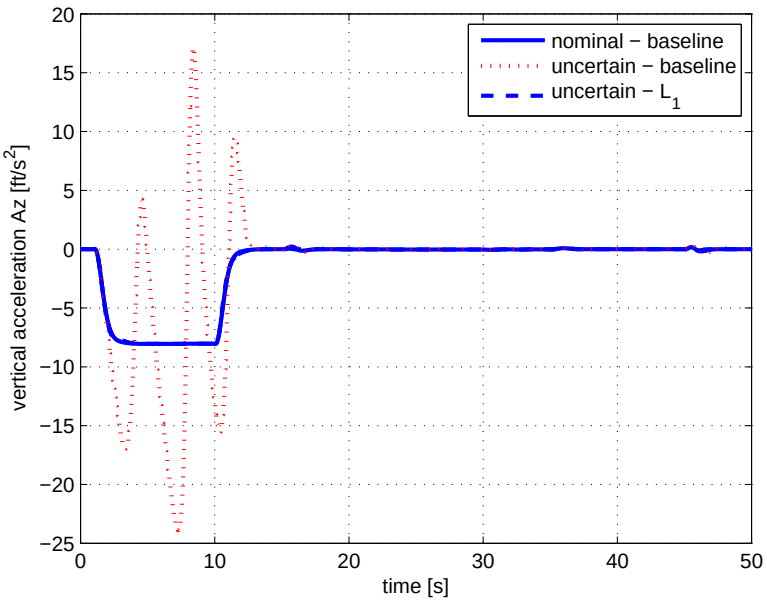

Figure 3.3: Zoomed subplot of Fig 2 to show guaranteed $\mathcal{L}_1$ performance

$(\dot{p}_p, \dot{q}_p, \dot{r}_p)$ command loops one at a time keeping the other two loops closed. This is shown in Table 3.1.

To calculate the time-delay margin for the adaptive system, the time-delay at the plant input is introduced, and the margins are calculated using numerical simulations.

The time-delay margins for the $\mathcal{L}_1$ adaptive controller are summarized in Table 3.2 for $C(s) = \frac{1}{0.05s+1}$ and $\Gamma_c = 100000$. The worst case time-delay margin is 0.062 sec, which is

Table 3.1: Phase and time-delay margins for the inner loop

Loop Margin	$\dot{p}$	$\dot{q}$	$\dot{r}$
Phase Margin (deg)	85.6	65.6	66.1
Cross-over Frequency (rad/sec)	4.25	6.01	4.27
Time-delay Margin (sec)	0.3515	0.1905	0.2702

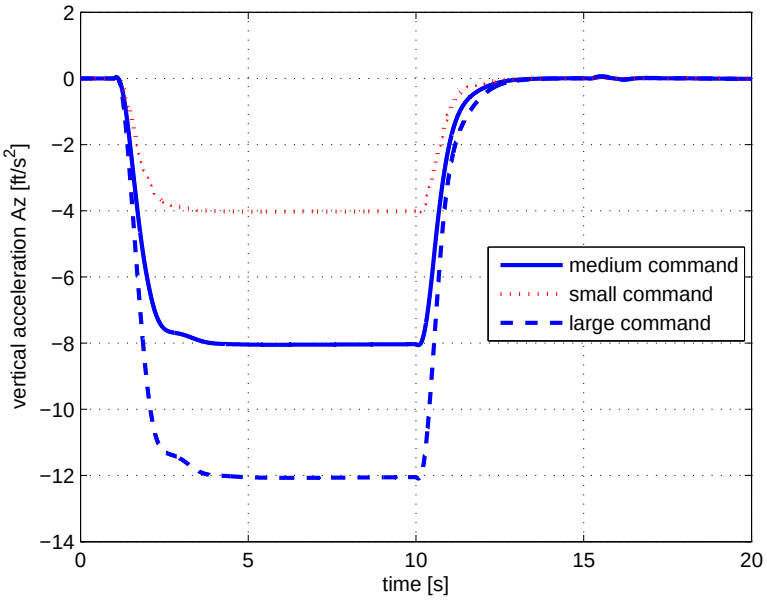

Figure 3.4: Inner-loop adaptation with control effectiveness reduction and pitch break phenomenon: scaled command tracking

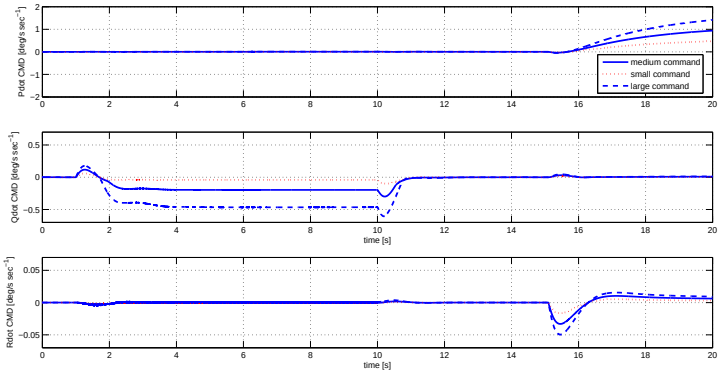

Figure 3.5: Inner-loop adaptation with control effectiveness reduction and pitch break phenomenon: scaled virtual control

Table 3.2: Time-delay margin for $\mathcal{L}_1$ for $C(s) = \frac{1}{0.05s+1}$

$\dot{p}$	$\dot{q}$	$\dot{r}$	
n/a	0.062	n/a	Individual
0.073	n/a	n/a	Individual
n/a	n/a	0.065	Individual
0.062	0.062	n/a	Two Loops
n/a	0.065	0.065	Two Loops
0.067	n/a	0.067	Two Loops
0.062	0.062	0.062	Simultaneous

small. Following the discussion from Section 3.3.4, the time-delay margin can be improved by tuning $C(s)$. Towards that end, consider the following low-pass filter

$$C_1(s) = \frac{1}{0.05s+1}\frac{(-6s+1)^2}{(8s+1)^2},$$

for which the $\mathcal{L}_1$ norm upper bound holds. The corresponding $D_1(s)$ will be

$$D_1(s) = \frac{(-6s+1)^2}{s(3.2s^2+28.8s+28.05)}\,.$$

The Bode plots of $D(s)$ and $D_1(s)$ are given in Figure 3.6. Note that a nonminimum phase filter is used to enhance the phase characteristic in the region of frequency-band in order to improve the phase margin.

The subplot of vertical acceleration of Figure 3.1 is repeated with $C_1(s)$ in Figure 3.7. Notice that there is some degradation in the tracking, however it is still satisfactory. For this choice of $C_1(s)$, the worst case time-delay obtained from simulation is 0.15 sec. In Table 3.2, it can be seen that worst case time-delay margin for $C(s)$ equal to 0.062sec, which implies that $C_1(s)$ doubles the time-delay margin. Thus, at this stage, it appears that improving the time-delay margin hurts the transient performance, which is consistent with the conventional claims in linear systems theory. From this perspective, the $\mathcal{L}_1$ adaptive control paradigm

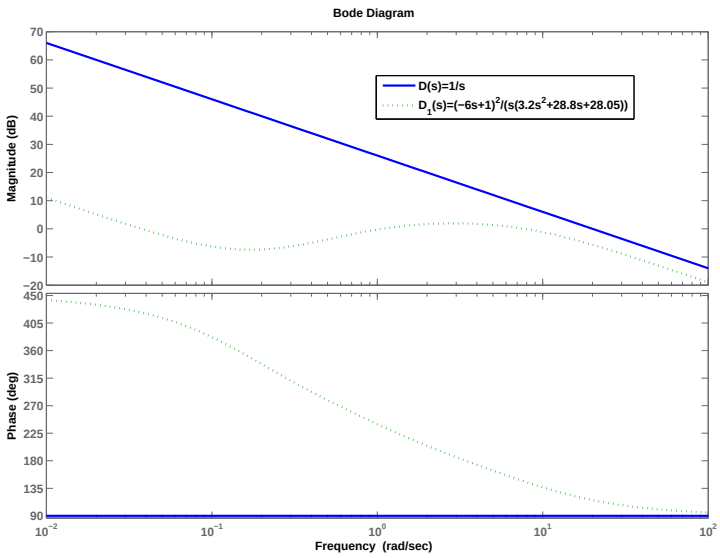

Figure 3.6: Choice of $C(s)$ to maximize the time-delay margin

achieves clear separation between adaptation and robustness: the adaptation can be as fast as the CPU permits, while robustness can be resolved via conventional methods well known from classical and robust control. Notice that all the time-delay margins are calculated for the case of control effectiveness reduction and in the presence of the pitch break uncertainty.

However, notice that a smaller value of Γ_c is preferable from an implementation point of view. Figure 3.8 shows the system response for different values of Γ_c for both low-pass filters. It can be seen that there is almost no degradation in the time response performance. However, for the low-pass filter $C(s) = \frac{1}{0.05s+1}$, if Γ_c decreases from 100000 to 10000, the worst case time-delay margin decreases from 0.062 to 0.022 (i.e. about 3 times). However, for $C_1(s)$ it decreases from 0.17 to 0.15 (i.e only 1.2 times). Thus, with smaller choice of Γ_c, $C_1(s)$ is more suitable in terms of robustness as compared to $C(s)$. Table 3.3 summarizes the margins for $C_1(s)$ with $\Gamma_c = 10000$.

Finally, the system with increased control effectiveness reduction (50% of each surface) with-

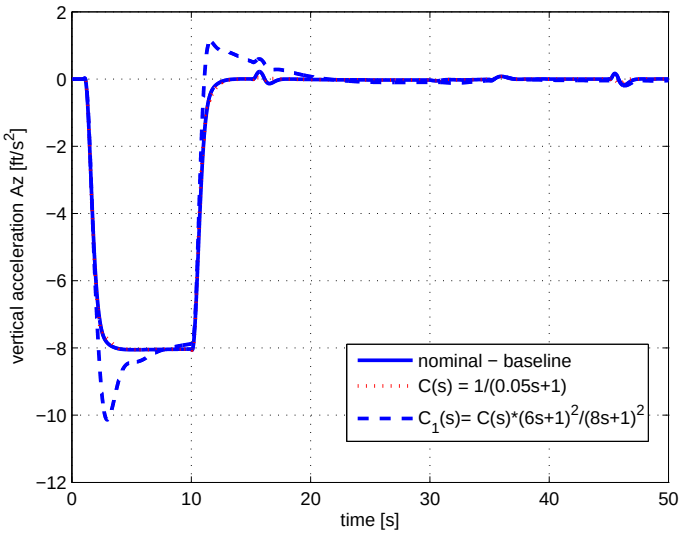

Figure 3.7: Inner-loop adaptation with control effectiveness reduction and pitch break phenomenon: command tracking (for different choice of $C(s)$)

Table 3.3: Time-delay margin of $\mathcal{L}_1$ for $C_1(s)$ and $\Gamma_c = 10000$

$\dot{p}$	$\dot{q}$	$\dot{r}$	
n/a	0.15	n/a	Individual
0.24	n/a	n/a	Individual
n/a	n/a	0.25	Individual
0.15	0.15	n/a	Two Loops
n/a	0.15	0.15	Two Loops
0.17	n/a	0.17	Two Loops
0.15	0.15	0.15	Simultaneous

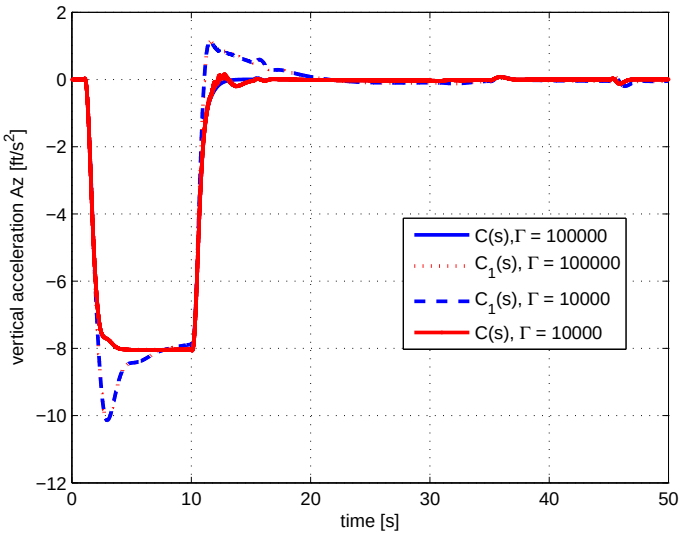

Figure 3.8: Inner-loop adaptation with control effectiveness reduction and pitch break phenomenon: command tracking (for different values of Γ_c)

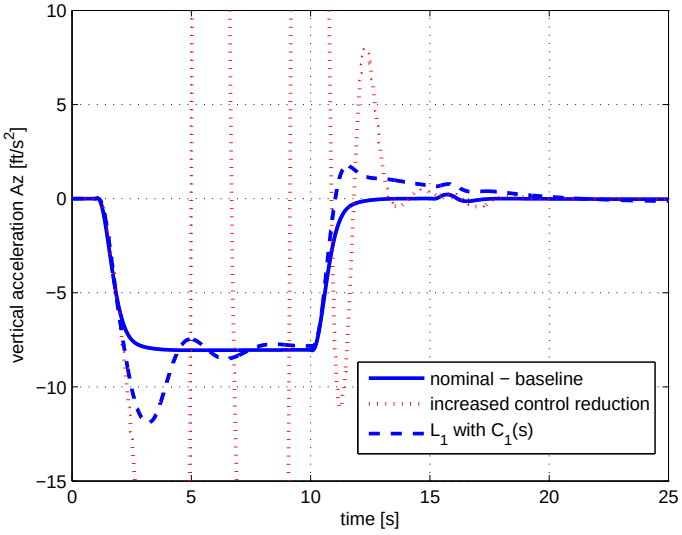

Figure 3.9: Baseline controller almost loses stability in the presence of increased control reduction, while $\mathcal{L}_1$ proves guaranteed tracking

Table 3.4: Worst case time-delay margin with 30% and 50% control effectiveness reduction

30% case	50% case		Γ_c
0.062	0.071	C(s)	100000
0.022	0.025	C(s)	10000
0.17	0.20	$C_1(s)$	100000
0.15	0.20	$C_1(s)$	10000

out any delays is simulated to test robustness of the $\mathcal{L}_1$ adaptive control scheme towards a different class of uncertainty. Figure 3.9 plots the vertical acceleration command tracking in the presence of pitch break uncertainty and 50% reduction of control effectiveness for each actuator channel. It can be seen that the $\mathcal{L}_1$ adaptive control architecture retains both its tracking property and as well the worst time-delay margin of 0.20, as predicted by the $\mathcal{L}_1$ theory. In Table 3.4, the worst-case time-delay margins for two cases of control effectiveness reduction are summarized.

3.4.2 Aerial Refueling

In this section the $\mathcal{L}_1$ adaptive controller is applied to Autonomous Aerial Refueling (AAR) autopilot design. The probe-and-drogue refueling procedure is adopted. This process has proven to be extremely difficult due to the aerodynamic coupling among the two aircraft, receiver and tanker, and the drogue. The autopilot has to compensate for the uncertainties due to the trailing vortices of the tanker when the receiver is flying from the observation point to the contact point. As compared to the earlier work of the authors [79], the control signal defined via (3.26), (3.27) and (3.29) subject to the $\mathcal{L}_1$-norm upper bound in (3.25), eliminates the need for selecting and tuning basis functions required by neural network based $\mathcal{L}_1$ adaptive control. This reduces the design effort significantly.

A decoupled six degree of freedom (6-DoF) aircraft model for the refueling aircraft is con-

sidered. It is assumed that both the receiver and the tanker aircraft are in straight and level flight in the beginning of the maneuver, and during the entire aerial refueling maneuver the receiver aircraft is subject only to small perturbations so that the linearized decoupled dynamics can be used to describe its motion with some level of fidelity with additive uncertainties coming from the trailing vortices induced by the tanker aircraft. For the aerial refueling maneuver all angles can be assumed small. Besides these assumptions, the influence of gravity, thrust, and elevator on the angle of attack are also neglected. The drogue position is known, served as reference command $z_c(t)$, and the control objective is to fly the receiver into a prescribed neighborhood of the drogue center within a prescribed finite time interval. The 6-DoF aircraft dynamics can be described as:

$$\begin{aligned}
\dot{l}_s &= V_t \\
\dot{V}_t &= X_V V_t - g\theta_p + X_q q_p + X_\alpha \alpha_p + X_{\delta_T}\Lambda_1(\delta_{T_{in}} + \delta_T) + \Delta_1(l_s, z_s, y_s) \\
\dot{\alpha}_p &= q_p + \frac{Z_\alpha}{V_0}\alpha_p \\
\dot{\theta}_p &= q_p \\
\dot{q}_p &= M_q q_p + M_\alpha \alpha_p + M_{\delta_e}\Lambda_2(\delta_{e_{in}} + \delta_e) + \Delta_2(l_s, z_s, y_s) \\
\dot{z}_s &= V_0(\theta_p - \alpha_p) \\
\dot{\phi}_p &= \frac{\cos\gamma_0}{\cos\theta_0}p_p + \frac{\sin\gamma_0}{\cos\theta_0}r_p \\
\dot{\beta}_p &= \frac{g\cos\theta_0}{V_0}\phi_p + \frac{Y_\beta}{V_0}\beta_p - r_p \\
\dot{p}_p &= L_\beta\beta_p + l_s p_p + L_r r_p + L_{\delta_a}\Lambda_3(\delta_{a_{in}} + \delta_a) + L_{\delta_r}\delta_{r_{in}} + \Delta_3(l_s, z_s, y_s) \\
\dot{r}_p &= N_\beta\beta_p + N_p p_p + N_r r_p + N_{\delta_r}\delta_{r_{in}} + N_{\delta_a}(\delta_{a_{in}} + \delta_a) \\
\dot{y}_s &= Y_\phi\phi_p + V_0\beta_p,
\end{aligned} \tag{3.101}$$

where $\Delta_1(l_s, z_s, y_s)$, $\Delta_2(l_s, z_s, y_s)$ and $\Delta_3(l_s, z_s, y_s)$ are the wake induced incremental changes to the horizontal acceleration, the pitch angle acceleration and the roll angle acceleration respectively. The coefficients $0 < \Lambda_i \leq 1$, $i = 1, 2, 3$, model the reduction in control effectiveness. The receiver dynamics are trimmed around $(V_0, \alpha_0, \theta_0)$, while the tanker is assumed to be trimmed for straight and level flight with the same trim conditions. The coordinate

system is the body-fixed system of the tanker aircraft. In (3.101), $\delta_{T_{in}}$, $\delta_{e_{in}}$, $\delta_{a_{in}}$ and $\delta_{r_{in}}$ are the inner-loop controllers, which are designed via proportional- integral feedback to keep θ_p, α_p, q_p, V_t, β_p, ϕ_p, p_p, r_p close to the trim conditions. We note that the inner-loop stabilization can be achieved via any of the conventional linear design methods (see e.g. in Ref. [100]) and is not elaborated in this dissertation for the sake of brevity. We will focus on the design of the outer-loop controllers δ_T, δ_e, δ_a and δ_r to enable the aerial refueling maneuver in the highly uncertain dynamic environment. With the inner-loop stabilization, the equations of motion can be expressed as:

$$\begin{aligned}
\dot{l}_s &= V_t \\
\dot{V}_t &= X'_V V_t + X_{\delta_T}\Lambda_1\delta_T + \Delta_1(l_s, z_s, y_s) \\
\dot{\alpha}_p &= q_p + \frac{Z_\alpha}{V_0}\alpha_p \\
\dot{\theta}_p &= q_p \\
\dot{q}_p &= M'_q q_p + M'_\alpha \alpha_p + M_{\delta_e}\Lambda_2\delta_e + \Delta_2(l_s, z_s, y_s) \\
\dot{z}_s &= V_0(\theta_p - \alpha_p) \\
\dot{\phi}_p &= \frac{\cos\gamma_0}{\cos\theta_0}p_p + \frac{\sin\gamma_0}{\cos\theta_0}r_p \\
\dot{\beta}_p &= \frac{g\cos\theta_0}{V_0}\phi_p + \frac{Y_\beta}{V_0}\beta_p - r_p \\
\dot{p}_p &= L'_\beta\beta_p + l'_s p_p + L'_r r_p + L_{\delta_a}\Lambda_3\delta_a + \Delta_3(l_s, z_s, y_s) \\
\dot{r}_p &= N'_\beta\beta_p + N'_p p_p + N'_r r_p \\
\dot{y}_s &= Y_\phi\phi_p + V_0\beta_p\,,
\end{aligned} \tag{3.102}$$

where X'_V, M'_q, M'_α, L'_β, L'_p, L'_r, N'_β, N'_p, N'_r are the redefined coefficients due to the proportional feedbacks used for the inner-loop stabilization. Usually, for the lateral axis the inner-loop control is designed using "aileron to rudder interconnect" to achieve stability axis roll without generating side-slip or yaw rate, which consequently reduces the term N_{δ_a} to zero, and therefore in (3.102) it has been neglected.

Consider a decoupled linearized six-degree-of-freedom (6-DOF) aircraft model for the receiver aircraft. Both the receiver and the tanker aircraft are in straight and level flight in the

beginning of the maneuver. The receiver is assumed to be subject only to small perturbations during the entire refueling maneuver so that the linearized decoupled dynamics can be used to describe its motion with some level of fidelity, with additive uncertainties coming from the trailing vortices induced by the tanker aircraft. For the aerial refueling maneuver all angles are assumed small. Besides these assumptions, the influence of gravity, thrust, and elevator on the angle of attack are also neglected. The drogue position is known, and serves as a reference command $z_c(t)$. The control objective is to fly the receiver into a prescribed neighborhood of the drogue center within a prescribed finite time interval. Upon incorporating inner-loop baseline controllers into the system dynamics, the system to be controlled has three inputs: thrust, elevator and aileron, and has three outputs: horizontal separation, vertical separation and lateral separation relative to the tanker. The control objective is to regulate three outputs to certain set points in the presence of aerodynamic uncertainties (drag, pitching moment and rolling moments) in three directions respectively, and in the presence of control surface failures.

The aircraft model is a flying-wing unmanned aerial vehicle (UAV), known as the Barrons Associates nonlinear tailless aircraft model (BANTAM) [77]. The wake-effect data which models the vortex are taken from a wind-tunnel test of a delta wing UAV behind KC-135R tanker [80]. The baseline controller is a Linear Quadratic Regulation (LQR) controller with integral action. For this LQR+PI controller structure, the feedforward gain K_z is zero. The system takes the form in (3.16), which is repeated here for the sake of completeness:

$$\dot{x}(t) \;=\; A_m x(t) + B_m z_c(t) + B_1\Big(\Lambda u_{ad}(t) + \Lambda K_0(t, x_p(t)) + k_x^\top x(t)\Big)\,, \qquad (3.103)$$

where $x(t) \in \mathbb{R}^{14}, u_{ad}(t) \in \mathbb{R}^3$ (thrust, elevator and aileron), $z_c(t) \in \mathbb{R}^3$ are the measured system states, control signals and reference inputs, respectively, $A_m \in \mathbb{R}^{14\times 14}$, $B_m \in \mathbb{R}^{14\times 3}$, $B_1 \in \mathbb{R}^{14\times 3}$ are known matrices with the three columns of B_1 being linearly independent. The definitions of Λ, k_x are given in (3.17). Notice that there is no k_z in equation (3.103). The state vector $x = (l_s, V_t, \alpha_p, \theta_p, q_p, z_s, \phi_p, \beta_p, p_p, r_p, y_s, l_I, h_I, y_I)^\top$ comprises eleven plant states (x_p), which include horizontal separation l_s, velocity V_t, angle of attack α_p, pitch

angle θ_p, pitch rate q_p, vertical separation z_s, roll angle ϕ_p, angle of sideslip β_p, body roll rate p_p, body yaw rate r_p, lateral separation y_s and three baseline controller (x_c) states, which include the integrator states of separations (l_I, h_I and y_I). The simulation results and the $\mathcal{L}_1$ controller parameters are given in this section. More details on system dynamics and baseline controller design can be found in [79].

The target point for the receiver aircraft is chosen to be the center of the outer cross section of the drogue. The aircraft is trimmed at the speed $V_0 = 500$ ft/sec, angle of attack $\alpha_0 = 0.042$ rad, pitch angle $\theta_0 = 0.042$ rad, and at the altitude of $h_p = 5000$ ft. The radius of the drogue is $r_d = 1$ ft. The initial position of the receiver aircraft is 165 ft behind the tanker and 50 ft below the tanker, and 10 ft to the left of the aircraft laterally. Relative to the tanker coordinate system the position of the drogue center is at the coordinates: $x_d = -15$ ft, $y_d = 30$ ft, $z_d = 10$ ft.

The closed-loop system with these baseline controller gains defines the nominal linear system response that has the desired convergence time for the probe to contact the drogue with desired performance specifications. The adaptive augmentation with the $\mathcal{L}_1$ controller is designed to track this system's response both in transient and steady state. In the absence of wake induced uncertainties and without any loss in control effectiveness, the probe reaches the 0.02 ft neighborhood of the drogue center within 25 sec. That is, $|x(25)-x_d(25)| = 0.012$, $|y(25) - y_d(25)| = 0.015$ and $|z(25) - z_d(25)| = 0.02$. Figure 3.10 plots the closed-loop trajectories in each axis. It compares the response in the absence of the wake and without any loss in control effectiveness with the response in the presence of the wake and loss in control effectiveness. The failures are 60% reduction of elevator effectiveness, and 60% reduction of aileron effectiveness, that is $\Lambda_2 = \Lambda_3 = 0.4$. From these figures it can seen that both the steady-state tracking and the transient performance are deteriorated in the presence of uncertainties. Figure 3.11 shows the other states (angle of attack α, pitch angle θ, roll angle ϕ, side-slip angle β, roll rate p, pitch rate q and yaw rate r) of the baseline controlled closed-loop system. Those states remain small during the whole aerial refueling process.

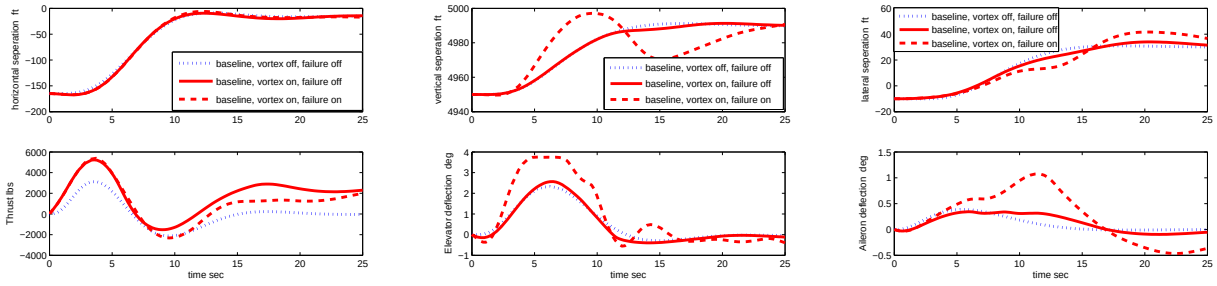

Figure 3.10: Horizontal, vertical, lateral separation -baseline controller

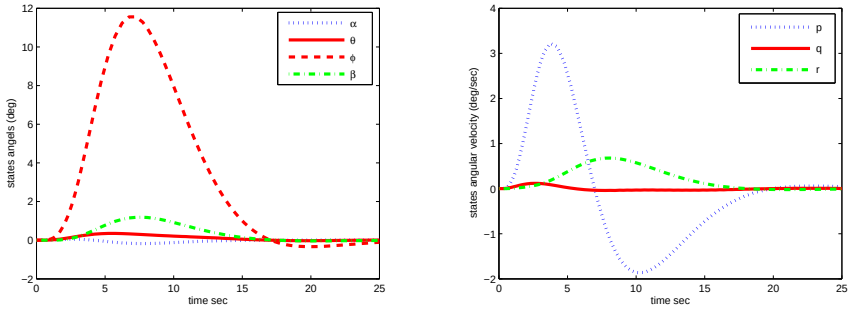

Figure 3.11: Angles and angular velocities - baseline controller

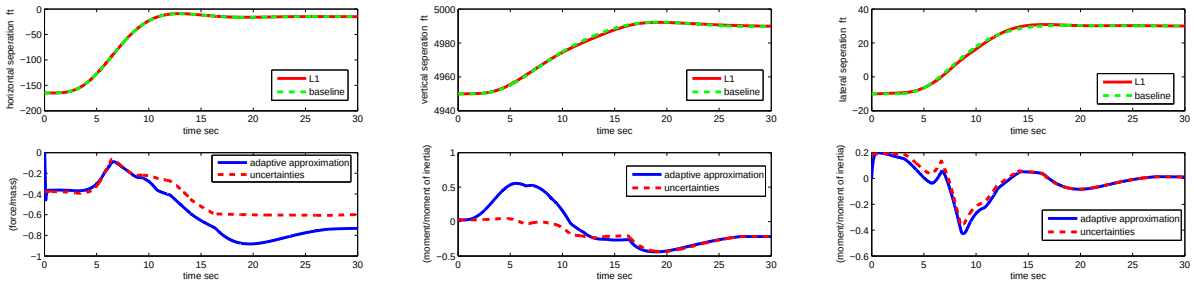

Figure 3.12: Horizontal, vertical, lateral separation -baseline + $\mathcal{L}_1$ controller

For the design of $\mathcal{L}_1$ controller we set $D_i(s) = \frac{1}{s}$, $i = 1, \cdots, m$. Conservative growth rates for the uncertainties are computed from the experimental data, implying that $\max L_{w_i} = 0.1$. The conservative maximum is given by $L_i = 10.1$. We choose $k_1 = k_2 = k_3 = 20$ leading to $C_1(s) = \frac{20}{s+20}$, $C_2(s) = \frac{8}{s+8}$ and $C_3(s) = \frac{8}{s+8}$. A uniform adaptive gain $\Gamma_c = 100000$ is set for the design of the adaptive controller in each axis. The closed-loop system response with $\mathcal{L}_1$ adaptive augmentation and the adaptive control signals are shown in Figure 3.12. Notice that $\mathcal{L}_1$ adaptive controller can recover the nominal performance of the baseline controller in the presence of the wake vortex and loss of control effectiveness. The tracking precision upon $t' = 25sec$ can be characterized with the bound $\|[y(t') \quad z(t')]^\top - [y_d(t') \quad z_d(t')]^\top\| = 0.05 \leq 1$, and $|x(t') - x_d(t')| = 0.04$. Notice that the in the thrust input channel, at the steady state there is a difference between the time histories of the adaptive approximation and the uncertainty. That is caused by the residue of the elevator control input coming into the horizontal direction. In the elevator and aileron plots, it can be seen that there are some differences between the adaptive signals and the uncertainties during the transient phase. If the actuator failure is turned off, the adaptive approximation will be much closer to the uncertainties, as shown in Figure 3.13.

Next it is shown that when the initial conditions change, $\mathcal{L}_1$ adaptive controller does not need any re-tuning.

The initial conditions of the receiver are changed. We keep the same values for Λ_1 and Λ_2, and run the simulations from 33.75 ft behind the tanker, 18 ft below the tanker and 22 ft to

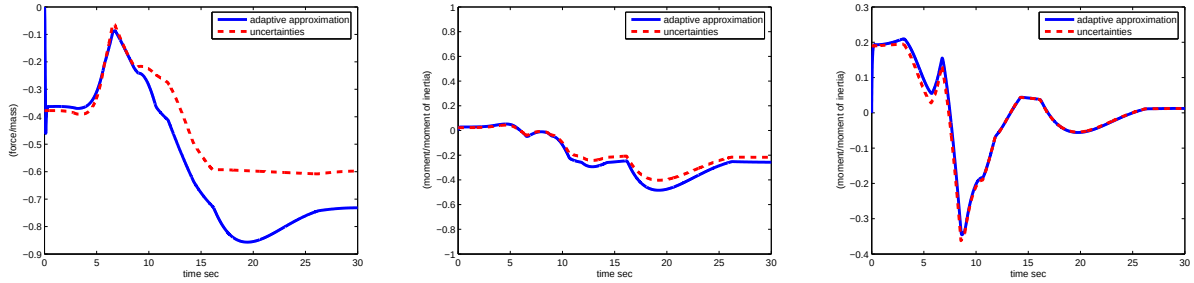

Figure 3.13: $\mathcal{L}_1$ adaptive control signals and uncertainties - failure OFF

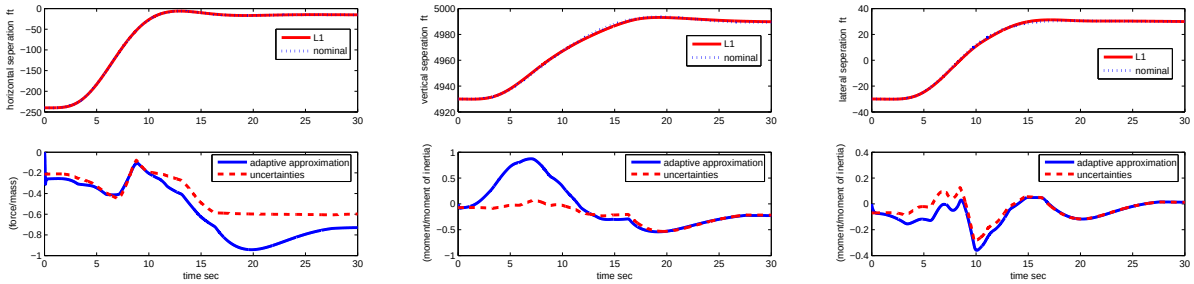

Figure 3.14: Horizontal, vertical and lateral Separation - second case

the right of the tanker, without any re-tuning of both controllers. The $\mathcal{L}_1$ adaptive controller achieves the tracking precision upon $t' = 25$ sec, which is $\|[y(t') \quad z(t')]^\top - [y_d(t') \quad z_d(t')]^\top\| = 0.021 \leq 1$, and $|x(t') - x_d(t')| = 0.020$, as seen in Figure 3.14. It can be observed that the $\mathcal{L}_1$ adaptive controller shows scaled system output responses (similar to linear systems).

Without re-tuning of the $\mathcal{L}_1$ controller, the simulation is further run by starting from various different initial conditions, as shown in Figure 3.15. It can be seen that the system outputs have scaled responses. The uncertainties are further increased, by multiplying the magnitude of the vortex data by two. This can approximately represent a different tanker if a modified horseshoe vortex model is considered. With fixed separations between the receiver and the tanker, the magnitude of the induced velocity is proportional to the strength of the vortex, which is in its turn proportional to the mean aerodynamic chord of the tanker and velocity of the tanker. So it is reasonable to scale our current induced aerodynamic coefficients by multiplying them by two to represent the change of tanker's wake effects. Figure 3.16 show

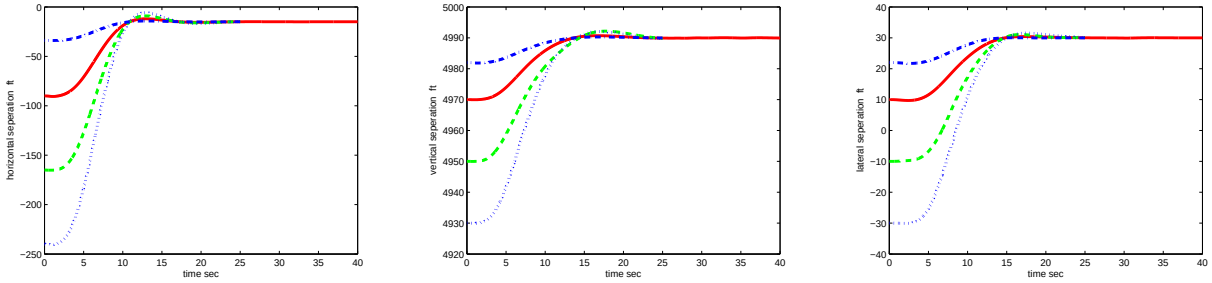

Figure 3.15: Horizontal, vertical and lateral Separation -scaled responses

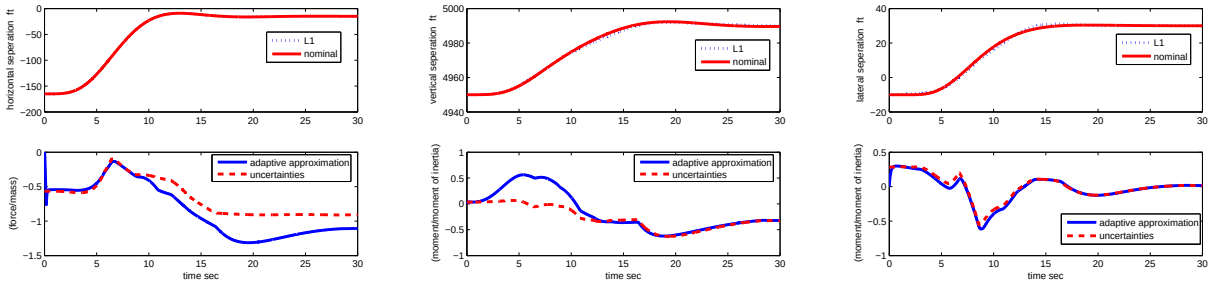

Figure 3.16: Horizontal, vertical and lateral Separation -increased vortex magnitude

that the the outputs are identical to the nominal performance, and Figure 3.17 shows that the adaptive control signals have scaled responses corresponding to the change of uncertainties.

Finally, the time-delay margin of the $\mathcal{L}_1$ adaptive controlled system similar to the UCAV model above is computed. First the low pass filters $C_2(s) = C_3(s) = \frac{25}{s+25}$ are used. The numerical values are shown in Table 3.5.

Next the low pass filter is changed to $C_2(s) = C_3(s) = \frac{8}{s+8}$. The time-delay margins are given in Table 3.6.

It can be seen that by applying different $C(s)$ the time-delay margin of the adaptive controlled system can be improved. This verifies the theoretical predictions.

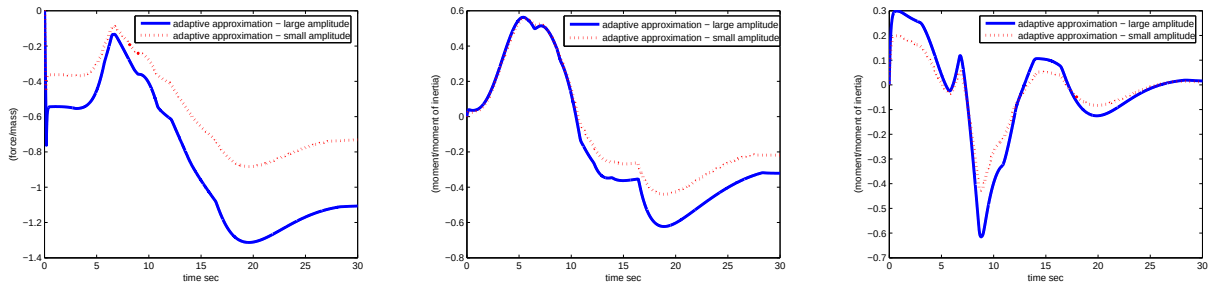

Figure 3.17: Adaptive signals vs uncertainties -increased vortex magnitude

Table 3.5: Time-delay margin of $\mathcal{L}_1$ for $C_2(s) = C_3(s) = \frac{25}{s+25}$ and $\Gamma_c = 100000$

elevator	aileron	
0.028	n/a	Individual
n/a	0.031	Individual
0.028	0.030	Simultaneous

Table 3.6: Time-delay margin of $\mathcal{L}_1$ for $C_2(s) = C_3(s) = \frac{8}{s+8}$ and $\Gamma_c = 100000$

elevator	aileron	
0.042	n/a	Individual
n/a	0.081	Individual
0.041	0.080	Simultaneous

3.5 Conclusion

The $\mathcal{L}_1$ state feedback adaptive controller is applied to two benchmark flight control applications in this section. The proposed adaptive control approach overcomes the drawbacks of conventional adaptive control methods. It has guaranteed performance bounds, both in transient and steady state, and systematic design methodology to achieve the desired control specifications. The bounded-away-from-zero time-delay margin of this adaptive controller can be improved by systematic choice of the underlying filters. These features hold a promise for the development of theoretically justified tools for Validation and Verification of adaptive systems.

Chapter 4

$\mathcal{L}_1$ Output Feedback Adaptive Control

4.1 Problem Formulation and Controller Architecture

Consider the linear SISO system

$$y(s) = A(s)\left[u(s) + d(s)\right], \quad y(0) = 0, \tag{4.1}$$

where $u(t) \in \mathbb{R}$ is the input, $y(t) \in \mathbb{R}$ is the system output, $A(s)$ is the unknown transfer function of the system, $d(s)$ is the Laplace transform of the time-varying disturbances $d(t, y)$. Notice that $d(t, y)$ can possibly depend also on the system output y, and the upper bound of the growth rate of $d(t, y)$ with respect to y is L, as stated in following assumption.

Assumption 4 *There exists a constant $L > 0$ such that the following inequality holds uniformly in $t \geq 0$ for all y, y':*

$$|d(t, y) - d(t, y')| \leq L|y - y'|.$$

The control objective is to design an adaptive output feedback controller $u(t)$ such that in the presence of uncertainties the system output $y(t)$ tracks the reference input $r(t)$ with satisfactory performance. This can be done by selecting a minimum-phase, strictly proper

and stable transfer function $M(s)$, and designing an adaptive control law to achieve $y(s) \approx M(s)r(s)$. The selection of $M(s)$ needs to satisfy the sufficient conditions for stability and performance, and the discussion on selection of $M(s)$ is postponed to Section 4.2. One important characteristic of $M(s)$ for the proposed adaptive controller is that it does not necessarily need to satisfy the Strict Positive Real (SPR) assumption for its structure. The system in (4.1) can be rewritten as:

$$\begin{aligned} y(s) &= M(s)\left(u(s)+\sigma(s)\right) && (4.2)\\ \sigma(s) &= \Big((A(s)-M(s))u(s)+A(s)d(s)\Big)/M(s)\,. && (4.3) \end{aligned}$$

Let ($A_m \in \mathbb{R}^{N\times N}$, $b_m \in \mathbb{R}^N$, $c_m \in \mathbb{R}^N$) be the minimal realization of $M(s)$. Hence, (A_m, b_m, c_m) is controllable and observable, with A_m being Hurwitz. Thus, the system in (4.2) can be rewritten as:

$$\begin{aligned} \dot{x}(t) &= A_m x(t) + b_m(u(t)+\sigma(t)) && (4.4)\\ y(t) &= c_m^\top x(t)\,, \quad x(0)=x_0=0. \end{aligned}$$

Next the closed-loop *reference system* that defines *an achievable control objective* for the $\mathcal{L}_1$ adaptive controller is introduced.

Closed-loop reference system: The reference system is given by

$$\begin{aligned} y_{ref}(s) &= M(s)(u_{ref}(s)+\sigma_{ref}(s)) && (4.5)\\ \sigma_{ref}(s) &= \big((A(s)-M(s))u_{ref}(s)+A(s)d_{ref}(s)\big)/M(s)\\ u_{ref}(s) &= C(s)(r(s)-\sigma_{ref}(s)) \end{aligned}$$

where $C(s)$ is a low pass filter with DC gain $C(0)=1$.

According to [11, Lemma 1] the selection of $C(s)$ and $M(s)$ must ensure that

$$H(s) = A(s)M(s)/\Big(C(s)A(s)+(1-C(s))M(s)\Big) \qquad (4.6)$$

is stable and that the $\mathcal{L}_1$-norm of the cascaded system is upper bounded as follows:

$$\|H(s)(1-C(s))\|_{\mathcal{L}_1} L < 1 \qquad (4.7)$$

Then the reference system in (4.5) is stable.

The elements of the $\mathcal{L}_1$ adaptive controller are introduced next.

State predictor (passive identifier): Let ($A_m \in \mathbb{R}^{n\times n}$, $b_m \in \mathbb{R}^n$, $c_m \in \mathbb{R}^n$) be the minimal realization of $M(s)$. Hence, (A_m, b_m, c_m) is controllable and observable with A_m being Hurwitz. Then the system in (4.1) can be rewritten as

$$\begin{aligned} \dot{x}(t) &= A_m x(t) + b_m(u(t) + \sigma(t)) \\ y(t) &= c_m^\top x(t) \end{aligned} \tag{4.8}$$

The state predictor is given by:

$$\begin{aligned} \dot{\hat{x}}(t) &= A_m \hat{x}(t) + b_m u(t) + \hat{\sigma}(t) \\ \hat{y}(t) &= c_m^\top \hat{x}(t) \end{aligned} \tag{4.9}$$

where $\hat{\sigma}(t) \in \mathbb{R}^n$ is the vector of adaptive parameters. Notice that in the state predictor equations $\hat{\sigma}(t)$ is not in the span of b_m, while in the equation (4.8) $\sigma(t)$ is in the span of b_m. Further, let $\tilde{y}(t) = \hat{y}(t) - y(t)$.

Adaptation law: Let P be the solution of the following algebraic Lyapunov equation:

$$A_m^\top P + P A_m = -Q$$

where $Q > 0$. From the properties of P it follows that there always exists a nonsingular $\sqrt{P}$ such that

$$P = \sqrt{P}^\top \sqrt{P}.$$

Given the vector $c_m^\top(\sqrt{P})^{-1}$, let D be the $(n-1)\times n$-dimensional nullspace of $c_m^\top(\sqrt{P})^{-1}$, i.e.

$$D(c_m^\top(\sqrt{P})^{-1})^\top = 0 \tag{4.10}$$

and let

$$\Lambda = \begin{bmatrix} c_m^\top \\ D\sqrt{P} \end{bmatrix} \in \mathbb{R}^{n\times n} \tag{4.11}$$

The update law for $\hat{\sigma}(t)$ is defined using the sampling time $T > 0$[1]:

$$\hat{\sigma}(iT) = -\Phi^{-1}(T)\mu(iT), \quad i = 1, 2, \cdots, \tag{4.12}$$

where

$$\Phi(T) = \int_0^T \mathrm{e}^{\Lambda A_m \Lambda^{-1}(T-\tau)}\Lambda d\tau \tag{4.13}$$

and

$$\mu(iT) = \mathrm{e}^{\Lambda A_m \Lambda^{-1} T}\mathbf{1}_1 \tilde{y}(iT), \quad i = 1, 2, \cdots \tag{4.14}$$

Here $\mathbf{1}_1$ denotes the basis vector in the space $\mathbb{R}^n$ with its first element equal to 1 and other elements being zero.

Control law: The control law is defined via the output of the low-pass filter:

$$u(s) = C(s)r(s) - \frac{C(s)}{M(s)}c_m^\top(s\mathbb{I} - A_m)^{-1}\hat{\sigma}(s)\,. \tag{4.15}$$

The complete $\mathcal{L}_1$ adaptive controller consists of the state predictor in (4.9), the adaptation law in (4.12), and the control law in (4.15), subject to the $\mathcal{L}_1$-norm upper bound in (4.7). The performance bounds of the $\mathcal{L}_1$ adaptive output feedback controller are given by the following theorem.

Theorem 3 *For the $\mathcal{L}_1$ adaptive controller given by (4.9), (4.12), (4.15), subject to the $\mathcal{L}_1$-norm upper bound in (4.7), we have*

$$\begin{aligned}
\lim_{T\to 0}\left(\|\tilde{y}\|_{\mathcal{L}_\infty}\right) &= 0\\
\lim_{T\to 0}\left(\|y - y_{ref}\|_{\mathcal{L}_\infty}\right) &= 0\\
\lim_{T\to 0}\left(\|u - u_{ref}\|_{\mathcal{L}_\infty}\right) &= 0
\end{aligned}$$

The result in this theorem follows immediately from [11, Theorem 1] and [11, Lemma 3].

[1] T defines the sampling rate of the available CPU.

4.2 The Design Issues of $\mathcal{L}_1$ Output Feedback Adaptive Control

4.2.1 Stability

The first step of designing an $\mathcal{L}_1$ output feedback adaptive controller is to guarantee stability of the closed-loop system. From Theorem 3 it can be seen that the output of the closed-loop system tracks that of the closed-loop reference system arbitrarily closely for all $t > 0$. Hence the goal of the first step in the design is to find $C(s)$ and $M(s)$ to satisfy the sufficient conditions given in (4.6) and (4.7). These two conditions can guarantee the stability of closed-loop reference system.

First the classes of systems that can satisfy (4.6) via the choice of $M(s)$ and $C(s)$ are discussed. It can be demonstrated that stability of $H(s)$ is equivalent to stabilization of $A(s)$ by

$$\frac{C(s)}{M(s)(1-C(s))}. \tag{4.16}$$

Consider the closed-loop system, comprised of the system $A(s)$ and negative feedback of (4.16). The closed-loop transfer function is:

$$\frac{A(s)}{1+A(s)\frac{C(s)}{M(s)(1-C(s))}}. \tag{4.17}$$

Letting

$$A(s)=\frac{A_n(s)}{A_d(s)}, \quad C(s)=\frac{C_n(s)}{C_d(s)}, \quad M(s)=\frac{M_n(s)}{M_d(s)}, \tag{4.18}$$

it follows from (4.6) that

$$H(s)=\frac{C_d(s)M_n(s)A_n(s)}{H_d(s)}, \tag{4.19}$$

where

$$H_d(s)=C_n(s)A_n(s)M_d(s)+M_n(s)A_d(s)(C_d(s)-C_n(s)). \tag{4.20}$$

Incorporating (4.18), one can verify that the denominator of the system in (4.17) is exactly

$H_d(s)$. Hence, stability of $H(s)$ is equivalent to the stability of the closed-loop system in (4.17).

The selection of $M(s)$ and $C(s)$ can be restricted due to the properties of the plant $A(s)$. Thus, it is not a trivial task. However, it can be done using tools from linear systems theory. The essential objective in this step is to design, based on the nominal system $A_0(s)$, a feedback controller that can be decomposed into $C(s)$ and $M(s)$ according to the equation (4.16), while achieving stability of $H(s)$ in (4.6) and verifying the condition in (4.7) based on conservative knowledge of parametric variations in $A(s)$. In the following subsection one method towards the selection of $C(s)$ and $M(s)$ is described.

Design via Pole Placement

A pole placement method (see examples in Ioannou and Sun [16]) is used to design a dynamic compensator for $A_0(s)$. The block diagram in Figure 4.1 shows the structure of the closed-loop system, where the dynamic controller $P(s)/L(s)$ is determined by the solution of the following equation

$$A_{0_n}(s)P(s) + A_{0_d}(s)L(s) = A_{cl}(s). \tag{4.21}$$

All terms in (4.21) are polynomials of s. The Hurwitz polynomial $A_{cl}(s)$ defines the desired pole locations of the closed-loop system. The coefficients of polynomials $P(s)$ and $L(s)$ may be obtained by solving the algebraic equation

$$\beta_l = {S_l}^{-1}\alpha_l$$

containing the Sylvester matrix S_l of A_{0_n} and A_{0_d}, while β_l is a vector containing coefficients of both $P(s)$ and $L(s)$, and α_l is a vector containing coefficients of $A_{cl}(s)$ (defined next).

Definition 12 *Given two polynomials* $a(s) = a_n s^n + a_{n-1}s^{n-1} + \cdots + a_0$, $b(s) = b_n s^n +$

$b_{n-1}s^{n-1}+\cdots+b_0$, *the Sylvester Matrix* S_l *is defined to be the following* $2n\times 2n$ *matrix:*

$$S_l=\begin{bmatrix}
a_n & 0 & 0 & \cdots & 0 & 0 & b_n & 0 & 0 & \cdots & 0 & 0\\
a_{n-1} & a_n & 0 & & 0 & 0 & b_{n-1} & b_n & 0 & & 0 & 0\\
\cdot & a_{n-1} & a_n & \ddots & & \vdots & \cdot & b_{n-1} & b_n & \ddots & & \vdots\\
\cdot & \cdot & \cdot & \cdot & \ddots & \vdots & \cdot & \cdot & \cdot & \cdot & \ddots & \vdots\\
\cdot & \cdot & \cdot & \cdot & \cdot & 0 & \cdot & \cdot & \cdot & \cdot & \cdot & 0\\
a_1 & \cdot & \cdot & \cdot & \cdot & a_n & b_1 & \cdot & \cdot & \cdot & \cdot & b_n\\
a_0 & a_1 & \cdot & \cdot & \cdot & a_{n-1} & b_0 & b_1 & \cdot & \cdot & \cdot & b_{n-1}\\
0 & a_0 & \cdot & \cdot & \cdot & \cdot & 0 & b_0 & \cdot & \cdot & \cdot & \cdot\\
0 & 0 & \cdot & \cdot & \cdot & \cdot & 0 & 0 & \cdot & \cdot & \cdot & \cdot\\
\vdots & & \ddots & \cdot & \cdot & \cdot & \vdots & 0 & \ddots & \cdot & \cdot & \cdot\\
\vdots & & & \ddots & a_0 & a_1 & \vdots & & & \ddots & b_0 & b_1\\
0 & 0 & \cdots & 0 & 0 & a_0 & 0 & 0 & \cdots & 0 & 0 & b_0
\end{bmatrix}.$$

Definition 13 *If* $L(s)=s^{n-1}+l_{n-2}s^{n-2}+\cdots+l_1s+l_0$, $P(s)=p_{n-1}s^{n-1}+p_{n-2}s^{n-2}+\cdots+p_1s+p_0$, *then*

$$\beta_l=[1,\ \ l_{n-2},\ \ l_{n-3},\ \ \cdots,\ \ l_1,\ \ l_0,\ \ p_{n-1},\ \ p_{n-2},\ \ \cdots,\ \ p_1,\ \ p_0]^\top.$$

If $A_{cl}(s)=s^{2n-1}+a^*_{2n-2}s^{2n-2}+\cdots+a^*_1s+a^*_0$, *then*

$$\alpha_l=[1,\ \ a^*_{2n-2},\ \ a^*_{2n-3},\ \ \cdots,\ \ a^*_1,\ \ a^*_0]^\top.$$

The polynomials $A_{0_n}(s)$ and $A_{0_d}(s)$ should be coprime to ensure the existence and uniqueness of solutions of $P(s)$ and $L(s)$, and non-singularity of S_l.

Incorporating (4.18) gives

$$\frac{C(s)}{M(s)\left(1-C(s)\right)}\ =\ \frac{C_n(s)M_d(s)}{M_n(s)\left(C_d(s)-C_n(s)\right)}. \tag{4.22}$$

Since the low pass filter $C(s)$ has DC gain of 1, the polynomial $C_d(s)-C_n(s)$ has no constant term, which means that the transfer function (4.22) has at least one pole at the origin. To

obtain suitable dynamic compensators which can be decomposed into $M(s)$ and $C(s)$, we need to design a dynamic compensator $\frac{\tilde{P}(s)}{\tilde{L}(s)}$ for the system $\frac{A_0(s)}{s}$. Observing Figure 4.2, it can be seen that the two closed-loop systems have the same characteristic equation. Hence it is possible to find $C(s)$ and $M(s)$ from the transfer function $\frac{1}{s}\frac{\tilde{P}(s)}{\tilde{L}(s)}$. Upon selection of the structure of $C(s)$ and $M(s)$, we can write explicitly the transfer function in (4.22) and obtain the coefficients of s by equating it to $\frac{1}{s}\frac{\tilde{P}(s)}{\tilde{L}(s)}$.

Upon obtaining the dynamic compensator $\frac{C(s)}{M(s)\left(1-C(s)\right)}$, one can apply Nyquist criterion or Root Locus methods to tune the gains of this compensator by changing the poles in $A_{cl}(s)$. If the low-pass filter $C(s)$ and the desired system $M(s)$ do not lead to satisfactory performance, re-selection of the desired locations of the closed-loop poles is needed. Notice that the above method is an *intuitive one*, and other methods from linear systems theory can be equivalently explored for determining a structure for $C(s)$ and $M(s)$.

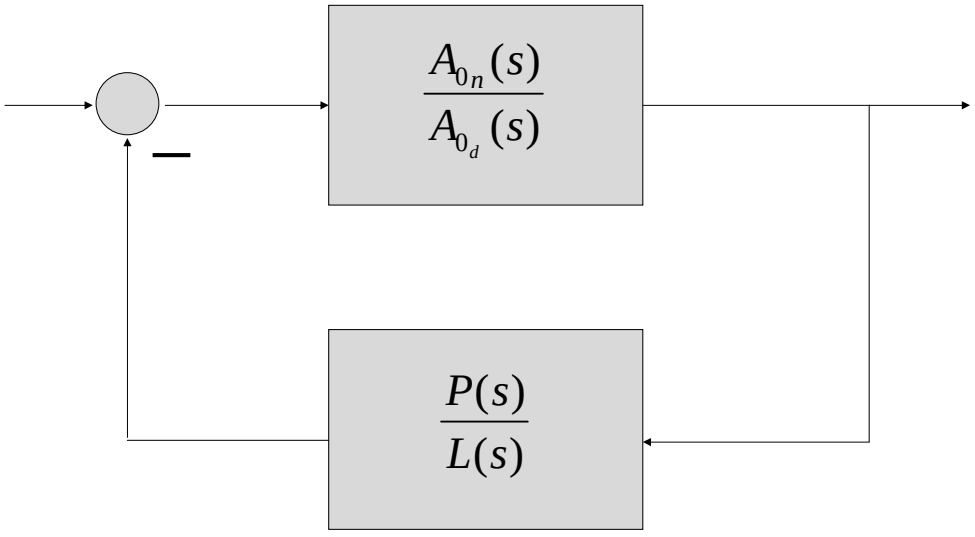

Figure 4.1: Block diagram of pole placement method.

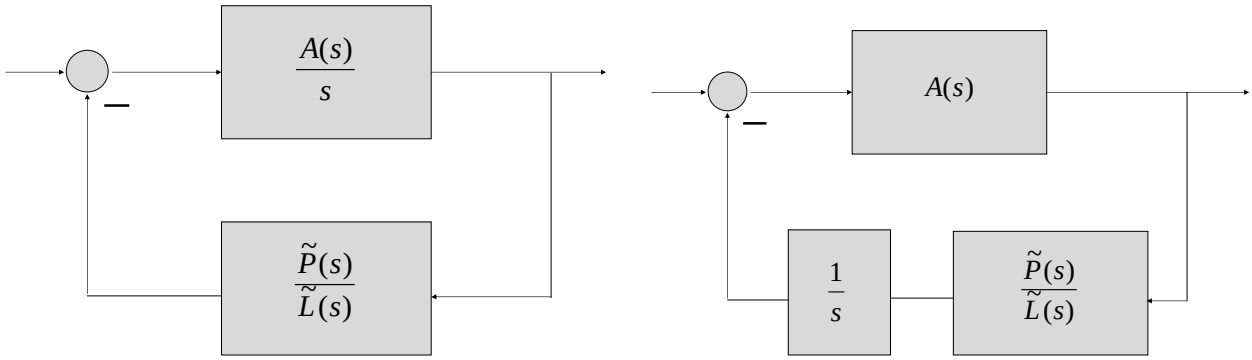

(a) (b)

Figure 4.2: Block Diagrams

Stability Check

Notice that the design of the dynamic compensator is based on our knowledge of the nominal plant $A_0(s)$. The bounds for the variation of the system parameters are known, but not the exact values of these parameters. The stability of the transfer function (4.17), or equivalently stability of the condition (4.6) can be checked by Kharitonov's Theorem. Towards that end, consider the set $\mathcal{I}(s)$ of real polynomials of degree n of the form

$$\delta(s) = \delta_0 + \delta_1 s + \delta_2 s^2 + \delta_3 s^3 + \cdots + \delta_n s^n \,,$$

where the coefficients lie within the given ranges:

$$\delta_0 \in [X_0, Y_0], \quad \delta_1 \in [X_1, Y_1], \quad \cdots, \delta_n \in [X_n, Y_n] \,.$$

Let $c_\delta = [\delta_0, \delta_1, \cdots, \delta_n]$ and consider the polynomial $\delta(s)$ with its coefficient vector c_δ. Introduce the hyper-rectangle box of the coefficients

$$\mathcal{B} := \left\{ c_\delta : c_\delta \in \mathbb{R}^{n+1},\ X_i \le \delta_i \le Y_i,\ i = 0, 1, \cdots, n \right\} \,.$$

It is assumed that the degree remains invariant over the family, so that $0 \notin [X_n, Y_n]$. Kharitonov's Theorem provides a (conservative) necessary and sufficient condition for Hurwitz stability of the entire family.

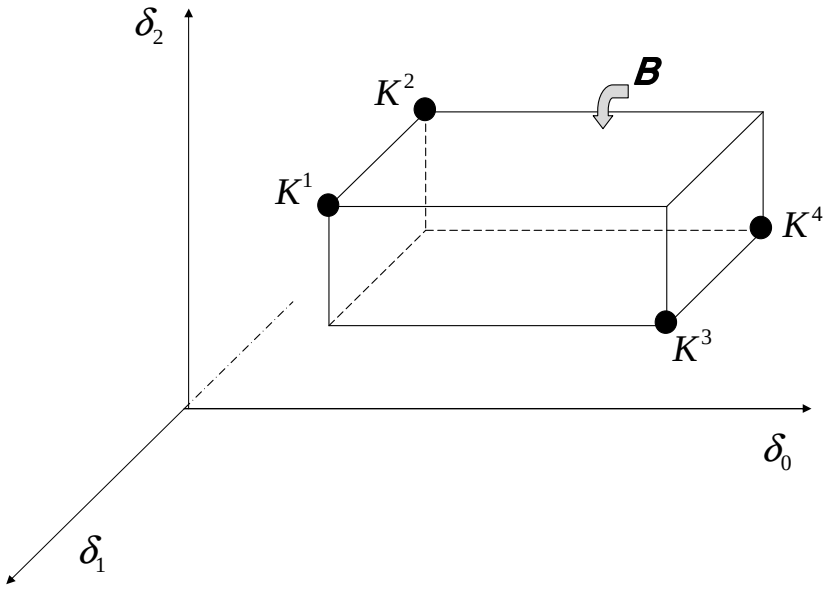

Figure 4.3: The box $\mathcal{B}$ and four Kharitonov vertices

Theorem 4 (Kharitonov Theorem) *[101]*

Every polynomial in the family $\mathcal{I}(s)$ is Hurwitz if and only if the following four extreme polynomials are Hurwitz:

$$\begin{aligned}
K^1(s) &= X_0 + X_1 s + Y_2 s^2 + Y_3 s^3 + X_4 s^4 + X_5 s^5 + Y_6 s^6 + \cdots, \\
K^2(s) &= X_0 + Y_1 s + Y_2 s^2 + X_3 s^3 + X_4 s^4 + Y_5 s^5 + Y_6 s^6 + \cdots, \\
K^3(s) &= Y_0 + X_1 s + X_2 s^2 + Y_3 s^3 + Y_4 s^4 + X_5 s^5 + X_6 s^6 + \cdots, \\
K^4(s) &= Y_0 + Y_1 s + X_2 s^2 + X_3 s^3 + Y_4 s^4 + Y_5 s^5 + X_6 s^6 + \cdots.
\end{aligned}$$

Proof of this theorem is omitted. To show the relationship between the box $\mathcal{B}$ and the vertices corresponding to extreme polynomials, a plot is shown for a family of second order polynomials [102], Figure 4.3.

Considering the bounds of parametric variations in $A(s)$ in (4.20) upon designing $C(s)$ and $M(s)$, the variation range $[X_i, Y_i]$, $i = 0, 1, \cdots, n$ of each coefficient of the polynomial $H_d(s)$ can be obtained. Substituting X_i and Y_i into the four extreme polynomials, we only need to check the stability of these four polynomials. If these four polynomials are stable, the

designed $C(s)$ and $M(s)$ are acceptable for verification of the condition in (4.6).

Upon the design of transfer functions $C(s)$ and $M(s)$, the condition (4.7) needs to be checked. This follows from the same procedure of the results in Cao and Hovakimyan [3, 6, 7].

4.2.2 Performance

The second step is to ensure satisfactory performance. Upon determining the structure of $M(s)$ and $C(s)$, which can satisfy the sufficient conditions for stability, it is possible to tune the parameters of $M(s)$ and $C(s)$ within the acceptable parameter space to achieve satisfactory performance. The tuning of parameters for $M(s)$ follows from conventional linear systems theory, which is omitted here. The guideline for tuning the low-pass filter $C(s)$ follows the same lines of Cao and Hovakimyan [6, 7]. The trade-off between the time-delay margin and the performance of the $\mathcal{L}_1$ adaptive controller depends solely upon $C(s)$. Increasing the bandwidth of $C(s)$ leads to improved performance at the price of reduced time-delay margin. In [78], constrained optimization of the performance and/or the robustness of $\mathcal{L}_1$ adaptive controller is studied by resorting to appropriate Linear Matrix Inequality (LMI) type conditions. If the corresponding LMI has a solution, then arbitrary desired performance bound can be achieved, while retaining a prespecified lower-bound on the time-delay margin.

In summary, to gain more freedom in design, it is important for designers to find the largest possible acceptable parameter space in the first step discussed in section 4.2.1.

4.3 Flight Control Example - Missile Longitudinal Autopilot: Scenario One

This section presents the application of the $\mathcal{L}_1$ output feedback adaptive controller to longitudinal autopilot design for a missile in the presence of uncertainties in system dynamics. The uncertainties include parametric variations in the transfer function and time-varying

disturbances. The parametric variations of the system's transfer function are caused by changes in aerodynamic coefficients. The missile model, taken from Mracek and Ridgely [103], is an unstable non-minimum phase system. The nominal optimal controller in Mracek and Ridgely [103] uses both system outputs (pitch rate and normal acceleration) to compute the feedback control signal. In this example the baseline controller is incorporated into plant dynamics to form a reference system. For augmentation purpose, the $\mathcal{L}_1$ adaptive output feedback controller is applied to the baseline controlled system, which is a stable but non-minimum phase system.

The longitudinal dynamics of a missile is considered in the presence of uncertainties in aerodynamics and time varying disturbances. The nominal optimal controller from Mracek and Ridgely [103], which is a "classic" three-loop topology autopilot designed by LQR methods, is introduced first. Then it is shown that the $\mathcal{L}_1$ output feedback adaptive controller can recover the nominal performance, defined by baseline controller, in the presence of uncertainties. For this adaptive controller, the selected reference system, which is a transfer function with desired step tracking response, does not satisfy the Strict Positive Realness (SPR) requirement.

4.3.1 System Dynamics

The missile's longitudinal dynamics can be described using the short period approximation of the longitudinal equations of motion [103]:

$$\dot{x}_p(t) = A_p x_p(t) + B_p \delta_p(t) \tag{4.23}$$

$$y_p(t) = C_p x_p(t) + D_p \delta_p(t) \tag{4.24}$$

$$y(t) = A_{z_m}(t)\,, \tag{4.25}$$

where $\delta_p(t)$ is the elevator input, $x_p(t)$ and $y_p(t)$ are the state and the output vectors respectively, given by

$$x_p(t) = \begin{bmatrix} \alpha(t) \\ q(t) \end{bmatrix}, \quad y_p(t) = \begin{bmatrix} A_{z_m}(t) \\ q_m(t) \end{bmatrix}, \tag{4.26}$$

while $\alpha(t)$ is angle of attack, $q(t)$ is pitch rate, $A_{z_m}(t)$ is normal acceleration and $q_m(t)$ is measured pitch rate. In (4.23) and (4.24) the system matrices are

$$A_p = \begin{bmatrix} \frac{1}{V_{m_0}} \left[\frac{\bar{Q}SC_{z_{\alpha 0}}}{m} - A_{X_0} \right] & 1 \\ \frac{\bar{Q}SdC_{m_{\alpha 0}}}{I_{YY}} & 0 \end{bmatrix}, \qquad B_p = \begin{bmatrix} \frac{\bar{Q}SC_{z_{\delta p_0}}}{mV_{m_0}} \\ \frac{\bar{Q}SdC_{m_{\delta p_0}}}{I_{YY}} \end{bmatrix},$$

$$C_p = \begin{bmatrix} \frac{\bar{Q}SC_{z_{\alpha 0}}}{mg} - \frac{\bar{Q}SdC_{m_{\alpha 0}}\bar{x}}{gI_{YY}} & 0 \\ 0 & 1 \end{bmatrix}, \qquad D_p = \begin{bmatrix} \frac{\bar{Q}SC_{z_{\delta p_0}}}{mg} - \frac{\bar{Q}SdC_{m_{\delta p_0}}\bar{x}}{gI_{YY}} \\ 0 \end{bmatrix}.$$

The numerical values of the simulation example in this section are listed in Table 4.1, and are taken from Mracek and Ridgely [103]. In this work, we consider uncertainties in the aerodynamic coefficients $C_{z_{\alpha 0}}$, $C_{m_{\alpha 0}}$, $C_{z_{\delta p_0}}$ and $C_{m_{\delta p_0}}$. These uncertainties do not satisfy the restrictive "matching condition" required by state feedback adaptive control schemes. Therefore the output feedback adaptive method from Cao and Hovakimyan [11] is applied. Time-varying disturbance, which enters the system at the same location as acceleration command $r(t)$ does, is considered. This disturbance, denoted by $d(t, y)$, possibly comes from uncertainties of guidance loop. We will show an illustration of the topology of the disturbance $d(t, y)$ and the baseline controller shortly.

It is assumed that the maximum possible variations of aerodynamic coefficients with respect to nominal values are known conservatively:

$$\|\Delta C_{z_{\alpha 0}}\| \leq 0.5 \cdot \|C_{z_{\alpha 0}}\|, \qquad \|\Delta C_{m_{\alpha 0}}\| \leq 0.5 \cdot \|C_{m_{\alpha 0}}\|,$$
$$\|\Delta C_{z_{\delta p_0}}\| \leq 0.5 \cdot \|C_{z_{\delta p_0}}\|, \qquad \|\Delta C_{m_{\delta p_0}}\| \leq 0.5 \cdot \|C_{m_{\delta p_0}}\|,$$

while the exact values of these coefficients are unknown. In simulations, the actual values of the aerodynamic coefficients are selected to be

$$C'_{z_{\alpha_0}} = 1.4 \cdot C_{z_{\alpha_0}}, \quad C'_{m_{\alpha_0}} = 1.5 \cdot C_{m_{\alpha_0}}, \quad C'_{z_{\delta_{p_0}}} = 0.8 \cdot C_{z_{\delta_{p_0}}}, \quad C'_{m_{\delta_{p_0}}} = 0.8 \cdot C_{m_{\delta_{p_0}}}. \tag{4.27}$$

Table 4.1: Numerical Values of Model

Variable	Value	Units	Description
V_{m_0}	3350	ft/sec	Total Missile Velocity
m	11.1	slug	Total Missile Mass
I_{YY}	137.8	slug $-$ ft^2	Pitch Moment of Inertia
$\bar{x}$	1.2	ft	Distance from CG to IMU Positive Forward
A_{X_0}	-60	ft/sec^2	Axial Acceleration Positive Forward
$C_{z_{\alpha 0}}$	-5.5313	-	Pitch Force Coefficient due to Angle of Attack
$C_{m_{\alpha 0}}$	6.6013	-	Pitch Moment Coefficient due to Angle of Attack
$C_{z_{\delta_{p_0}}}$	-1.2713	-	Pitch Force Coefficient due to fin Deflection
$C_{m_{\delta_{p_0}}}$	-7.5368	-	Pitch Moment Coefficient due to fin Deflection
$\bar{Q}$	13332	lb/ft^2	Dynamic Pressure
S	0.5454	ft^2	Reference Area
d	0.8333	ft	Reference Length
g	32.174	ft/sec^2	Gravity Constant

The control objective is to design an adaptive output feedback controller to achieve satisfactory tracking performance for the output $A_{z_m}(t)$, in the presence of parametric uncertainties and time varying disturbances.

4.3.2 Controller Design

LQR Solution

First the "classical" three-loop topology for the nominal controller design [103] is shown, assuming that the required output signals in the three-loop topology are available. The system is augmented by considering $z(t) = \delta_p(t)$ as an additional state:

$$\begin{aligned} \dot{x}_1(t) &= A_1 x_1(t) + B_1 u(t) \\ y_1(t) &= C_1 x_1(t)\,, \end{aligned} \tag{4.28}$$

where

$$x_1(t) = \begin{bmatrix} \alpha(t) \\ q(t) \\ z(t) \end{bmatrix}, \qquad u(t) = \dot{\delta}_p(t), \qquad y_1(t) = \begin{bmatrix} A_{z_m}(t) \\ q_m(t) \\ \dot{q}_m(t) \end{bmatrix}, \tag{4.29}$$

and the transformed state space matrices are

$$A_1 = \begin{bmatrix} A_p & B_p \\ [0] & 0 \end{bmatrix}, \qquad B_1 = \begin{bmatrix} [0] \\ 1 \end{bmatrix}, \qquad C_1 = \begin{bmatrix} C_p & D_p \\ A_p(2,:) & B_p(2,:) \end{bmatrix}. \tag{4.30}$$

The optimal Linear Quadratic Regulator (LQR) solution in [103] is given by:

$$u(t) = \dot{\delta}_p(t) = K_{opt} \begin{bmatrix} A_{z_m}(t) - K_{ss} r_0 \\ q_m(t) \\ \dot{q}_m(t) \end{bmatrix}, \tag{4.31}$$

where K_{ss} is chosen to ensure zero steady-state error for step commands, while r_0 is the steady-state value of the reference command $r(t)$. Based on the nominal numerical values

given in Table 4.1, the optimal controller gains are:

$$K_{opt} = [-1.3028 \;\; 11.7544 \;\; 0.3277], \quad K_{ss} = 1.0855. \tag{4.32}$$

In the current setup, $\dot{q}_m(t)$ is not measurable, and the above computed optimal controller is actually the derivative of $\delta_p(t)$. Since this is a linear system, both sides of (4.31) can be integrated to determine $\delta_p(t)$ (assuming constant gains) as:

$$\delta_p(t) = K_{opt} \begin{bmatrix} \int_0^t \left(A_{z_m}(\tau) - K_{ss} r_0\right) d\tau \\ \int_0^t q_m(\tau) d\tau \\ \int_0^t \dot{q}_m(\tau) d\tau \end{bmatrix} = K_{opt} \begin{bmatrix} \int_0^t \left(A_{z_m}(\tau) - K_{ss} r_0\right) d\tau \\ \int_0^t q_m(\tau) d\tau \\ q_m(t) \end{bmatrix}. \tag{4.33}$$

Augmentation of the Baseline Controller

Denote

$$K_{I_A} = K_{opt}(1), \;\; K_\theta = K_{opt}(2), \;\; K_q = K_{opt}(3).$$

The control input for elevator $\delta_p(t)$ is

$$\delta_p(t) = [0 \;\; K_q] y_p(t) + x_c(t),$$

where the additional state $x_c(t)$ is obtained from

$$\begin{aligned} \dot{x}_c(t) &= K_\theta q_m(t) + K_{I_A} \left[K_{ss}(u_{ad}(t) + d(t, y(t))) - A_{z_m}(t)\right] \\ &= [-K_{I_A} \;\; K_\theta] y_p(t) + K_{I_A} K_{ss} u_{ad}(t) \end{aligned}$$

with $d(t, y(t))$ being a time-varying disturbance dependent on the system output. The disturbance satisfies Assumption 4. This disturbance may come from the uncertainties in the guidance loop. The topology of this controller structure is shown in Figure 4.4. It is straight-

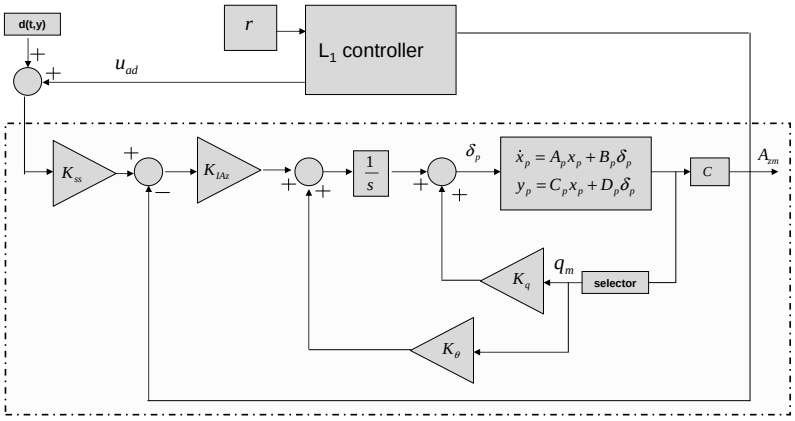

Figure 4.4: Topology of adaptive augmentation to baseline

forward to derive the following partially closed loop system dynamics:

$$\begin{bmatrix} \dot{x}_p(t) \\ \dot{x}_c(t) \end{bmatrix} = \underbrace{\begin{bmatrix} A_p + B_p K_{c0} C_p & B_p \\ K_{c1}[\mathbb{I} + D_p K_{c0}] C_p & K_{c1} D_p \end{bmatrix}}_{A_2} \underbrace{\begin{bmatrix} x_p(t) \\ x_c(t) \end{bmatrix}}_{x_2(t)} + \underbrace{\begin{bmatrix} 0 \\ K_{I_A} K_{ss} \end{bmatrix}}_{B_2} [u_{ad}(t) + d(t, y(t))]$$

$$y(t) = \underbrace{[C_p(1,:) + D_p(1,:) K_{c0} C_p \quad D_p(1,:)]}_{C_2} \begin{bmatrix} x_p(t) \\ x_c(t) \end{bmatrix}, \tag{4.34}$$

where $K_{c0} = [0 \;\; K_q]$ and $K_{c1} = [-K_{I_A} \;\; K_\theta]$. The transfer function from u_{ad} to y in system (4.34), denoted by $A(s)$, is a stable and non-minimum phase system.

$\mathcal{L}_1$ Adaptive Output Feedback Control Design

In system (4.34), the longitudinal dynamics of the missile can be presented in the following form:

$$y(s) = A(s)\left[u_{ad}(s) + d(s)\right], \quad y(0) = 0, \tag{4.35}$$

where $u_{ad}(t) \in \mathbb{R}$ is the input to the partially closed loop system, $y(t) = A_{z_m}(t) \in \mathbb{R}$ is the system output, $A(s) = C_2^\top (s\mathbb{I} - A_2)^{-1} B_2$ is the unknown transfer function of the system, $d(s)$ is the Laplace transform of the time-varying disturbances in (4.34). Substituting the numerical values from Table 4.1 and K_{opt} into the system in (4.34), the nominal system of

$A(s)$ is obtained

$$A_0(s) = \frac{A_{0_n}}{A_{0_d}} = \frac{-19.13s^2 + 23.06s + 63410}{s^3 + 92.09s^2 + 3767s + 63410}. \tag{4.36}$$

For this example, we show two methods of selection for $M(s)$ and $C(s)$. The first method is based on observation and trial, and the second one is the pole placement method we have discussed. It is shown that these two methods can have similar performance. However, for an unstable and non-minimum phase system, observation and trial method can hardly work, and we have to apply the pole placement method for design of $M(s)$ and $C(s)$, as shown in later section.

Method One

The plant $A(s)$ has desired dynamics since it is obtained by including baseline controller in the dynamics. However, the system $M(s)$ needs to be stable and minimum phase. Hence we use the denominator of $A(s)$ as the denominator of $M(s)$, and for the numerator of $M(s)$ we only keep the constant term of the numerator of $A(s)$. Next, we construct a second order low-pass filter $C(s)$, and tune its bandwidth. The final selection of $M(s)$ and $C(s)$ are:

$$M(s) = \frac{63410}{s^3 + 92.09s^2 + 3767s + 63410}, \tag{4.37}$$

$$C(s) = \frac{3000}{s^2 + 46.56s + 3000}, \tag{4.38}$$

and one can verify from (4.20) that $H(s)$ is stable.

Method Two

When designing the dynamic compensator $\frac{P(s)}{L(s)}$ for the system $\frac{A_0(s)}{s}$ via pole placement method, we can choose the desired pole locations following the controller design for cart-pendulum system. We first start with the desired pole locations $-27 \pm 31j$, $-27 \pm 31j$, -36, -36 and -36, then

$$A_{cl}(s) = s^7 + 216s^6 + 21848s^5 + 1.3\text{E}06s^4 + 5.2\text{E}07s^3 + 1.3\text{E}09s^2 + 1.9\text{E}10s + 1.3\text{E}11\,.$$

The Sylvester Matrix is determined by the coefficients of $A_{0_n}(s)$ and $sA_{0_d}(s)$. The vectors

containing the coefficients of $A_{0_n}(s)$ and $sA_{0_d}(s)$, respectively, are shown below

$$[0 \quad -19.125 \quad 23.055 \quad 63406]^\top, \qquad [1 \quad 92.092 \quad 3766.8 \quad 63406 \quad 0]^\top.$$

The Sylvester Matrix S_l is

$$S_l = \begin{bmatrix} 1 & 0 & 0 & 0 & 0 & 0 & 0 & 0 \\ 92.092 & 1 & 0 & 0 & 0 & 0 & 0 & 0 \\ 3766.8 & 92.092 & 1 & 0 & -19.125 & 0 & 0 & 0 \\ 63406 & 3766.8 & 92.092 & 1 & 23.055 & -19.125 & 0 & 0 \\ 0 & 63406 & 3766.8 & 92.092 & 63406 & 23.055 & -19.125 & 0 \\ 0 & 0 & 63406 & 3766.8 & 0 & 63406 & 23.055 & -19.125 \\ 0 & 0 & 0 & 63406 & 0 & 0 & 63406 & 23.055 \\ 0 & 0 & 0 & 0 & 0 & 0 & 0 & 63406 \end{bmatrix}$$

The following algebraic equation

$$\beta_l = {S_l}^{-1}\alpha_l$$

can be solved to get the vector β_l:

$$\beta_l = [1 \quad 123.91 \quad 7304.4 \quad 1.8\text{E}05 \quad 33.152 \quad 3052 \quad 1.25\text{E}05 \quad 2.1\text{E}06]^\top,$$

where α_l is the vector of the coefficients of $A_{cl}(s)$.

The first four elements of β_l are the coefficients of $L(s)$, and the rest of the elements are the coefficients of $P(s)$. Hence,

$$L(s) = s^3 + 123.91s^2 + 7304s + 1.8\text{E}05,$$

$$P(s) = 33.152s^3 + 3052s^2 + 1.2\text{E}05s + 2.1\text{E}06.$$

If $C(s)$ is selected to be a fourth order, relative degree 4 transfer function, and $M(s)$ be third order, relative degree 3 transfer function, the transfer function in (4.22) can be written explicitly. The coefficients of $M(s)$ and $C(s)$ are obtained by equating (4.22) to $\frac{1}{s}\frac{P(s)}{L(s)}$. This

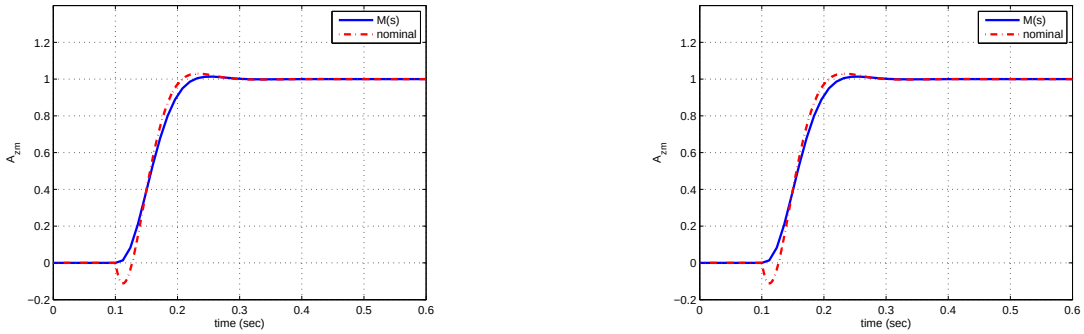

(a) Method one (b) Method two

Figure 4.5: Step response of $M(s)$

generates the initial guess values for $M(s)$ and $C(s)$. After several iterations for selecting coefficients of $M(s)$ and $C(s)$, the final transfer functions are:

$$M(s) = \frac{2.1\text{E}04}{0.3315s^3 + 30.52s^2 + 1248s + 2.1\text{E}04}, \tag{4.39}$$

$$C(s) = \frac{7.5\text{E}09}{s^4 + 2790s^3 + 2.5\text{E}06s^2 + 1.99\text{E}08s + 7.5\text{E}09}. \tag{4.40}$$

This selection of $M(s)$ and $C(s)$ generate satisfactory performance according to simulation results shown below.

The design process can become more complicated if the system $A(s)$ is unstable and non-minimum phase. This is shown in the example of Section 4.4.

4.3.3 Simulation Results

The sampling time is chosen as $T = 0.001$. Figure 4.5 shows the step response of $M(s)$ for both methods (one and two). They are also compared to the response of nominal performance defined by baseline controller. It can be seen that the selected reference systems $M(s)$ for both cases have satisfactory response.

The time-varying disturbance is set

$$d(t, y(t)) = 0.1y(t) + 0.2\sin(0.3t),$$

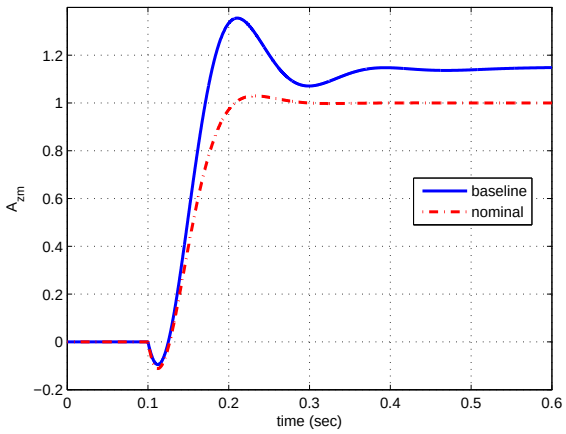

Figure 4.6: Baseline control with uncertainties.

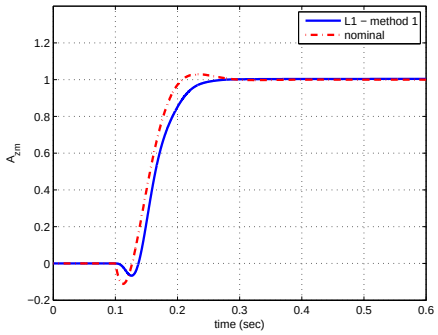

(a) Method one

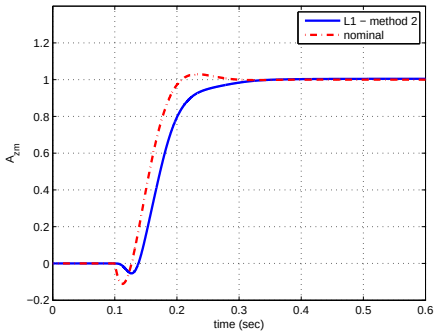

(b) Method two

Figure 4.7: Performance of $\mathcal{L}_1$ control

which deteriorates the performance of baseline controlled system, as shown in Figure 4.6

Then $\mathcal{L}_1$ adaptive output feedback controller is applied to the system in the presence of uncertainties, Figure 4.7. Both of the two methods can recover the nominal performances. The adaptive control signal is shown in Figure 4.8.

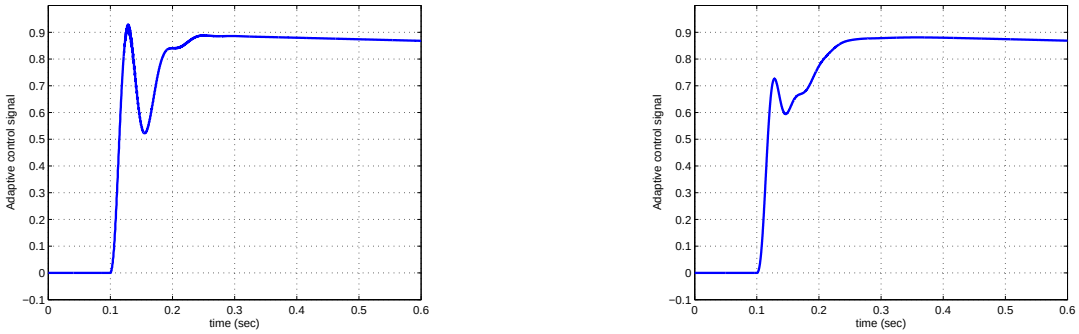

(a) Method one (b) Method two

Figure 4.8: Control signal of $\mathcal{L}_1$ control

Looking into the closed loop reference system (4.5), it can be shown that

$$\begin{aligned} y_{ref}(s) &= M(s)\left[C(s)r(s) + (1-C(s))\sigma_{ref}(s)\right] \\ &= M(s)\Big[C(s)r(s) + \frac{C(s)(1-C(s))(A(s)-M(s))}{M(s)+(A(s)-M(s))C(s)}r(s) + \\ &\quad \frac{(1-C(s))A(s)}{M(s)+(A(s)-M(s))C(s)}d(s)\Big]. \end{aligned}$$

The transfer function from $d(s)$ to $y_{ref}(s)$ can be expressed as

$$\frac{(C_d(s)-C_n(s))A_n(s)M_n(s)}{(C_d(s)-C_n(s))A_d(s)M_n(s)+A_n(s)M_d(s)C_n(s)}. \tag{4.41}$$

For the case of method one, the magnitude curve of the Bode diagram of the transfer function from $d(s)$ to $y_{ref}(s)$ is given in Figure 4.9, which shows disturbance attenuation at low and high frequencies. This behavior of the reference system can be improved by manipulating the bandwidths of $M(s)$ and $C(s)$.

Finally the parametric uncertainties are changed due to the change in the aerodynamic coefficients given below:

$$C'_{z_{\alpha_0}} = 1.2 \cdot C_{z_{\alpha_0}}, \quad C'_{m_{\alpha_0}} = 1.4 \cdot C_{m_{\alpha_0}}, \quad C'_{z_{\delta_{p_0}}} = 0.8 \cdot C_{z_{\delta_{p_0}}}, \quad C'_{m_{\delta_{p_0}}} = 0.8 \cdot C_{m_{\delta_{p_0}}}, \tag{4.42}$$

and the time-varying disturbance is changed to:

$$d(t, y(t)) = 0.2y(t) + 0.5\sin(0.1t).$$

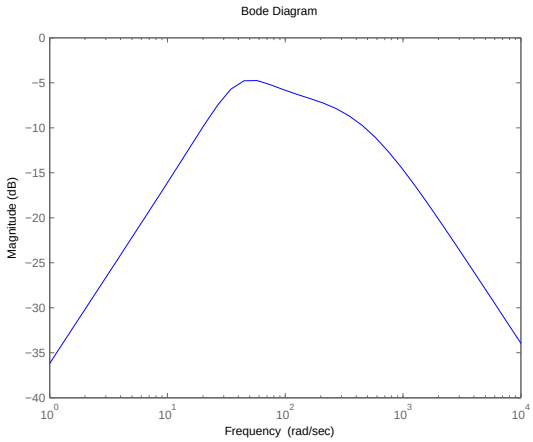

Figure 4.9: Frequency response of transfer function from d to y_{ref} - method one

The system output is shown in Figure 4.10. It can be seen that the $\mathcal{L}_1$ adaptive output feedback control has uniform performance.

4.4 Flight Control Example - Missile Longitudinal Autopilot: Scenario Two

In this example, the problem setup and the system dynamics are the same as in scenario one in Section 4.3, except that the only measurable feedback signal is the acceleration $A_{z_m}(t)$, and the time-varying disturbance enters the system at the same place with the elevator input $\delta_p(t)$. In this scenario, the $\mathcal{L}_1$ output feedback adaptive controller needs to control an unstable, non-minimum phase system, which brings additional challenges to the design. Since the only available feedback signal is the acceleration, the original baseline controller described in the previous section cannot be applied. For comparison purposes, we design a Linear Quadratic Gaussian (LQG) controller with Loop Transfer Recovery (LTR) design to recover the robustness of the baseline LQR controller. This serves as the nominal output feedback controller in the absence of uncertainties. In the presence of uncertainties, the nominal

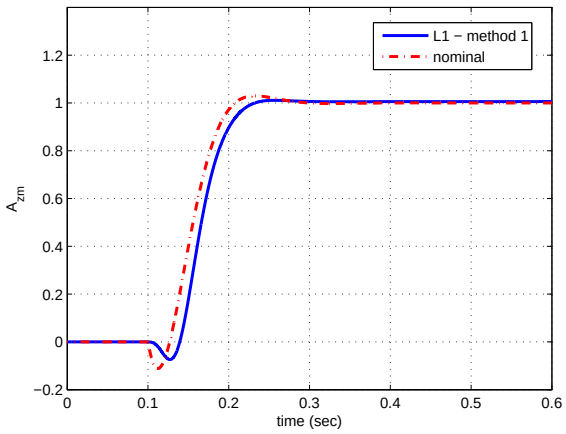

Figure 4.10: Closed loop response of $\mathcal{L}_1$ controller with different uncertainties

performance defined by the LQG with LTR controller deteriorates, and the maximum amount of recoverable robustness of the baseline LQG controller is limited due to the unstable zero of the missile system. On the other hand, the $\mathcal{L}_1$ adaptive controller has uniform performance independent of the nature of uncertainties, which is beneficial under detrimental conditions, e.g., unavailability of certain feedback signals as in current scenario.

4.4.1 System Dynamics

The missile's longitudinal dynamics are described as:

$$\dot{x}_p(t) = A_p x_p(t) + B_p \left[\delta_p(t) + v(t, y(t))\right] \tag{4.43}$$

$$y_p(t) = C_p x_p(t) + D_p \left[\delta_p(t) + v(t, y(t))\right] \tag{4.44}$$

$$y(t) = A_{z_m}(t)\,, \tag{4.45}$$

where $v(t, y(t))$ is time-varying disturbance and depends on $y(t)$. Other signals and matrices are defined in (4.23) and (4.24).

The system is augmented by considering $z(t) = \delta_p(t) + v(t, y(t))$ as an additional state, and

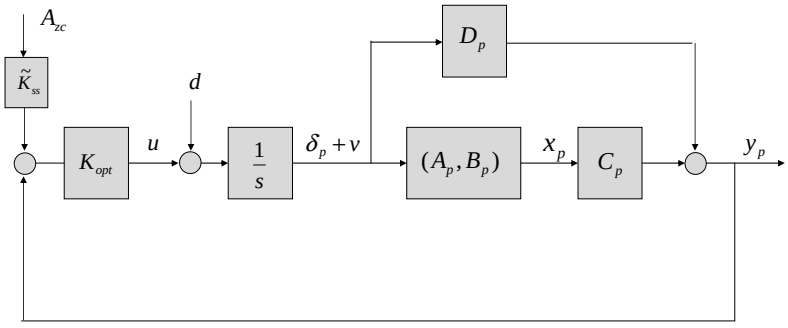

Figure 4.11: Block diagram of system.

the system in (4.28) takes the form

$$\begin{aligned} \dot{x}_1(t) &= A_1 x_1(t) + B_1 \left(u(t) + d(t, y(t))\right) \\ y_1(t) &= C_1 x_1(t)\,, \end{aligned} \tag{4.46}$$

where

$$x_1(t) = \begin{bmatrix} \alpha(t) \\ q(t) \\ z(t) \end{bmatrix}, \quad u(t) = \dot{\delta}_p(t), \quad d(t, y(t)) = \dot{v}(t, y(t)), \quad y_1(t) = \begin{bmatrix} A_{z_m}(t) \\ q_m(t) \\ \dot{q}_m(t) \end{bmatrix}, \tag{4.47}$$

and the transformed state space matrices are

$$A_1 = \begin{bmatrix} A_p & B_p \\ [0] & 0 \end{bmatrix}, \quad B_1 = \begin{bmatrix} [0] \\ 1 \end{bmatrix}, \quad C_1 = \begin{bmatrix} C_p & D_p \\ A_p(2,:) & B_p(2,:) \end{bmatrix}. \tag{4.48}$$

Notice that we assume that the disturbance $d(t, y(t))$ satisfies Assumption 4. A block diagram of the plant and the controller structure is shown in Figure 4.11. The controller gains K_{ss} and K_{opt} are the same as in (4.32).

4.4.2 Control Design

Output Feedback Solution: LQG/LTR

Based on the LQR solution of the above nominal optimal controller, we can design a Linear Quadratic Gaussian (LQG) with Loop Transfer Recovery (LTR) controller using only the

output A_{z_m}. Since the LQR controller is ready, we only need to design the Kalman filter, which can help to recover the robustness of the LQR controller. We note that due to the non-minimum phase property of the system, the robustness recovery is limited.

In Mracek and Ridgely [103], the LQR design is based on the transformed system with state transformation $x_2 = C_1 x_1$, as shown below

$$\begin{aligned} \dot{x}_2(t) &= A_2 x_2(t) + B_2 u(t), \\ y_2(t) &= x_2(t) \end{aligned} \tag{4.49}$$

where

$$x_2(t) = \begin{bmatrix} A_{z_m}(t) \\ q_m(t) \\ \dot{q}_m(t) \end{bmatrix}, \qquad A_2 = C_1 A_1 C_1^{-1}, \qquad B_2 = C_1 B_1.$$

We design Kalman filter based on this LQR solution. We consider the system structure

$$\begin{aligned} \dot{x}_2(t) &= A_2 x_2(t) + B_2 u(t) + B_2 \omega(t) \\ y_k(t) &= A_{z_m}(t) = [1 \quad 0 \quad 0] x_2(t) + v(t), \end{aligned} \tag{4.50}$$

where the plant noise $\omega(t)$ and the measurement noise $v(t)$ are white noise with the spectral densities S_ω and S_v respectively, and they are uncorrelated and orthogonal. Furthermore, the plant noise and the initial states of the system (4.50) are assumed to be uncorrelated and orthogonal; so are the measurement noise and the states. The Kalman filter equation is

$$\dot{\hat{x}}_2(t) = A_2 \hat{x}_2(t) + B_2 u(t) + G\left(y_k(t) - [1 \quad 0 \quad 0]\hat{x}_2(t)\right), \tag{4.51}$$

where G is the Kalman gain. The Loop Transfer Recovery design is done by increasing the spectral density S_ω of the plant noise $\omega(t)$. We choose different values of S_ω to design the Kalman filter, and compare the results to the LQR results. The spectral density of the measurement noise is set as $S_v = 0.1$. The Kalman filter gain is obtained by MATLAB command "*kalman*". Next we show the system response of LQG/LTR control.

First, the unit step responses of the LQR and the LQG/LTR control are shown. In Figure 4.12, the LQG controller is designed with $S_\omega = 1$ and $S_v = 0.1$. It can be seen that

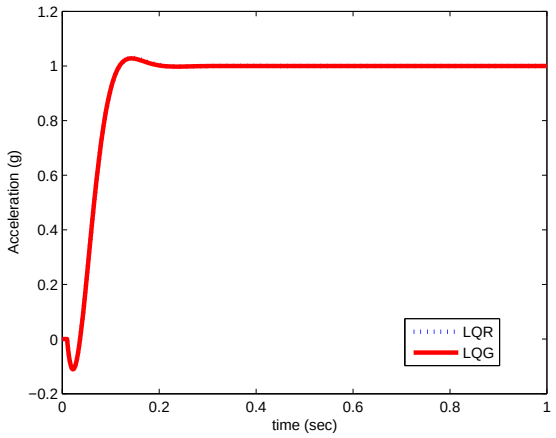

Figure 4.12: Comparison between LQR and LQG - no uncertainty, no disturbance

the time responses of these two controllers are identical. However, the robustness of these two controllers are different, due to the small value of the spectral density S_ω, which means that the loop transfer recovery is not enough. This can be seen in Figure 4.13. In this figure, additional parametric uncertainties in (4.27) are present. The LQR controller has certain inherent robustness to parametric uncertainties, hence its performance is acceptable. However, the LQG controller has degraded performance due to lack of robustness. We need to increase the spectral density S_ω to recover as much as possible the robustness of the LQR controller. In Figure 4.14, the spectral density is increased to 100, and we can see that the performance is improved in the presence of parametric uncertainties. This robustness recovery is limited by the system's non-minimum phase zero. Hence, increasing S_ω cannot recover the robustness completely, as shown in Figure 4.15. With very large value of S_ω, the system's performance is no better than that in the case of smaller S_ω.

We now introduce the disturbance $d(t) = 0.1\sin(0.5\pi t)$ into the system. In Figure 4.16, the system output under the LQR controller drifts from the desired steady state position. The performance of LQG/LTR is unacceptable. This is expected because of the limitation of the loop transfer recovery applied to a non-minimum phase system.

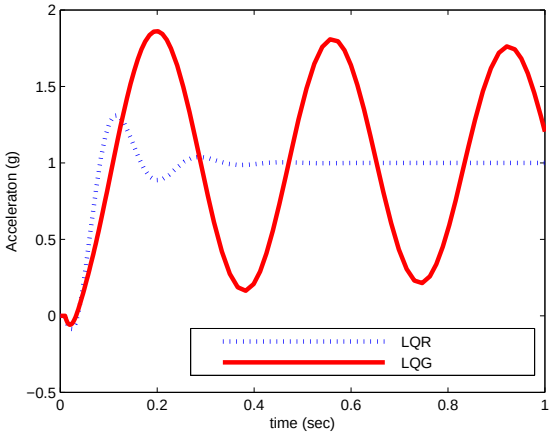

Figure 4.13: Comparison between LQR and LQG - with uncertainty, no disturbance

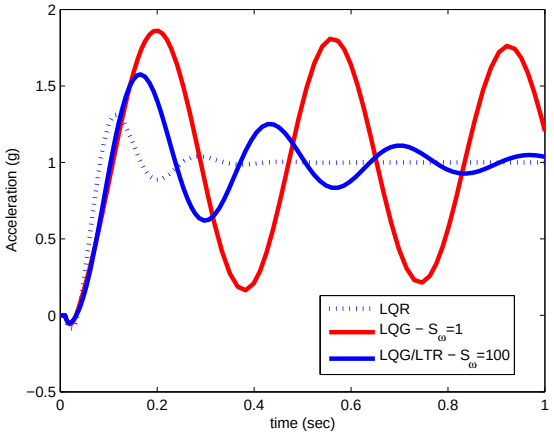

Figure 4.14: Comparison between LQR, LQG and LQG/LTR - with uncertainty, no disturbance

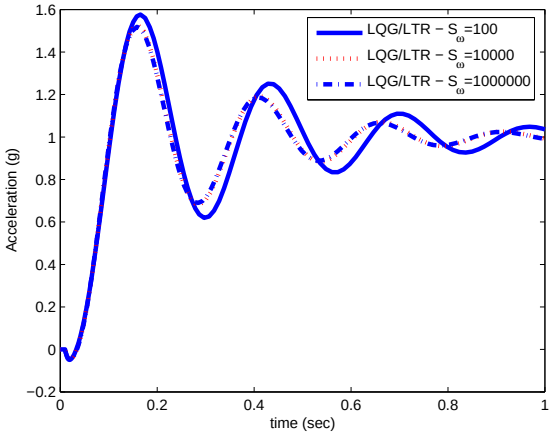

Figure 4.15: Different values of S_ω for LQG/LTR designs - with uncertainties, no disturbance

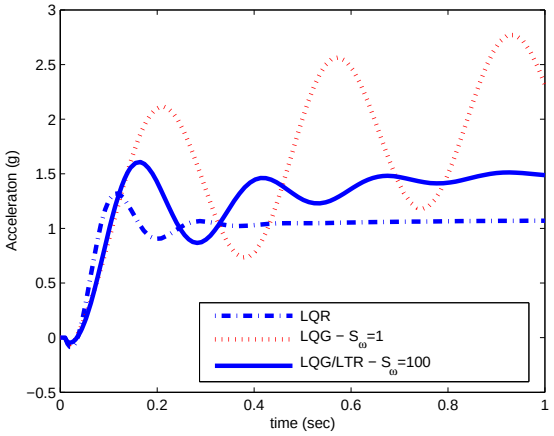

Figure 4.16: Comparison between LQR, LQG and LQG/LTR - with uncertainties and disturbance

$\mathcal{L}_1$ Adaptive Output Feedback Control Design

In the system (4.46), if we let $y(t) = C_1(1,:)x_1(t) = c^\top x_1(t) = A_{z_m}(t)$, the longitudinal dynamics of the missile can be presented in the following form:

$$y(s) = A(s)\left[u(s) + d(s)\right], \quad y(0) = 0\,, \tag{4.52}$$

where $u(t) = \dot{\delta}_p(t) \in \mathbb{R}$ is the input, $y(t) = A_{z_m}(t) \in \mathbb{R}$ is the system output, $A(s) = c^\top(s\mathbb{I} - A_1)^{-1}B_1$ is the unknown transfer function of the system, $d(s)$ is the Laplace transform of the time-varying disturbances in (4.46). Notice that $d(t, y)$ depends on the system output y, and the upper bound of the growth rate of $d(t, y)$ with respect to y is L, as stated in Assumption 4.

Substituting the numerical values from Table 4.1 into the system in (4.46), we get the nominal system of $A(s)$

$$A_0(s) = \frac{A_{0_n}}{A_{0_d}} = \frac{-13.51s^2 + 16.46s + 44800}{s^3 + 1.064s^2 - 290.3s}. \tag{4.53}$$

Since the system $A(s)$ is unstable and non-minimum phase, the method based on observation and trial can hardly work. We apply the pole placement method to design $M(s)$ and $C(s)$. Due to the limited choices of parameters for $M(s)$, the system performance is not as good as that defined by baseline LQR controller. However, as shown in simulation results, the $\mathcal{L}_1$ output feedback adaptive controller has better performance than LQG (LTR) controller does in the presence of uncertainties, and the $\mathcal{L}_1$-performance is uniform and independent of uncertainties provided the sufficient conditions for stability are satisfied.

We now show how to select $M(s)$ and $C(s)$ for the missile model. If we choose the desired pole locations as $-200 \pm 200j$, $-200 \pm 200j$, -20, -20 and -20, then

$$A_{cl}(s) = s^7 + 860s^6 + 3.7\text{E}05s^5 + 8.4\text{E}07s^4 + 1.0\text{E}10s^3 + 4.6\text{E}11s^2 + 8.2\text{E}12s + 5.1\text{E}13\,.$$

The Sylvester Matrix is determined by the coefficients of $A_{0_n}(s)$ and $sA_{0_d}(s)$. The vectors containing the coefficients of $A_{0_n}(s)$ and $sA_{0_d}(s)$, respectively, are shown below

$$[0 \quad -13.5 \quad 16.5 \quad 44796]^\top, \qquad [1 \quad 1.06 \quad -290.3 \quad 0 \quad 0]^\top.$$

The Sylvester Matrix S_l is

$$S_l = \begin{bmatrix} 1 & 0 & 0 & 0 & 0 & 0 & 0 & 0 \\ 1.06 & 1 & 0 & 0 & 0 & 0 & 0 & 0 \\ -290.3 & 1.06 & 1 & 0 & -13.5 & 0 & 0 & 0 \\ 0 & -290.3 & 1.06 & 1 & 16.5 & -13.5 & 0 & 0 \\ 0 & 0 & -290.3 & 1.06 & 44796 & 16.5 & -13.5 & 0 \\ 0 & 0 & 0 & -290.3 & 0 & 44796 & 16.5 & -13.5 \\ 0 & 0 & 0 & 0 & 0 & 0 & 44796 & 16.5 \\ 0 & 0 & 0 & 0 & 0 & 0 & 0 & 44796 \end{bmatrix}$$

We solve the following algebraic equation

$$\beta_l = {S_l}^{-1}\alpha_l$$

to get the vector β_l:

$$\beta_l = [1 \;\; 858 \;\; 4.6\text{E}06 \;\; 2.4\text{E}08 \;\; 3.1\text{E}05 \;\; 1.2\text{E}07 \;\; 1.8\text{E}08 \;\; 1.1\text{E}09]^\top,$$

where α_l is the vector of the coefficients of $A_{cl}(s)$.

The first four elements of β_l are the coefficients of $L(s)$, and the rest of the elements are the coefficients of $P(s)$. Hence,

$$L(s) = s^3 + 858s^2 + 4.6\text{E}06s + 2.4\text{E}08,$$

$$P(s) = 3.1\text{E}05s^3 + 1.2\text{E}07s^2 + 1.8\text{E}08s + 1.1\text{E}09.$$

If we select $C(s)$ to be a second order, relative degree 2 transfer function, and $M(s)$ be third order, relative degree 1 transfer function, we can write explicitly the transfer function in (4.22) and obtain the coefficients of $M(s)$ and $C(s)$ by equating (4.22) to $\frac{1}{s}\frac{P(s)}{L(s)}$. The transfer functions for $C(s)$ and $M(s)$ take the form:

$$M(s) = \frac{s^2 + 806s + 4.5\text{E}06}{s^3 + 39.02s^2 + 585s + 3665}, \tag{4.54}$$

$$C(s) = \frac{3.1\text{E}05}{s^2 + 52.61s + 3.1\text{E}05}. \tag{4.55}$$

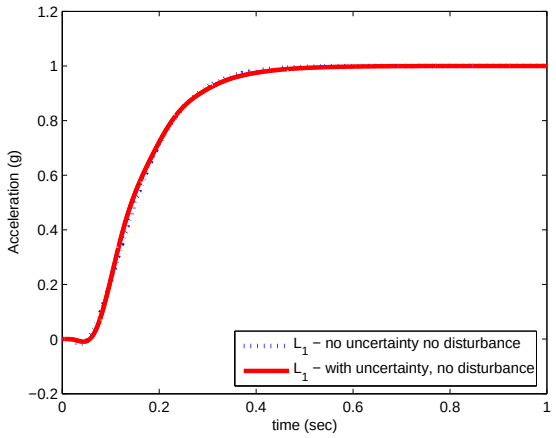

Figure 4.17: Closed loop response of $\mathcal{L}_1$ controller - with/without uncertainties, no disturbance

4.4.3 Simulation Results

We select $T = 0.0001$. The $\mathcal{L}_1$ output feedback adaptive control approach is applied to this system. Figure 4.17 shows the system outputs with $\mathcal{L}_1$ controller, in the absence and in the presence of parametric uncertainties. We can see that the system output tracks the step command satisfactorily. Although this response is different from that of the baseline LQR controller, we demonstrate later that in different unknown scenarios, the $\mathcal{L}_1$ controlled system still has a uniform response close to the one shown in Figure 4.17, independent of the nature of the uncertainty. This verifies the theoretical claim on uniform approximation of the corresponding signals of a bounded reference system. In Figure 4.18 the control signal is shown, which is guaranteed to stay in low frequency range.

The disturbance is then introduced, as shown in Figure 4.19. Since $d(t)$ does not depend on the system output $y(t)$, the condition in (4.7) is satisfied automatically. We see that the output response is slightly different than that of the nominal $\mathcal{L}_1$ case, but is still satisfactory.

Finally the parametric uncertainties are changed due to a change in aerodynamic coefficients

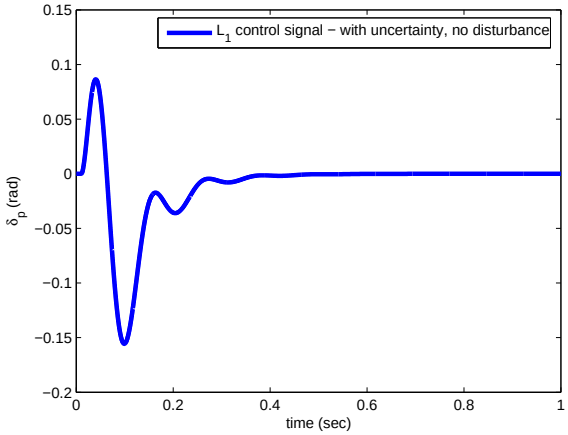

Figure 4.18: Control signal of $\mathcal{L}_1$ controller

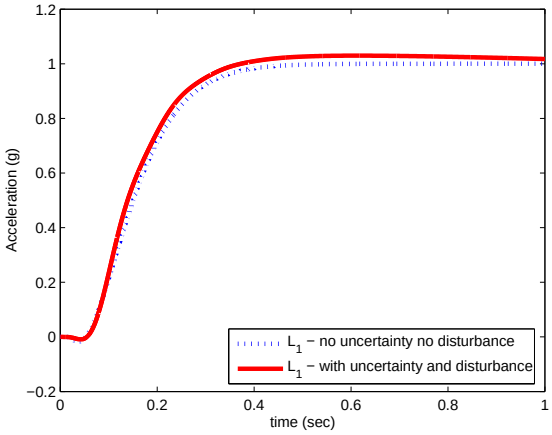

Figure 4.19: Closed loop response of $\mathcal{L}_1$ controller - with uncertainties and disturbance

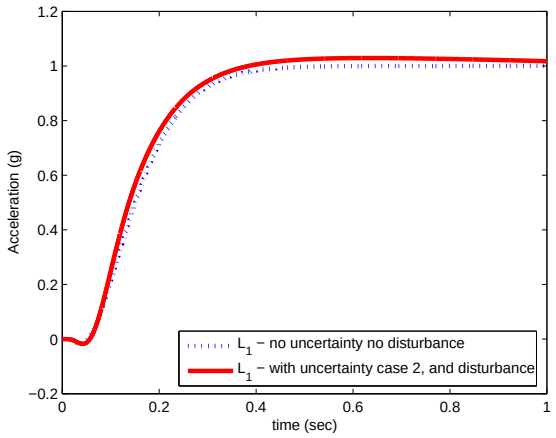

Figure 4.20: Closed loop response of $\mathcal{L}_1$ controller with different uncertainties

given below:

$$C'_{z_{\alpha_0}} = 1.2 \cdot C_{z_{\alpha_0}}, \quad C'_{m_{\alpha_0}} = 1.5 \cdot C_{m_{\alpha_0}}, \quad C'_{z_{\delta_{p0}}} = 0.8 \cdot C_{z_{\delta_{p0}}}, \quad C'_{m_{\delta_{p0}}} = 0.7 \cdot C_{m_{\delta_{p0}}}. \quad (4.56)$$

The system output is shown in Fig. 4.20. We can see that the $\mathcal{L}_1$ output feedback adaptive controller holds its uniform performance.

4.5 Conclusion

Longitudinal autopilot design for a missile model is performed using $\mathcal{L}_1$ adaptive output feedback controller, appropriate for non-SPR reference system dynamics. The new piecewise constant adaptive law along with the low-pass filtered control signal ensures uniform performance bounds for system's both input/output signals as compared to the corresponding signals of a non-SPR reference system. The simulation results demonstrate the benefits of the $\mathcal{L}_1$ adaptive controller.

Chapter 5

$\mathcal{L}_1$ State Feedback Adaptive Controller: Time-Varying Reference Systems

In this section we present the $\mathcal{L}_1$ adaptive controller for time-varying reference systems. This is important for augmentation of baseline gain-scheduled controller, which naturally leads to time-varying reference system. The objective of the adaptive augmentation is twofold. First, it aims to recover the nominal performance of the gain-scheduled controlled system at different operating points, without overruling the performance of the baseline controller. Second, the design of the adaptive augmentation should be pursued in a way so that in the absence of uncertainties the output of it is zero. Thus, the adaptive augmentation must include the dynamics of the closed-loop system, controlled by the baseline gain-scheduled controller, as a part of its feedback. The dynamics of the gain-scheduled controller change dependent upon the scheduling variables, resulting in a time-varying closed-loop reference system. To match the dynamics of the closed-loop baseline gain-scheduled controlled system, the reference system of the adaptive controller needs to be time-varying too. This motivates the study of $\mathcal{L}_1$ adaptive control for time-varying reference systems in this dissertation.

In this section, we analyze the stability and the performance of the $\mathcal{L}_1$ adaptive controller for a time-varying reference system. We further illustrate how the theory can be used for adaptive augmentation of a baseline gain-scheduled controller.

5.1 $\mathcal{L}_1$ Adaptive Control Problem Formulation

Consider a linear time-varying system:

$$\dot{x}(t) = A_m(t)x(t) + b(t)\left(\Lambda u(t) + \theta^\top(t)x(t) + \sigma(t)\right), \quad y(t) = c^\top x(t), \quad x(0) = x_0\,, \tag{5.1}$$

where $x(t) \in \mathbb{R}^n$ is the system state vector (measurable), $u(t) \in \mathbb{R}$ is the control signal, $y(t) \in \mathbb{R}$ is the regulated output, $b(t) \in \mathbb{R}^n$ is a known vector, $c \in \mathbb{R}^n$ is a known constant vector, $A_m(t)$ is a known $n \times n$ matrix which satisfies the point-wise eigenvalue condition, $\Lambda \in \mathbb{R}$ is an unknown constant with known sign, $\theta(t) \in \mathbb{R}^n$ is a vector of time-varying unknown parameters, while $\sigma(t) \in \mathbb{R}$ is a time-varying disturbance.

Assumption 5 *Without loss of generality, we assume that*

$$\Lambda \in \Omega_0 = [\omega_{l_0},\ \omega_{u_0}]\,, \quad \theta(t) \in \Theta, \quad |\sigma(t)| \le \Delta_0\,, \quad t \ge 0\,, \tag{5.2}$$

where $\omega_{u_0} > \omega_{l_0} > 0$ are given known upper and lower bounds, Θ is a known compact set and $\Delta_0 \in \mathbb{R}^+$ is a known (conservative) bound of $\sigma(t)$.

Assumption 6 *We further assume that $\theta(t)$ and $\sigma(t)$ are continuously differentiable and their derivatives are uniformly bounded:*

$$\|\dot{\theta}(t)\|_2 \le d_\theta < \infty, \quad |\dot{\sigma}(t)| \le d_\sigma < \infty, \quad \forall\ t \ge 0\,, \tag{5.3}$$

where the numbers d_θ, d_σ can be arbitrarily large.

Assumption 7 *The vector $b(t)$ is continuously differentiable, bounded away from zero, and its derivative is uniformly bounded:*

$$\|\dot{b}(t)\|_2 \le d_b < \infty, \ \ \forall\ t \ge 0.$$

Assumption 8 *There exists ζ such that $\|\dot{A}_m(t)\|_\infty \leq \zeta$ for all $t \geq 0$.*

Assumption 9 *The representation $[A_m(t), b(t)]$ is strongly controllable, and $A_m(t)$ and $b(t)$ are uniformly bounded and smooth.*

The control objective is to design a full-state feedback adaptive controller to ensure that $y(t)$ tracks a given bounded reference signal $r(t)$ *both in transient and steady state*, while all other error signals remain bounded.

5.2 $\mathcal{L}_1$ Adaptive Controller

In this section, we develop a novel adaptive control architecture for the system in (5.1) that permits complete transient characterization for both $u(t)$ and $x(t)$. The elements of the $\mathcal{L}_1$ adaptive controller are introduced next:

State Predictor: We consider the following state predictor

$$\dot{\hat{x}}(t) = A_m(t)\hat{x}(t) + b(t)\left(\hat{\Lambda}(t)u(t) + \hat{\theta}^\top(t)x(t) + \hat{\sigma}(t)\right), \quad \hat{y}(t) = c^\top\hat{x}(t), \quad \hat{x}(0) = x_0, \tag{5.4}$$

which has the same structure as the system in (5.1). The only difference is that the unknown parameters $\Lambda, \theta(t), \sigma(t)$ are replaced by their adaptive estimates $\hat{\Lambda}(t), \hat{\theta}(t), \hat{\sigma}(t)$ that are governed by the adaptive laws.

Adaptive Laws: The adaptive estimates are given by

$$\dot{\hat{\theta}}(t) = \Gamma_\theta \text{Proj}(-x(t)\tilde{x}^\top(t)P(t)b(t), \hat{\theta}(t)), \quad \hat{\theta}(0) = \hat{\theta}_0 \tag{5.5}$$

$$\dot{\hat{\sigma}}(t) = \Gamma_\sigma \text{Proj}(-\tilde{x}^\top(t)P(t)b(t), \hat{\sigma}(t)), \quad \hat{\sigma}(0) = \hat{\sigma}_0 \tag{5.6}$$

$$\dot{\hat{\Lambda}}(t) = \Gamma_\Lambda \text{Proj}(-\tilde{x}^\top(t)P(t)b(t)u(t), \hat{\Lambda}(t)), \quad \hat{\Lambda}(0) = \hat{\Lambda}_0, \tag{5.7}$$

where $\tilde{x}(t) = \hat{x}(t) - x(t)$, $\Gamma_\theta = \Gamma_c I_{n\times n} \in \mathbb{R}^{n\times n}$, $\Gamma_\sigma = \Gamma_\Lambda = \Gamma_c > 0$ are the adaptation rates, and $P(t) = P^\top(t) > 0$ is the solution of the algebraic Lyapunov equation $A_m^\top(t)P(t) +$

$P(t)A_m(t) = -\mathbb{I}$. The existence of $P(t)$ follows from the proof of Lemma 5 and Assumption 8. Moreover, from (2.9) we can see that there exists $\epsilon_P > 0$ such that

$$\|\dot{P}(t)\|_\infty \leq \epsilon_P < 1.$$

The slow rate of variation of $A_m(t)$ leads to smaller ϵ_P.

In the implementation of the projection operator we use the compact set Θ as given in (5.2).

Control Law: The control signal is the output of the following system

$$\chi(s) = D(s)r_u(s)\,, \quad u(s) = -k\chi(s)\,, \tag{5.8}$$

where $k > 0$ is a feedback gain, $r_u(s)$ is the Laplace transformation of $r_u(t) = \hat{\Lambda}(t)u(t) + \bar{r}(t)$, $\bar{r}(t) = \hat{\theta}^\top(t)x(t) + \hat{\sigma}(t) - k_g(t)r(t)$, and $k_g(t) = -1/(c^\top A_m^{-1}(t)b(t))$ for each $t \geq 0$, while $D(s)$ is any transfer function that leads to strictly proper stable

$$C(s) = \Lambda k D(s)/(1 + \Lambda k D(s)) \tag{5.9}$$

with DC gain $C(0) = 1$. One simple choice is $D(s) = 1/s$, which yields a first order strictly proper $C(s)$ in the following form $C(s) = \Lambda k/(s + \Lambda k)$. Further, let

$$L = \max_{\theta(t)\in\Theta} \sum_{i=1}^{n} |\theta_i(t)|\,, \tag{5.10}$$

where $\theta_i(t)$ is the i^{th} element of $\theta(t)$, Θ is the compact set introduced in (5.2).

The $\mathcal{L}_1$ adaptive controller consists of (5.4), (5.5)-(5.7), (5.8) subject to the following $\mathcal{L}_1$-norm upper bound for the choice of $D(s)$:

$$\|G\|_{\mathcal{L}_1} L < 1\,, \tag{5.11}$$

where $G = H\bar{C}$, with $H : \mathbb{R} \to \mathbb{R}^n$ being the input-output map of the linear time-varying system $\dot{x}(t) = A_m(t)x(t) + b(t)u(t)$, and $\bar{C}$ being the input-output map of $\bar{C}(s) = 1 - C(s)$. Thus, $G : \mathbb{R} \to \mathbb{R}^n$.

5.3 Analysis of $\mathcal{L}_1$ Adaptive Controller

5.3.1 Closed-loop Reference System

Next we consider the following closed-loop LTV reference system with its control signal and system response being defined as follows:

$$\dot{x}_{ref}(t) = A_m(t)x_{ref}(t) + b(t)\left(\Lambda u_{ref}(t) + \theta^\top(t)x_{ref}(t) + \sigma(t)\right), \; x_{ref}(0) = x_0 \quad (5.12)$$

$$u_{ref}(s) = C(s)\frac{\bar{r}_{ref}(s)}{\Lambda}, \quad y_{ref}(t) = c^\top x_{ref}(t), \quad (5.13)$$

where $\bar{r}_{ref}(s)$ is the Laplace transformation of the signal $\bar{r}_{ref}(t) = -\theta^\top(t)x_{ref}(t) - \sigma(t) + k_g(t)r(t)$.

Lemma 13 *If $D(s)$ verifies the condition in (5.11), the reference system in (5.12)-(5.13) is stable.*

Proof: Let $C : \mathbb{R} \to \mathbb{R}$ be the input-output map of the transfer function $C(s)$, and the map $H_{in} : \mathbb{R}^n \to \mathbb{R}^n$ represent the zero-input response of the linear time-varying system $\dot{x}(t) = A_m(t)x(t)$. It follows from (5.12)-(5.13) that $x_{ref} = Gr_1 + HCk_gr + H_{in}x_0$, where $r_1(t) = \theta^\top(t)x_{ref}(t) + \sigma(t)$ is subject to the following bound: $\|r_1\|_{\mathcal{L}_\infty} \leq L\|x_{ref}\|_{\mathcal{L}_\infty} + \|\sigma\|_{\mathcal{L}_\infty}$. We consider G and $\theta^\top(t)$ as the two interconnected systems defined in Theorem 1. The block diagram is shown in Figure 5.1. Since $D(s)$ verifies the condition in (5.11), and the signals $\sigma(t)$, HCk_gr and $H_{in}x_0$ are bounded, Theorem 1 ensures that the closed-loop system in (5.12)-(5.13) is stable.

□

5.3.2 Transient and Steady State Performance

To prove uniform transient and steady state tracking between the closed-loop adaptive system with $\mathcal{L}_1$ adaptive controller (5.1), (5.4), (5.5)-(5.7), (5.8) and the reference system in (5.12)-

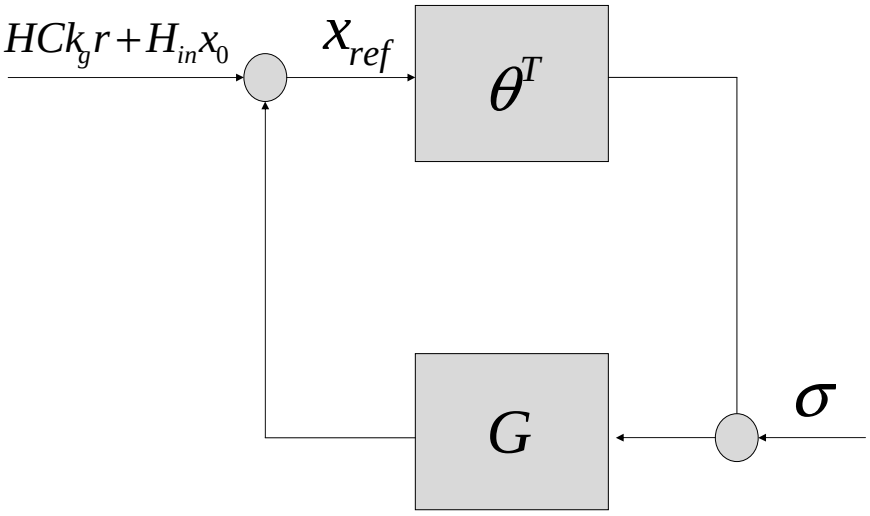

Figure 5.1: Block diagram of the closed loop reference system.

(5.13), we first need to quantify the prediction error performance that is used in the adaptive law.

Lemma 14 *For the system in (5.1) and the $\mathcal{L}_1$ adaptive controller in (5.4), (5.5)-(5.7) and (5.8), the prediction error between the system state and the predictor is bounded $\|\tilde{x}\|_{\mathcal{L}_\infty} \leq \sqrt{\frac{\theta_m}{\lambda_{P_{\min}} \Gamma_c}}$, where $\lambda_{P_{\min}} = \min_{t\in[0,\infty)} \lambda_{\min}(P(t))$,*

$$\theta_m \triangleq \max_{\theta\in\Theta} \sum_{i=1}^{n} 4\theta_i^2 + 4\Delta^2 + 4\left(\omega_u - \omega_l\right)^2 + 4\frac{\lambda_{P_{\max}}}{1-\epsilon_P}\left(\max_{\theta\in\Theta} \|\theta\|_\infty d_\theta + d_\sigma \Delta\right),$$

and $\lambda_{P_{\max}} = \max_{t\in[0,\infty)} \lambda_{\max}(P(t))$.

Proof: Consider the candidate Lyapunov function:

$$V(\tilde{x}(t), \tilde{\theta}(t), \tilde{\Lambda}(t), \tilde{\sigma}(t)) = \tilde{x}^\top(t) P(t) \tilde{x}(t) + \Gamma_\theta^{-1} \tilde{\theta}^\top(t) \tilde{\theta}(t) + \Gamma_\Lambda^{-1} \tilde{\Lambda}^2(t) + \Gamma_\sigma^{-1} \tilde{\sigma}^2(t),$$

where $\tilde{\theta}(t) \triangleq \hat{\theta}(t) - \theta(t)$, $\tilde{\sigma}(t) \triangleq \hat{\sigma}(t) - \sigma(t)$, $\tilde{\Lambda}(t) \triangleq \hat{\Lambda}(t) - \Lambda$. It follows from (5.1) and (5.4) that

$$\dot{\tilde{x}}(t) = A_m(t)\tilde{x}(t) + b(t)(\tilde{\Lambda}(t)u(t) + \tilde{\theta}^\top(t)x(t) + \tilde{\sigma}(t)), \quad \tilde{x}(0) = 0. \tag{5.14}$$

Using the projection based adaptation laws from (5.5)-(5.7), one has the following upper bound:

$$\begin{aligned}\dot{V}(t) &= \dot{\tilde{x}}^\top(t)P(t)\tilde{x}(t)+\tilde{x}^\top(t)P(t)\dot{\tilde{x}}(t)+\tilde{x}^\top(t)\dot{P}(t)\tilde{x}(t)+2\Gamma_\theta^{-1}\tilde{\theta}^\top(t)\dot{\tilde{\theta}}(t)\\ &\quad +2\Gamma_\Lambda^{-1}\tilde{\Lambda}^\top(t)\dot{\tilde{\Lambda}}(t)+2\Gamma_\sigma^{-1}\tilde{\sigma}^\top(t)\dot{\tilde{\sigma}}(t)\\ &= -\tilde{x}^\top(t)\left(\mathbb{I}-\dot{P}(t)\right)\tilde{x}(t)-2\Gamma_\theta^{-1}\tilde{\theta}^\top(t)\dot{\theta}(t)-2\Gamma_\sigma^{-1}\tilde{\sigma}^\top(t)\dot{\sigma}(t)\\ &\leq -\tilde{x}^\top(t)\left(\mathbb{I}-\dot{P}(t)\right)\tilde{x}(t)+2\Gamma_c^{-1}\left|\tilde{\theta}^\top(t)\dot{\theta}(t)+\tilde{\sigma}(t)\dot{\sigma}(t)\right|. \end{aligned} \tag{5.15}$$

The projection algorithm ensures that $\hat{\theta}(t)\in\Theta$, $\hat{\Lambda}(t)\in\Omega$, $\hat{\sigma}(t)\in\Delta$ for all $t\geq 0$, and therefore

$$\begin{aligned}&\max_{t\geq 0}\left(\Gamma_c^{-1}\tilde{\theta}^\top(t)\tilde{\theta}(t)+\Gamma_c^{-1}\tilde{\Lambda}^2(t)+\Gamma_c^{-1}\tilde{\sigma}^2(t)\right)\\ \leq\ &\left(\max_{\theta\in\Theta}\sum_{i=1}^{n}4\theta_i^2+4\Delta^2+4\left(\omega_u-\omega_l\right)^2\right)/\Gamma_c\end{aligned} \tag{5.16}$$

for any $t\geq 0$.

If $V(t)\geq\theta_m/\Gamma_c$ at some t, then it follows from (5.16) that $\tilde{x}^\top(t)P(t)\tilde{x}(t)\geq 4\frac{\lambda_{P_{\max}}}{\Gamma_c(1-\epsilon_P)}\Big(d_\sigma\Delta+\max_{\theta\in\Theta}\|\theta\|_\infty d_\theta\Big)$, and hence

$$\tilde{x}^\top(t)(\mathbb{I}-\dot{P}(t))\tilde{x}(t)\geq\frac{1-\epsilon_P}{\lambda_{P_{\max}}}\tilde{x}^\top(t)P(t)\tilde{x}(t)\geq\frac{4(\max\limits_{\theta\in\Theta}\|\theta\|_\infty d_\theta+d_\sigma\Delta)}{\Gamma_c}. \tag{5.17}$$

The upper bounds in (5.3) along with the projection based adaptive laws lead to the following upper bound: $\left|\tilde{\theta}^\top(t)\dot{\theta}(t)+\tilde{\sigma}(t)\dot{\sigma}(t)\right|\leq 2\max\limits_{\theta\in\Theta}\|\theta\|_\infty d_\theta+d_\sigma\Delta$. Hence, if $V(t)\geq\theta_m/\Gamma_c$, then from (5.15) and (5.17) we have

$$\dot{V}(t)\leq 0. \tag{5.18}$$

Since we have set $\hat{x}(0)=x(0)$, we can verify that $V(0)\leq\Big(\max_{\theta\in\Theta}\sum_{i=1}^{n}4\theta_i^2+4\Delta^2+4\left(\omega_u-\omega_l\right)^2\Big)/\Gamma_c<\theta_m/\Gamma_c$. It follows from (5.18) that $V(t)\leq\dfrac{\theta_m}{\Gamma_c}$ for any $t\geq 0$.

Since $\lambda_{P_{\min}}\|\tilde{x}(t)\|_{\mathcal{L}_\infty}^2\leq\tilde{x}^\top(t)P(t)\tilde{x}(t)\leq V(t)$, then $||\tilde{x}(t)||_{\mathcal{L}_\infty}^2\leq\dfrac{\theta_m}{\lambda_{P_{\min}}\Gamma_c}$, which concludes the proof. □

We further notice that this bound is proportional to the rate of variation of uncertainties and is inverse proportional to the adaptation gain. The next theorem is in charge for both transient and steady-state performance of the $\mathcal{L}_1$ adaptive controller.

Theorem 5 *Given the system in (5.1) and the $\mathcal{L}_1$ adaptive controller defined via (5.4), (5.5)-(5.7) and (5.8) subject to (5.11), we have:*

$$\|x - x_{ref}\|_{\mathcal{L}_\infty} \leq \gamma_1\,, \quad \|u - u_{ref}\|_{\mathcal{L}_\infty} \leq \gamma_2\,, \tag{5.19}$$

where $\gamma_1 = \frac{\|C\|_{\mathcal{L}_1}}{1-\|H\bar{C}\|_{\mathcal{L}_1}L}\sqrt{\frac{\theta_m}{\lambda_{P_{\max}}\Gamma_c}}$, $\gamma_2 = \left\|\frac{C}{\Lambda}\right\|_{\mathcal{L}_1} L\gamma_1 + \frac{\hat{\beta}c_{\max}}{\Lambda}\sqrt{\frac{\theta_m}{\lambda_{P_{\max}}\Gamma_c}}$ *with* $\hat{\beta} > 0$ *and* $c_{\max} > 0$ *being constants.*

Proof: Let $\tilde{r}(t) = \tilde{\Lambda}(t)u(t) + \tilde{\theta}^\top(t)x(t) + \tilde{\sigma}(t)\,,\ r_2(t) = \theta^\top(t)x(t) + \sigma(t)\,.$ It follows from (5.8) that $\chi(s) = D(s)r_u(s)$, where $r_u(t) = \Lambda u(t) + r_2(t) - k_g(t)r(t) + \tilde{r}(t)$. Consequently

$$\chi(s) = \frac{D(s)}{1 + k\Lambda D(s)}r_3(s)\,, \quad u(s) = -\frac{kD(s)}{1 + k\Lambda D(s)}r_3(s)\,,$$

where $r_3(t) = (r_2(t) - k_g(t)r(t) + \tilde{r}(t))$. Using the definition of $C(s)$ from (5.9), we can write

$$\Lambda u(s) = -C(s)r_3(s)\,, \tag{5.20}$$

and the system in (5.1) consequently takes the form:

$$x = H\bar{C}r_2 + HCk_g r - HC\tilde{r}. \tag{5.21}$$

It follows from (5.12)-(5.13) that $x_{ref} = H\bar{C}r_1 + HCk_g r$. Let $e(t) = x(t) - x_{ref}(t)$. Using (5.21) one gets

$$e = H\bar{C}r_4 - HC\tilde{r}, \quad e(0) = 0\,, \tag{5.22}$$

where

$$r_4(t) = \theta^\top(t)e(t)\,. \tag{5.23}$$

Lemma 14 gives the following upper bound:

$$\|e_t\|_{\mathcal{L}_\infty} \leq \|H\bar{C}\|_{\mathcal{L}_1}\|r_{4_t}\|_{\mathcal{L}_\infty} + \|r_{5_t}\|_{\mathcal{L}_\infty}\,, \tag{5.24}$$

where $r_5 = CH\tilde{r}$. From the relationship in (5.14) we have $\tilde{x} = H\tilde{r}$, which leads to $r_5 = C\tilde{x}$, and hence $\|r_{5_t}\|_{\mathcal{L}_\infty} \leq \|C\|_{\mathcal{L}_1}\|\tilde{x}_t\|_{\mathcal{L}_\infty}$. Using the definition of L in (5.10), one can verify straightforwardly that $\|(\theta^\top e)_t\|_{\mathcal{L}_\infty} \leq L\|e_t\|_{\mathcal{L}_\infty}$, and from (5.23) we have $\|r_{4_t}\|_{\mathcal{L}_\infty} \leq L\|e_t\|_{\mathcal{L}_\infty}$. From (5.24) we have $\|e_t\|_{\mathcal{L}_\infty} \leq \|H\bar{C}\|_{\mathcal{L}_1}L\|e_t\|_{\mathcal{L}_\infty} + \|C\|_{\mathcal{L}_1}\|\tilde{x}_t\|_{\mathcal{L}_\infty}$. The upper bound from Lemma 14 and the $\mathcal{L}_1$-norm upper bound from (5.11) lead to the following upper bound

$$\|e_t\|_{\mathcal{L}_\infty} \leq \frac{\|C\|_{\mathcal{L}_1}}{1 - \|H\bar{C}\|_{\mathcal{L}_1}L}\sqrt{\frac{\theta_m}{\lambda_{P_{\max}}\Gamma_c}},$$

which holds uniformly for all $t \geq 0$ and therefore leads to the first bound in (5.19).

To prove the second bound in (5.19), we notice that from (5.13) and (5.20) that $u(s) - u_{ref}(s) = -\frac{C(s)}{\Lambda}r_7(s) - r_6(s)$, where $r_7(t) = \theta^\top(t)(x(t) - x_{ref}(t))$ and $r_6(s) = \frac{C(s)}{\Lambda}\tilde{r}(s)$. Therefore,

$$\|u - u_{ref}\|_{\mathcal{L}_\infty} \leq (L/\Lambda)\|C\|_{\mathcal{L}_1}\|x - x_{ref}\|_{\mathcal{L}_\infty} + \|r_6\|_{\mathcal{L}_\infty}. \tag{5.25}$$

We now analyze the signal $r_6(t)$. The term $\tilde{r}(t)$ in $r_6(t)$ is the input to the system (5.14), the output of which is $\tilde{x}(t)$. We have already computed the uniform bound on $\|\tilde{x}\|_{\mathcal{L}_\infty}$. Hence, we need to find a relationship between the norm of $\tilde{r}(t)$ and the norm of $\tilde{x}(t)$ of a linear system. The low-pass filter $C(s)$ appears to be critical for deriving the bound on $\|r_6\|_{\mathcal{L}_\infty}$ in terms of the bound on $\|\tilde{x}\|_{\mathcal{L}_\infty}$.

According to Assumption 9, the representation $[A_m(t), b(t)]$ is strongly controllable, and $A_m(t)$, $b(t)$ are uniformly bounded and smooth. For the system

$$\dot{\tilde{x}}(t) = A_m(t)\tilde{x}(t) + b(t)\tilde{r}(t),$$

from Lemma 8 we know that there exists a uniformly bounded transformation $T(t)$, such that $\hat{x}(t) = T(t)\tilde{x}(t) = [\alpha_1(t), \cdots, \alpha_n(t)]^\top$, and the transformed system takes the controllable

canonical form

$$\begin{bmatrix} \dot{\alpha}_1(t) \\ \dot{\alpha}_2(t) \\ \vdots \\ \dot{\alpha}_{n-1}(t) \\ \dot{\alpha}_n(t) \end{bmatrix} = \begin{bmatrix} 0 & 1 & 0 & \cdots & 0 \\ 0 & 0 & 1 & \cdots & 0 \\ \vdots & \vdots & \vdots & \ddots & \vdots \\ 0 & 0 & 0 & \cdots & 1 \\ -a_1(t) & -a_2(t) & -a_3(t) & \cdots & -a_n(t) \end{bmatrix} \begin{bmatrix} \alpha_1(t) \\ \alpha_2(t) \\ \vdots \\ \alpha_{n-1}(t) \\ \alpha_n(t) \end{bmatrix} + \begin{bmatrix} 0 \\ 0 \\ \vdots \\ 0 \\ 1 \end{bmatrix} \tilde{r}(t), \tag{5.26}$$

where $a_i(t),\ i = 1, \cdots, n$ are bounded. The relationship between $\alpha(t) = \alpha_1(t)$ and $\tilde{r}(t)$ can be described by the following ODE:

$$\alpha^n(t) + a_n(t)\alpha^{n-1}(t) + \cdots + a_1(t)\alpha(t) = \tilde{r}(t). \tag{5.27}$$

Let

$$z(t) = \bar{c}^\top \hat{x}(t) = \bar{c}_1\alpha(t) + \bar{c}_2\alpha^{(1)}(t) + \cdots + \bar{c}_n\alpha^{(n-1)}(t), \tag{5.28}$$

where $\bar{c}_i,\ i = 1, \cdots, n$ are the coefficients of a stable polynomial $\bar{c}_n s^{n-1} + \cdots + \bar{c}_1$. Consider $z(t) = c^\top(t)\tilde{x}(t)$, where $c^\top(t) = \bar{c}^\top T(t)$. It follows from (5.28) that

$$\begin{aligned} \alpha(s) &= \frac{1}{\bar{c}_n s^{n-1} + \cdots + \bar{c}_1} z(s) \\ &\vdots \\ \alpha^{(n-1)}(s) &= \frac{s^{n-1}}{\bar{c}_n s^{n-1} + \cdots + \bar{c}_1} z(s) \\ \alpha^{(n)}(s) &= \frac{s^n}{\bar{c}_n s^{n-1} + \cdots + \bar{c}_1} z(s) \end{aligned} \tag{5.29}$$

Considering the linearity of equation (5.27), we can divide $\tilde{r}(t)$ into two parts $\tilde{r}_1(t)$ and $\tilde{r}_2(t)$, $\tilde{r}(t) = \tilde{r}_1(t) + \tilde{r}_2(t)$, and write

$$\alpha^{(n)}(t) = \tilde{r}_1(t), \tag{5.30}$$

$$a_n(t)\alpha^{(n-1)}(t) + \cdots + a_1(t)\alpha(t) = \tilde{r}_2(t). \tag{5.31}$$

Since $\tilde{x}(t)$ has been proved to be bounded and $c^\top(t)$ is bounded, the signal $z(t)$ is bounded. It follows from (5.28) that $\alpha(t), \cdots, \alpha^{n-1}(t)$ are all bounded. From (5.29) and (5.30), since

$\alpha_i(t)$ are bounded, $\tilde{r}_2(t)$ is bounded. We notice that the transfer functions

$$\frac{1}{\bar{c}_n s^{n-1} + \cdots + \bar{c}_1} \ , \ \cdots \ , \ \frac{s^{n-1}}{\bar{c}_n s^{n-1} + \cdots + \bar{c}_1}$$

are proper and stable transfer functions. Hence, there exist finite positive numbers $(\beta_1)_i$, $i = 0, \cdots, n-1$ such that

$$\|\alpha^{(i)}\|_{\mathcal{L}_\infty} \leq (\beta_1)_i \|z\|_{\mathcal{L}_\infty} .$$

From $\tilde{r}(t) = \tilde{r}_1(t) + \tilde{r}_2(t)$, we can have

$$C(s)\tilde{r}(s) = \mu_1(s) + \mu_2(s),$$

where

$$\mu_1(s) = C(s)\tilde{r}_1(s), \qquad \mu_2(s) = C(s)\tilde{r}_2(s).$$

Since $C(s)$ is a strictly proper stable transfer function, its $\mathcal{L}_1$ norm is finite positive number. Since $(\beta_1)_i$, $a_i(t)$, $i = 0, \cdots, n-1$ and the $\mathcal{L}_1$ norm of $C(s)$ are finite, we have

$$\|\mu_2\|_{\mathcal{L}_\infty} \leq \beta_2 \|z\|_{\mathcal{L}_\infty} ,$$

where β_2 is a finite positive number. From (5.29) we have

$$\tilde{r}_1(s) = \frac{s^n}{\bar{c}_n s^{n-1} + \cdots + \bar{c}_1} z(s).$$

Substituting the above expression into $\mu_1(s) = C(s)u_1(s)$ gives

$$\mu_1(s) = C(s)\frac{s^n}{\bar{c}_n s^{n-1} + \cdots + \bar{c}_1} z(s).$$

Since $C(s)$ is strictly proper and stable, the cascaded transfer function $C(s)\frac{s^n}{\bar{c}_n s^{n-1}+\cdots+\bar{c}_1}$ is stable and proper. Hence, its $\mathcal{L}_1$ norm, denoted by β_3, is a positive number. We then have

$$\|\mu_1\|_{\mathcal{L}_\infty} \leq \beta_3 \|z\|_{\mathcal{L}_\infty} .$$

From the existence of $(\beta_1)_i$, β_2 and β_3, it follows that there exists a finite positive number $\hat{\beta}$ such that

$$\|\mu\|_{\mathcal{L}_\infty} \leq \hat{\beta} \|z\|_{\mathcal{L}_\infty} .$$

Let $||c(t)|| \leq c_{\max}$. Then the above inequality takes the form:

$$\|C\tilde{r}\|_{\mathcal{L}_\infty} \leq \hat{\beta} c_{\max} \|\tilde{x}\|_{\mathcal{L}_\infty} .$$

Notice that $r_6(s) = \frac{1}{\Lambda}\mu(s)$. Lemma 14 consequently leads to the upper bound:

$$\|r_6\|_{\mathcal{L}_\infty} \leq \frac{\hat{\beta} c_{\max}}{\Lambda} \sqrt{\frac{\theta_m}{\lambda_{P_{\max}} \Gamma_c}} ,$$

which, when substituted into (5.25), leads to the second bound in (5.19). □

Thus, the tracking error between $x(t)$ and $x_{ref}(t)$, as well between $u(t)$ and $u_{ref}(t)$, is uniformly bounded by a constant inverse proportional to Γ_c. This implies that during the transient phase one can achieve arbitrarily close tracking performance for both signals simultaneously by uniformly increasing the adaptation rate Γ_c.

5.3.3 Design Guidelines

We notice that the control law $u_{ref}(t)$ in the closed-loop reference system, which is used in the analysis of $\mathcal{L}_\infty$ norm bounds, is not implementable since its definition involves the unknown parameters. Theorem 5 ensures that the $\mathcal{L}_1$ adaptive controller approximates $u_{ref}(t)$ both in transient and steady state. So, it is important to understand how these bounds can be used for ensuring uniform transient response with *desired* specifications. We notice that the following *ideal* control signal

$$u_{ideal}(t) = \frac{k_g(t) r(t) - \theta^\top(t) x_{ref}(t) - \sigma(t)}{\Lambda} \tag{5.32}$$

is the one that leads to desired system response:

$$\dot{x}_{ref}(t) = A_m(t) x_{ref}(t) + b(t) k_g(t) r(t), \quad y_{ref}(t) = c^\top x_{ref}(t) \tag{5.33}$$

by cancelling the uncertainties exactly. In the closed-loop reference system (5.12)-(5.13), $u_{ideal}(t)$ is further low-pass filtered by $C(s)$ to have guaranteed low-frequency range. Thus,

the reference system in (5.12)-(5.13) has a different response as compared to (5.33) achieved with (5.32). In [3, 7], specific design guidelines are suggested for selection of $C(s)$ to ensure that in case of constant A_m, b, θ and σ the response of $x_{ref}(t)$ and $u_{ref}(t)$ can be made as close as possible to (5.33).

5.4 Augmentation of the Gain-Scheduled Controller

The gain-scheduled baseline controller can be combined with the linear time-varying plant to generate a linear time-varying reference system. Then the proposed $\mathcal{L}_1$ adaptive controller can augment the baseline gain scheduled controller. We give a brief review of gain-scheduled control design. It usually involves the following steps.

Step One

We start with a nonlinear system without considering any uncertainties:

$$\begin{aligned} \dot{X}(t) &= f(X(t), U(t), w(t)), \quad X(t_0) = X_0, \\ Z(t) &= h_1(X(t), U(t), w(t)), \\ Y(t) &= h_2(X(t), w(t)), \end{aligned} \tag{5.34}$$

where $X(t) \in \mathbb{R}^{n_1}$, $U(t) \in \mathbb{R}$ are the state and the input, $w(t) \in \mathbb{R}^{m_w}$ is the vector of exogenous variables, $Z(t) \in \mathbb{R}$ denotes the error signal to be controlled, $Y(t) \in \mathbb{R}^m$ is the measured output that can be used for feedback.

Gain-scheduling proceeds by computing a linear parameter-varying model for the plant. For that purpose two approaches are studied extensively, linearization based scheduling and quasi-LPV based scheduling. The linearization scheduling is based on the linearization of the nonlinear plant (5.34) about a family of equilibrium points, also called operating points or set points. Assuming that the scheduling variables change slowly and can be treated as constants

in the neighborhood of the equilibrium points, one obtains a family of linear time-invariant systems valid for each operating point. Next, linear controllers, parameterized by the fixed-values of the scheduling variables, are designed for each of these systems, implementation of which for the original nonlinear system leads to the nonlinear gain-scheduled design due to the continuous (slow) change in the scheduling variables.

In quasi-LPV scheduling, the plant dynamics are rewritten converting the nonlinearities into time-varying parameters, which are further used as scheduling variables. Quasi-LPV description gives a linear system with time-varying parameters without applying any linearization technique. Since the nonlinear terms in the plant involve the states, some state variables must be treated as parameters in various parts of the model, while they remain dynamical variables elsewhere. This introduces additional challenges for the control design. Furthermore, the quasi-LPV description requires insight into the specific nonlinear dynamics of the system. Hence, although the quasi-LPV description is not local, it has more complexity to its design.

In this dissertation we only show the linearization approach for obtaining a linear time-varying model dependent upon the scheduling variables. We denote the scheduling variable $\eta(t)$, and assume that $\eta(t)$ includes the exogenous scheduling signal and can possibly depend on the output $Y(t)$ as well. For example, we can use Mach number as a scheduling variable for aircraft flight control. It is a function of altitude and velocity. The dependence of the aircraft dynamics on altitude is characterized by $w(t)$ that can capture pressure, density, etc., while velocity is a part of the system states (or output). Hence we can write the scheduling variable as $\eta(t) = \eta(w(t), Y(t))$. However, in this step we treat each fixed value of $\eta(t)$ as a parameter of the system and denote it by η, and do the linearization with respect to system states and inputs, but not with respect to η. This leads to a parameterized family of linear systems. An important issue arises, when η depends on state variables through the measured output $Y(t)$, in addition to $w(t)$. In that case, the scheduling variables appear both as parameters (components of the vector η) and as dynamical variables (components of $Y(t)$) at different places in the linearized plant.

Definition 14 *The functions $X_e(\eta)$, $U_e(\eta)$ and $w_e(\eta)$ define an equilibrium family for the plant (5.34) on the set $\eta \in \Xi$, if*

$$f(X_e(\eta), U_e(\eta), w_e(\eta)) = 0, \qquad \eta \in \Xi. \tag{5.35}$$

Associated with this equilibrium family one has the output equilibrium family

$$\begin{aligned} Z_e(\eta) &= h_1(X_e(\eta), U_e(\eta), w_e(\eta)), \qquad \eta \in \Xi, \\ Y_e(\eta) &= h_2(X_e(\eta), w_e(\eta)), \qquad \eta \in \Xi. \end{aligned}$$

Let $X_\delta(t) = X(t) - X_e(\eta)$, $U_\delta(t) = U(t) - U_e(\eta)$, $Z_\delta(t) = Z(t) - Z_e(\eta)$ and $Y_\delta(t) = Y(t) - Y_e(\eta)$. Then the linearization of (5.34) around equilibrium points can be expressed as:

$$\begin{aligned} \dot{X}_\delta(t) &= A(\eta(t))X_\delta(t) + B(\eta(t))U_\delta(t) \\ Z_\delta(t) &= C_1(\eta(t))X_\delta(t) + D_1(\eta(t))U_\delta(t) \\ Y_\delta(t) &= C_2(\eta(t))X_\delta(t). \end{aligned} \tag{5.36}$$

Assumption 10 *There exists sufficiently small $\epsilon > 0$, such that for all $t \geq 0$, $\|X(t) - X_e(t)\| \leq \epsilon$.*

Remark 4 *Assumption 10 implies that the linear time-varying model in (5.36) is almost always valid.*

Step Two

Next, we design a parameterized family of linear controllers. For each fixed value of $\eta(t)$, denoted by η, we design a family of linear controllers parameterized by η. Notice that the scheduling variable η is considered as a fixed parameter throughout the design process, but it becomes a time-varying input signal to the gain-scheduled controller implementation due to its dependence on system's measured state and exogenous signal. This is the key to the

gain scheduling philosophy. Let the family of linear controllers be given by the following dynamics:

$$\begin{bmatrix} \dot{X}_\delta^c(t) \\ U_\delta(t) \end{bmatrix} = \begin{bmatrix} F(\eta) & G(\eta) \\ H(\eta) & E(\eta) \end{bmatrix} \begin{bmatrix} X_\delta^c(t) \\ Y_\delta(t) \end{bmatrix}, \qquad \eta \in \Xi \tag{5.37}$$

Step Three

The objective of this step is to compute, based on the linear controller family (5.37), a controller that has the general form

$$\begin{aligned} \dot{X}^c(t) &= f_g(X^c(t), Y(t), w(t)), \\ U(t) &= h_g(X^c(t), Y(t), w(t)), \end{aligned} \tag{5.38}$$

with the obvious input and output signals corresponding to the original nonlinear plant (5.34). The controller (5.38) is the one that is going to be implemented. Notice that the linear controller family (5.37) is not necessarily the controller being implemented in the final step.

The design of the gain-scheduled controller (5.38) needs to ensure that the linearization of the nonlinear feedback system consisting of the gain-scheduled controller (5.38) and the nonlinear plant produces the same linear closed-loop system what one would otherwise obtain from application of the linear controller (5.37) to the linearized plant. This can be achieved if following two conditions hold.

First, the linearization scheduling needs to ensure that the equilibrium family of the controller (5.38) matches the plant equilibrium family, i.e. there exists a function $X_e^c(\eta)$ such that

$$\begin{aligned} 0 &= f_g(X_e^c(\eta), Y_e(\eta), w_e(\eta)), \\ U_e(\eta) &= h_g(X_e^c(\eta), Y_e(\eta), w_e(\eta)), \qquad \eta \in \Xi. \end{aligned} \tag{5.39}$$

Second, it needs to ensure that the linearization family of the controller (5.38) is the designed

family of linear controllers (5.37). Thus we require that

$$\begin{aligned}
&\frac{\partial f_g}{\partial X^c}\Big(X_e^c(\eta), Y_e(\eta), w_e(\eta)\Big) = F(\eta),\\
&\frac{\partial f_g}{\partial Y}\Big(X_e^c(\eta), Y_e(\eta), w_e(\eta)\Big) = G(\eta),\\
&\frac{\partial h_g}{\partial X^c}\Big(X_e^c(\eta), Y_e(\eta), w_e(\eta)\Big) = H(\eta),\\
&\frac{\partial h_g}{\partial Y}\Big(X_e^c(\eta), Y_e(\eta), w_e(\eta)\Big) = E(\eta), \qquad \eta \in \Xi.
\end{aligned} \tag{5.40}$$

One direct way to get (5.38) is to specify the controller, in terms of the coefficients in (5.37), as follows:

$$\begin{aligned}
\dot{X}^c(t) &= F(\eta(t))[X^c(t) - X_e^c(\eta(t))] + G(\eta(t))[Y(t) - Y_e(\eta(t))],\\
U(t) &= H(\eta(t))[X^c(t) - X_e^c(\eta(t))] + E(\eta(t))[Y(t) - Y_e(\eta(t))] + U_e(\eta(t)).
\end{aligned} \tag{5.41}$$

Step Four

Check nonlocal performance of the gain scheduled controller by simulations.

In step 2, we might be able to directly design a family of controllers via particular design methods, like, for example, LPV methods. However, in most of the situations one adopts interpolation on point design controllers due to their simplicity. Theoretically justified interpolation methods were reported in [89, 90, 91, 92]. We notice that even if the interpolated family of linear controllers is theoretically justified for stabilization of the system for each value of the scheduling variable, implementation of the gain-scheduled controller based on the interpolation of a family of linear controllers still needs careful treatment in terms of performance and stability. This important issue has been acknowledged in literature [93, 94, 96, 98, 97].

Since we are focusing on how to augment the existing baseline controller, we assume a well-designed gain-scheduled controller is available. For details on the design of gain-scheduled

controllers, refer to [93, 94, 96, 98, 97, 40]. For analysis of stability, we assume that the scheduling variable changes slowly, such that the condition from Assumption 8 can hold. That is, $\|\dot{A}(t)\| \leq \zeta$. This "slow varying" condition is one of the rule-of-thumb guidelines for gain-scheduled control design.

5.5 Gain Scheduling Design of Aerial Refueling Racetrack Maneuver

The complete autonomous aerial refueling process consists of three phases: approaching, station-keeping and flying away. In previous chapter the approaching of the receiver to the tanker is shown. In this section, station-keeping with racetrack shape maneuver of the receiver aircraft is studied. Racetrack maneuver includes flights at straight wings level condition, coordinated steady turn and transitions in between, which correspond to different operating conditions. The baseline controller which can work for racetrack maneuver is gain-scheduled, which means it is time-varying. The newly developed $\mathcal{L}_1$ adaptive controller for time-varying reference system can be applied to ensure that aerial refueling in this scenario can be done with guaranteed and desired performance bounds.

We first start with 6DoF nonlinear equations of motion of the receiver aircraft. The derivations of the equations of motion follow commonly used approaches, e.g., in [100, 111]. The dynamics are derived with respect to inertial frame, but expressed in stability axis. All notations are defined in Nomenclature.

Translational Kinematic Equations

$$\begin{aligned}
\dot{l}_p(t) &= V_t(t)\Big[\cos\beta_p\cos\alpha_p\cos\theta_p\cos\psi_p+\sin\beta_p(-\cos\phi_p\sin\psi_p \\
&\quad +\sin\phi_p\sin\theta_p\cos\psi_p)+\cos\beta_p\sin\alpha_p(\sin\phi_p\sin\psi_p+\cos\phi_p\sin\theta_p\cos\psi_p)\Big] \\
\dot{y}_p(t) &= V_t(t)\Big[\cos\beta_p\cos\alpha_p\cos\theta_p\sin\psi_p+\sin\beta_p(\cos\phi_p\cos\psi_p+\sin\phi_p\sin\theta_p\cos\psi_p) \\
&\quad +\cos\beta_p\sin\alpha_p(-\sin\phi_p\cos\psi_p+\cos\phi_p\sin\theta_p\cos\psi_p)\Big] \\
\dot{h}_p(t) &= V_t(t)\Big[-\cos\beta_p\cos\alpha_p\sin\theta_p+\sin\beta_p\sin\phi_p\cos\theta_p \\
&\quad +\cos\beta_p\sin\alpha_p\cos\phi_p\cos\theta_p\Big]
\end{aligned} \tag{5.42}$$

Translational Dynamic Equations

$$\begin{aligned}
\dot{V}_t(t) &= g\Big[\cos\theta_p\sin\beta_p\sin\phi_p+\cos\beta_p(\cos\phi_p\cos\theta_p\sin\alpha_p-\cos\alpha_p\sin\theta_p)\Big] \\
&\quad +\frac{1}{m_p}\Big[-D_p(t)+T_p(t)\cos\alpha_p\cos\beta_p\Big] \\
\dot{\beta}_p(t) &= -r_p(t)\cos\alpha_p+p_p(t)\sin\alpha_p-\frac{1}{m_pV_t(t)}\Big[S_p(t)+T_p(t)\cos\alpha_p\sin\beta_p\Big] \\
&\quad \frac{g}{V_t(t)}\Big[-\cos\phi_p\cos\theta_p\sin\alpha_p\sin\beta_p+\cos\beta_p\cos\theta_p\sin\phi_p+\cos\alpha_p\sin\beta_p\sin\theta_p\Big] \\
\dot{\alpha}_p(t) &= q_p(t)-(p_p(t)\cos\alpha_p+r_p(t)\sin\alpha_p)\tan\beta_p+\frac{g\sec\beta_p}{V_t(t)}\Big[\cos\alpha_p\cos\phi_p\cos\theta_p+\sin\alpha_p\sin\theta_p\Big] \\
&\quad -\frac{\sec\beta_p}{m_pV_t(t)}\Big[L_p+T_p\sin\alpha_p\Big]
\end{aligned} \tag{5.43}$$

Rotational Kinematic Equations

$$\begin{aligned}
\dot{\phi}_p(t) &= p_p(t)+q_p(t)\sin\phi_p\tan\theta_p+r_p(t)\cos\phi_p\tan\theta_p \\
\dot{\theta}_p(t) &= q_p(t)\cos\phi_p-r_p(t)\sin\phi_p \\
\dot{\psi}_p(t) &= \Big[q_p(t)\sin\phi_p+r_p(t)\cos\phi_p\Big]/\cos\theta_p
\end{aligned} \tag{5.44}$$

Rotational Dynamic Equations

$$\begin{aligned}
\dot{p}_p(t) &= \frac{1}{I_{xx}I_{zz}-I_{xz}^2}\Big[I_{xx}-I_{yy}+I_{zz}I_{xz}p_p(t)q_p(t)+(I_{yy}-I_{zz}I_{zz}^2-I_{xz}^2)q_p(t)r_p(t)+ \\
&\quad +I_{zz}\mathcal{L}_p+I_{xz}\mathcal{N}_p\Big] \\
\dot{q}_p(t) &= \frac{1}{I_{yy}}\Big[(I_{zz}-I_{xx})p_p(t)r_p(t)+(r_p^2(t)-p_p^2(t))I_{xz}+\mathcal{M}_p\Big] \\
\dot{r}_p(t) &= \frac{1}{I_{xx}I_{zz}-I_{xz}^2}\Big[(I_{xx}^2-I_{xx}I_{yy}+I_{xz}^2)p_p(t)q_p(t)+(-I_{xx}+I_{yy}-I_{zz})I_{xz}q_p(t)r_p(t) \\
&\quad +I_{xz}\mathcal{L}_p+I_{xx}\mathcal{N}_p\Big]
\end{aligned} \tag{5.45}$$

Notice that the rolling moment and pitching moment include uncertainties as shown below:

$$\mathcal{L}_p(t)=\Lambda_1 u_{ail}(t)+\Delta_1(t),\quad \mathcal{M}_p=\Lambda_2 u_{ele}(t)+\Delta_2(t)\,,$$

where Λ_i is the scaling factor that represents actuator effectiveness reduction, $\Delta_i(t)$ represents unknown rolling and pitching moments respectively, $u_{ail}(t)$ and $u_{ele}(t)$ are control inputs from aileron and elevator.

For successful aerial refueling, the receiver is required to make the same steady coordinated turn with the tanker. Coordinated turn requires the aircraft to fly with constant yaw rate $\dot{\psi}_p$ and zero sideslip angle β_p. Furthermore, the deviation in altitude and speed should be small, while starting and ending the turn. When the racetrack maneuver starts, the aircraft is at wing level straight flight condition, while at the steady turning phase, it has constant nonzero yaw rate $\dot{\psi}_p$, constant pitch and roll angles (θ_p, ϕ_p), constant airspeed V_t and angle of attack α_p, zero sideslip angle β_p, and constant angular velocities (p_p, q_p, r_p). Hence, the start of the maneuver has one equilibrium operating condition, and the steady turning corresponds to another equilibrium operating condition. Gain-scheduling is needed to control the aircraft for transition from one operating point to another.

We schedule the baseline controller by yaw rate $\dot{\psi}_p$. A tracking controller for yaw rate is designed. The yaw rate command starts with zero, then gradually increases to a constant value, which corresponds to the steady state value of the yaw rate at the steady turning phase. Upon that, the yaw rate command will decrease to zero gradually. The timing of

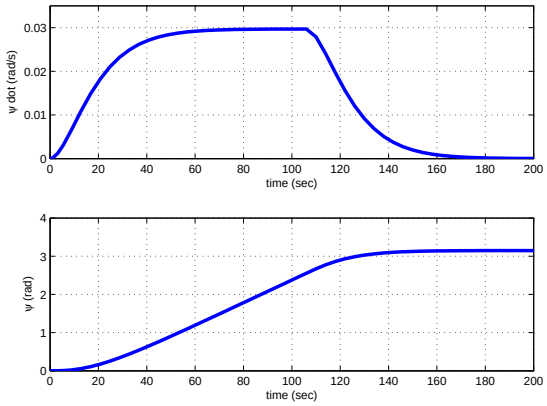

Figure 5.2: Yaw rate command and yaw angle.

this command is decided such that the yaw angle changes up to 180 degree. It is shown in Figure 5.2. The baseline controller also includes speed hold and altitude hold controllers. A LQR-based integral MIMO controller is designed for two nominal conditions: 1) straight level flight condition at $V_t = 500$ ft/s, $\dot{\psi}_p = 0$ rad/s; 2) steady coordinated turn at $V_t = 500$ ft/s, $\dot{\psi}_p = 0.0297$ rad/s.

Upon linearization at the above nominal conditions, the system states (ΔV_t, $\Delta\beta_p$, $\Delta\alpha_p$, Δp_p, Δq_p, Δr_p, $\Delta\theta_p$, $\Delta\phi_p$ Δh_p) are obtained. Notice that these states are deviations from nominal values. All the states are available for feedback, so the measured output y is equal to x. The performance output, which we want to control, includes airspeed, altitude and yaw rate. We have

$$\begin{aligned} x(t) &= [\Delta V_t(t)\ \Delta\beta_p(t)\ \Delta\alpha_p(t)\ \Delta p_p(t)\ \Delta q_p(t)\ \Delta r_p(t)\ \Delta\theta_p(t)\ \Delta\phi_p(t)\ \Delta h_p(t)]^\top \\ y(t) &= x(t) \\ z(t) &= [\Delta V_t(t)\ \Delta h_p(t)\ \Delta\dot{\psi}_p(t)]^\top \\ u(t) &= [\delta_a(t)\ \delta_e(t)\ \delta_r(t)\ \xi_T(t)]^\top, \end{aligned} \tag{5.46}$$

where the aileron input δ_a, the elevator input δ_e, the rudder input δ_r and the thrust input ξ_T are the control inputs. Corresponding to the two operating points, two linear time-invariant

systems are obtained:

$$\begin{aligned} \dot{x}_1(t) &= A_1 x_1(t) + B_1 u_1(t), \\ \dot{x}_2(t) &= A_2 x_2(t) + B_2 u_2(t). \end{aligned} \tag{5.47}$$

Due to the difficulty of calculating $A(t)$ and $B(t)$ analytically, the linear time-varying dynamics are obtained via interpolation. For example,

$$A(t) = (1 - \lambda(t))A_1 + \lambda(t)A_2\,,$$

where

$$\lambda(t) = \frac{\dot{\psi}_p(t) - \dot{\psi}_1}{\dot{\psi}_2 - \dot{\psi}_1},$$

and $\dot{\psi}_1 = 0$, $\dot{\psi}_2 = 0.0297$. The baseline control input is interpolated from the nominal controllers u_{10} and u_{20}, designed for two operating points:

$$u_0(t) = \frac{\dot{\psi}_p(t) - \dot{\psi}_2}{\dot{\psi}_1 - \dot{\psi}_2} u_{10} + \frac{\dot{\psi}_p(t) - \dot{\psi}_1}{\dot{\psi}_2 - \dot{\psi}_1} u_{20}.$$

Then the linear time-varying system is obtained

$$\begin{aligned} \dot{x}(t) &= A(t)x(t) + B(t)\Big(\Lambda u(t) + \theta^\top(t)x(t) + \sigma(t)\Big) \\ y(t) &= Cx(t) \\ z(t) &= Hx(t), \end{aligned} \tag{5.48}$$

where Λ, $\theta(t)$ and $\sigma(t)$ are uncertainties that will be discussed later in simulation section. The numerical values of A_1, A_2, B_1 and B_2 are shown in Appendix. The two nominal conditions for operating points are also shown in Appendix.

The baseline controller is designed for the nominal LTI systems (5.47) in the absence of uncertainties, using LQR and PI method. We first design a controller without considering the state "altitude $h_p(t)$". The response of $h_p(t)$ is relatively slow and can be controlled by an outer loop feedback controller. The reason we decouple altitude state from other states in the design is that if the altitude is included in the LQR design, the resulting controller has

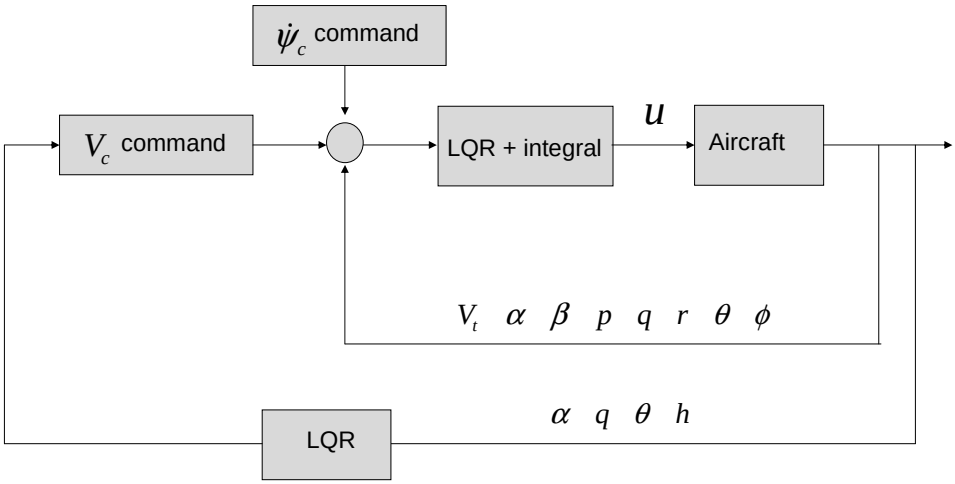

Figure 5.3: Block diagram of baseline controller.

slow response of yaw rate tracking. Hence we first design a LQR+integral baseline controller for subsystem whose states are

$$[\Delta V_t(t)\ \Delta\beta_p(t)\ \Delta\alpha_p(t)\ \Delta p_p(t)\ \Delta q_p(t)\ \Delta r_p(t)\ \Delta\theta_p(t)\ \Delta\phi_p(t)]^\top.$$

Then we design an outer loop controller using the LQR method to hold the altitude during the coordinated turn. The outer loop controller takes the states α_p, q_p, θ_p and h_p and generates a command signal V_{tc} for the air speed V_t. The illustration of this scheme is shown in Figure 5.3.

Upon obtaining the gain-scheduled baseline controller, we are able to calculate nominal dynamics $A_m(t)$ as described in (5.1). Then we can verify some of the assumptions given in Section 5.1. This process is done through numerical calculations.

- *Slow variation assumption* : at each fixed t, $A_m(t)$ has negative real part of eigenvalues. We have solved the Lyapunov equation $A_m^\top(t)P(t) + P(t)A_m(t) = -\mathbb{I}$ for $P(t)$ over the time range $t \in [0, 200]$ seconds. And calculate numerically $\|\dot{P}(t)\|_\infty$ over this time range. They are uniformly less than one. Hence the sufficient condition for stability is verified.

- *Strong controllability assumption*: at each fixed t in the time range $t \in [0, 200]$ seconds, the controllability matrix $Q_c(t)$ is calculated, and they are all nonsingular.

5.6 Simulations

We first look at the baseline controller. The design parameters for the two baseline controllers are shown below. For condition 1 we have:

$$Q_1 = \text{diag}([0.9,\ 0.09,\ 0.09,\ 0.09,\ 0.09,\ 0.9,\ 0.09,\ 0.09,\ 1,\ 9]),\ Q_{h1} = \text{diag}([10,\ 20,\ 20,\ 50]),$$

and

$$R_1 = \text{diag}([0.9,\ 0.9,\ 4.5,\ 45]), \quad R_{h1} = 0.6.$$

For condition 2 we have:

$$Q_2 = \text{diag}([1,\ 0.1,\ 0.1,\ 0.1,\ 0.1,\ 1,\ 0.1,\ 0.5,\ 1,\ 10]), \quad Q_{h2} = \text{diag}([10,\ 20,\ 20,\ 50]),$$

and

$$R_2 = \text{diag}([1,\ 1,\ 5,\ 50]), \quad R_{h2} = 0.05.$$

The experimental vortex effect data that we applied to the simulation in previous chapter describe the induced drag, rolling and pitching moments generated from wing tip vortices of the tanker. They are functions of the relative distance between the receiver and the tanker. Therefore, during the coordinated turn, when the probe has already captured the drogue, the vortex induced uncertainties can be treated as constants according to experimental data. However, in real flight conditions, more uncertainties in the air flow field may exist, and the experimental data from wind tunnel test can not model the real vortex effect perfectly. Hence, considering them as pure constant disturbances and applying conventional disturbance rejection techniques may not ensure satisfactory performance. This is the reason that we design adaptive controller to compensate for time-varying and state dependent uncertainties. These uncertainties are not available from our current experimental data, so we

introduce some "artificial worst-case" type disturbances to show the ability of the proposed adaptive controller for handling these.

We inject induced rolling moment and pitching moment into $\dot{p}_p$ and $\dot{q}_p$ equations. The induced rolling moment is

$$f_{roll}(t) = p_p(t) + \phi_p(t) + 0.5\sin(0.1t),$$

and the induced pitching moment is

$$f_{pitch} = 0.5.$$

In equation (5.48), Λ models the reduction of actuator surface effectiveness. In the simulation, we set $\Lambda_i = 0.45$, $i = 1, 2, 3$, i.e. the aileron, the elevator and the rudder lose their effectiveness by 55%.

The $\mathcal{L}_1$ adaptive controller design has the following parameters. For each control channel, the low-pass filter is chosen as

$$D(s) = \frac{1}{s^2 + 7s},$$

while the feedback gains k_i, $i = 1, \cdots, 4$ are chosen as

$$k_1 = 50, \quad k_2 = 50, \quad k_3 = 50, \quad k_4 = 7.$$

The adaptation gain is selected $\Gamma_c = 80000$.

The simulation results first show the nominal performance of the racetrack maneuver in the absence of uncertainties. In. Figure 5.4, the air speed, the yaw rate and the altitude response are shown. The tracking of yaw rate is satisfactory and the deviations of air speed and altitude are small. Then in Figure 5.5 the projection of flight trajectory on the horizontal plane is shown, which is in a racetrack shape. In Figure 5.6 the remaining system states are shown. Figure 5.7 shows the control inputs.

Next the induced rolling and pitching moment are considered. Figure 5.8 shows the degradation of the yaw rate tracking performance and flight trajectory. If control effectiveness

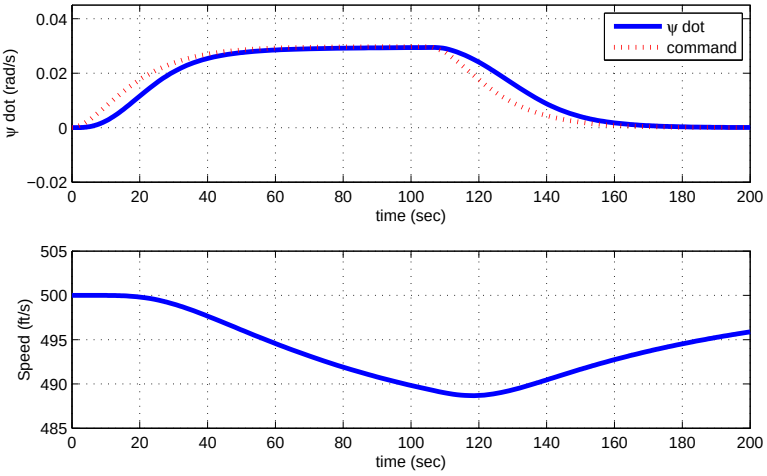

Figure 5.4: Nominal output performance of baseline .

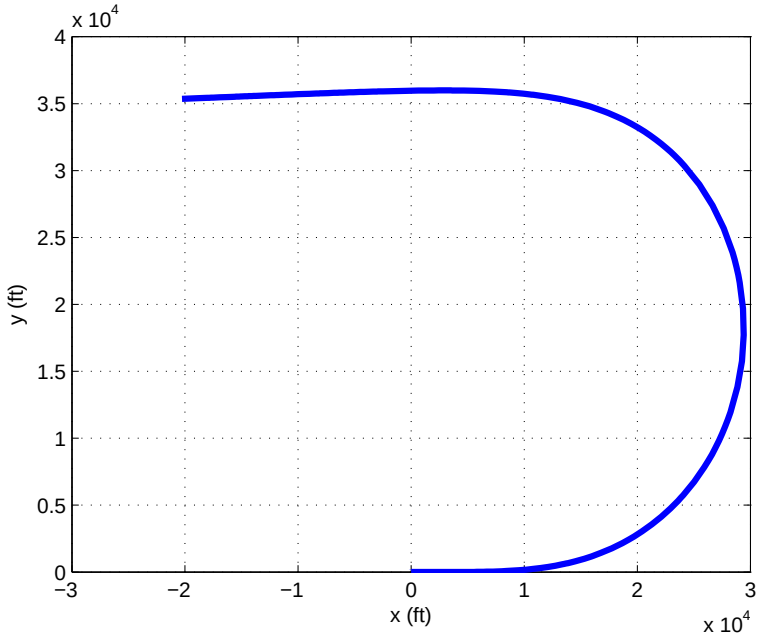

Figure 5.5: Projection of flight trajectory on horizontal plane.

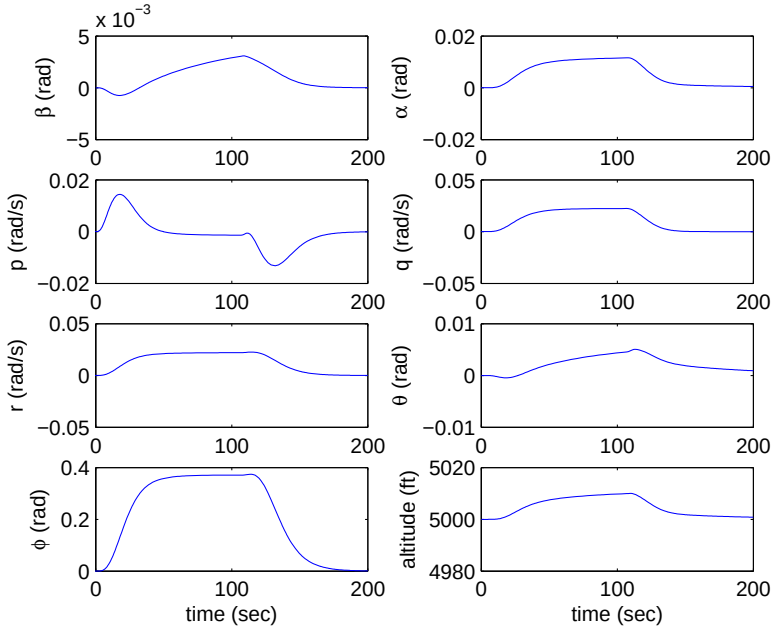

Figure 5.6: System states of nominal performance.

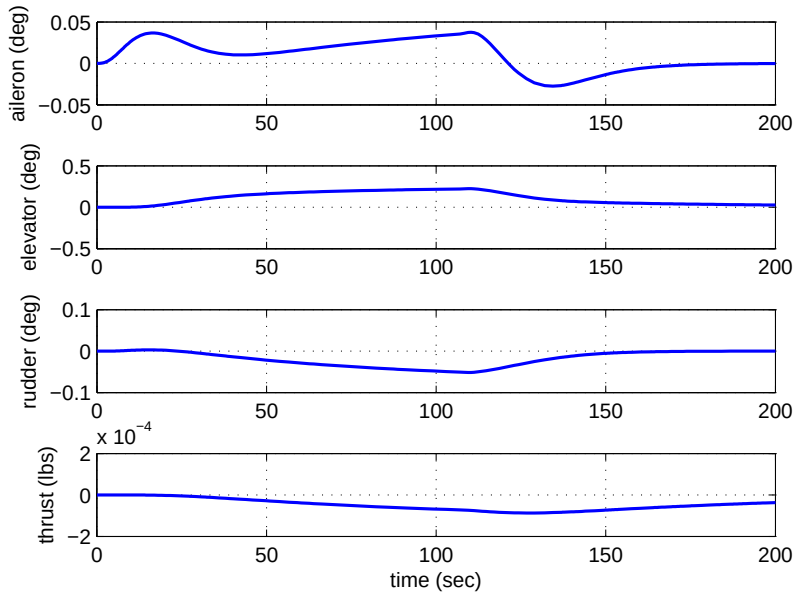

Figure 5.7: System control inputs of nominal performance.

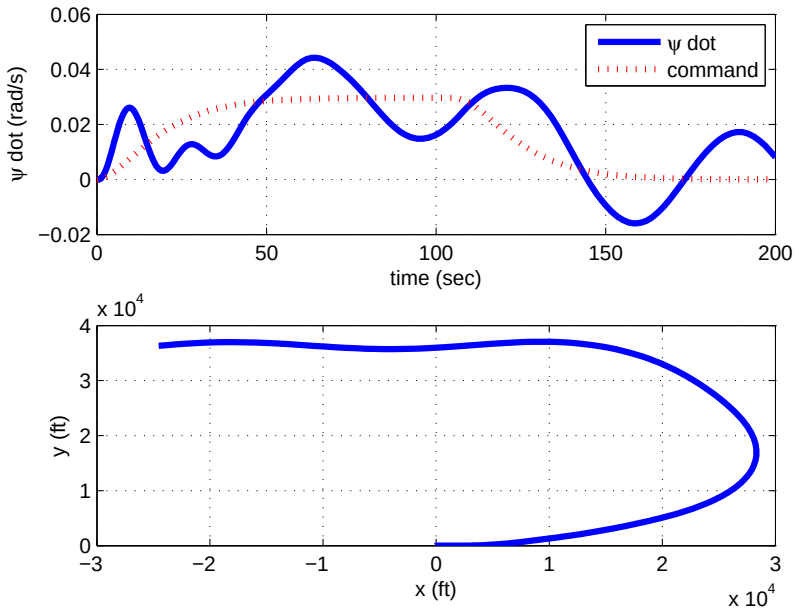

Figure 5.8: Performance under rolling and pitching uncertainties.

uncertainty is introduced, the performance is degraded too. Figure 5.9 shows the degradations in the presence of actuator effectiveness reduction.

When we apply the $\mathcal{L}_1$ adaptive controller to the system in the presence of uncertainties, the nominal performance can be recovered satisfactorily. When considering induced roll and pitch moment uncertainties, the responses in Figure 5.10 and Figure 5.11 show the recovery of nominal performance. In Figure 5.12 the adaptive control signals are shown, which are augmentations of the baseline controller and stay within reasonable range. In Figures 5.13 and 5.14, the $\mathcal{L}_1$ adaptive controller performance in the presence of control effectiveness reduction is shown for the entire maneuver, and Figure 5.15 shows the adaptive control signal for this case.

If the coordinated turn is done at a different yaw rate, the yaw rate command is different. The $\mathcal{L}_1$ adaptive controller has scaled tracking performance, which is typical for linear system's response. We increase the amplitude of the original yaw rate command by 25%, that is,

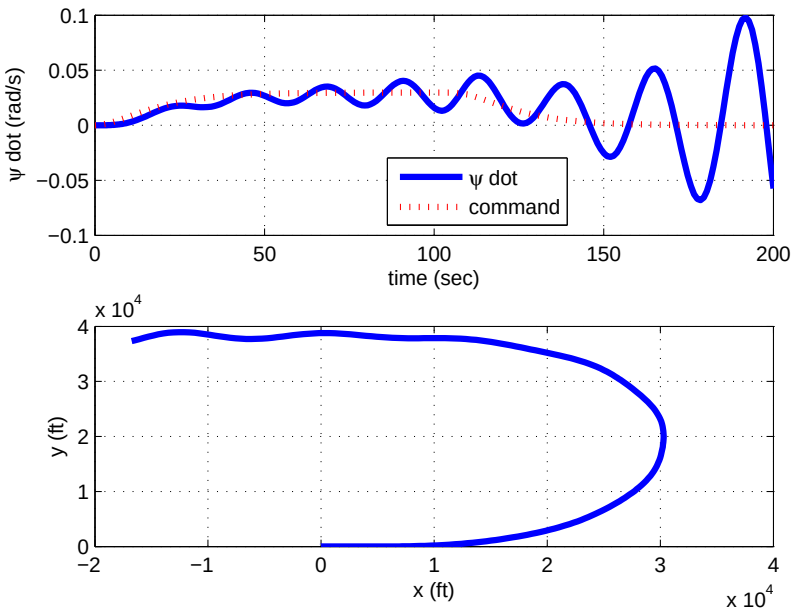

Figure 5.9: Performance under actuator effectiveness reduction.

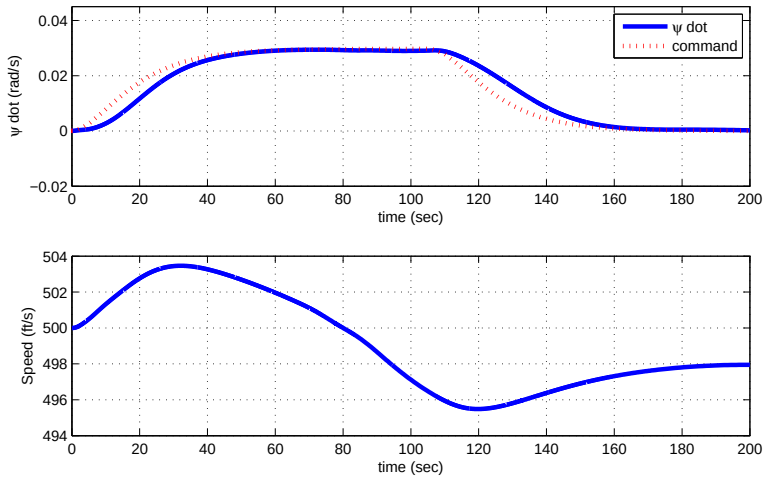

Figure 5.10: Output performance of $\mathcal{L}_1$ control - rolling and pitching moment uncertainties.

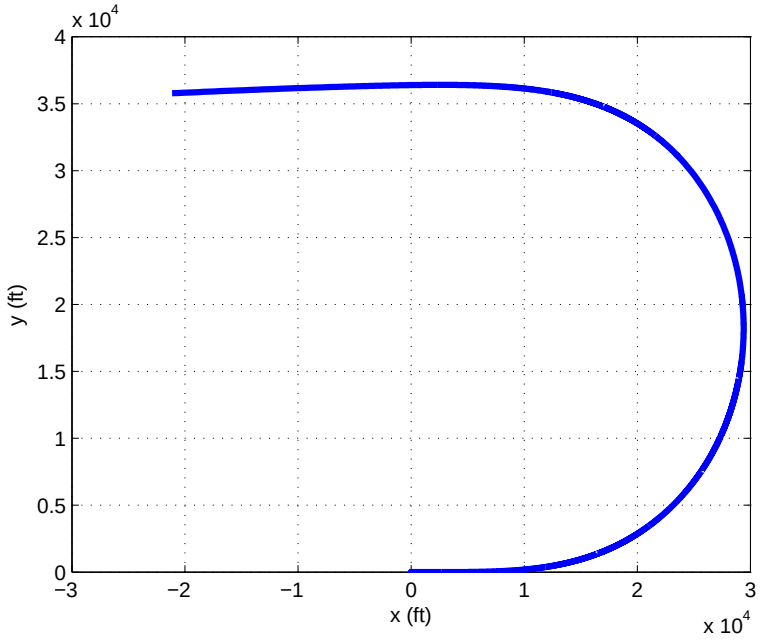

Figure 5.11: Flight trajectory with rolling and pitching moment uncertainties.

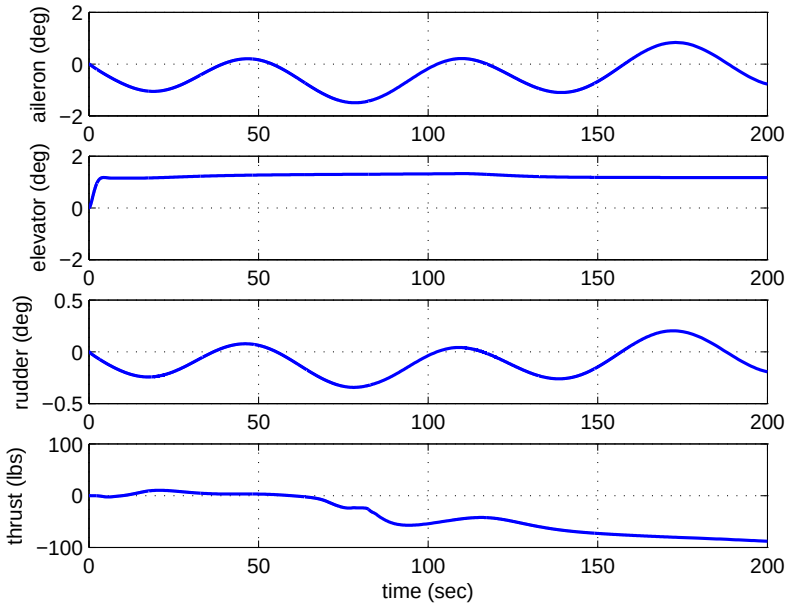

Figure 5.12: Adaptive control signals - rolling and pitching moment uncertainties.

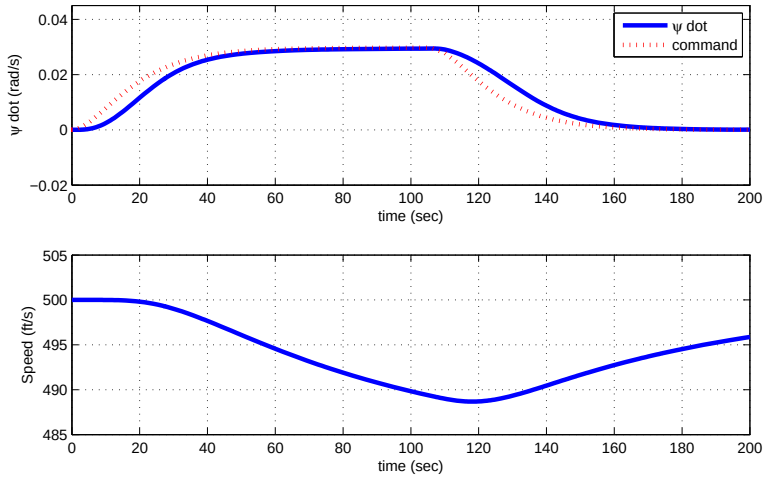

Figure 5.13: Output performance of $\mathcal{L}_1$ control - control effectiveness reduction.

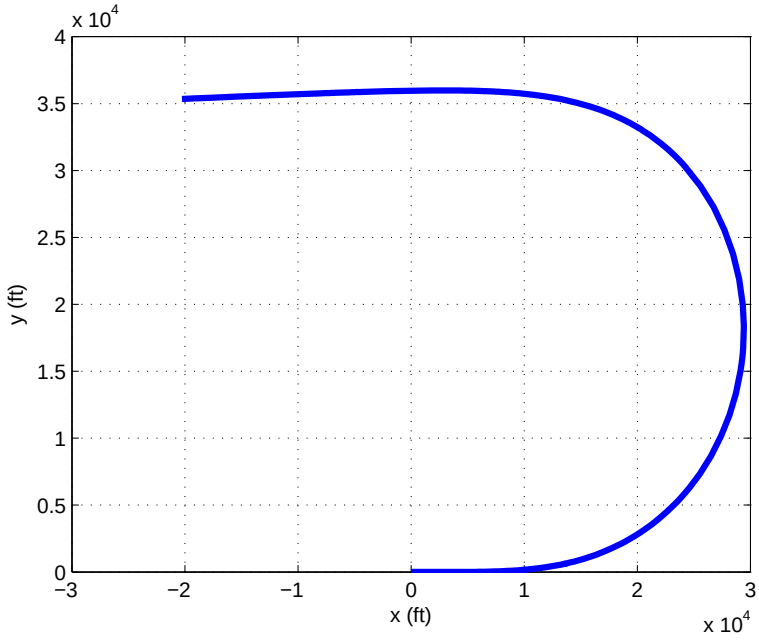

Figure 5.14: Flight trajectory with control effectiveness reduction.

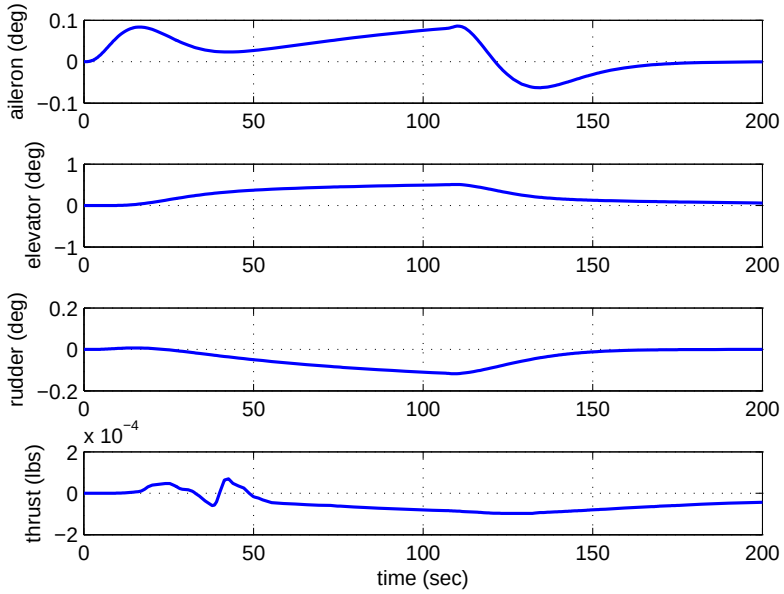

Figure 5.15: Adaptive control signals - control effectiveness reduction.

$\dot{\psi} = 0.0371$ rad/s. It is obvious that the coordinated turning maneuver can be finished sooner in this case. The new yaw rate command and original yaw rate command are shown in Figure 5.16. The performance in the presence of rolling and pitching moment uncertainties is shown in Figure 5.17 , and it can be seen that the performance degrades.

The $\mathcal{L}_1$ adaptive controller is applied to this scenario without any re-tuning of the controller. The output performance is shown in Figure 5.18. If we compare it to the yaw rate commands shown in Figure 5.16, we can see that the $\mathcal{L}_1$ adaptive controller has scaled tracking performance. The adaptive control signal is plotted in Figure 5.19.

5.7 Conclusion

In this chapter, $\mathcal{L}_1$ state feedback adaptive controller is extended to time-varying reference systems. The adaptive controller intends to augment a gain-scheduled baseline controller.

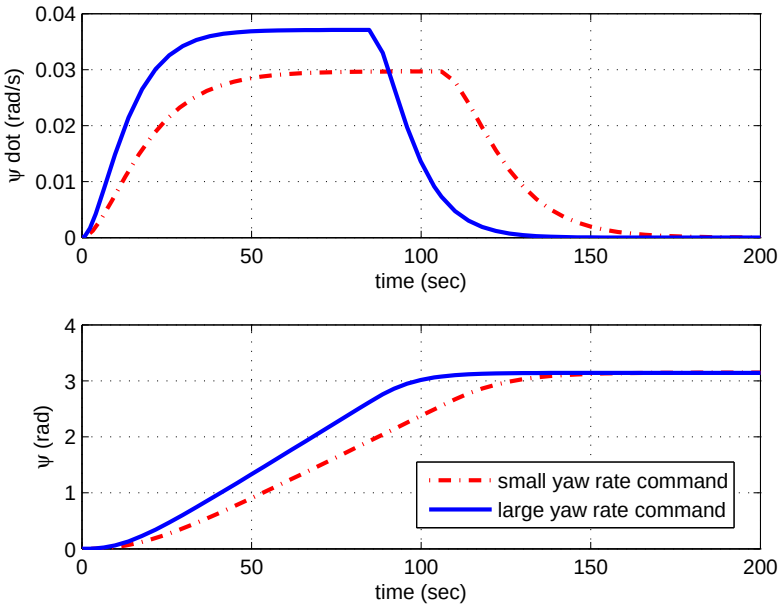

Figure 5.16: Comparison of yaw rate commands in two scenarios.

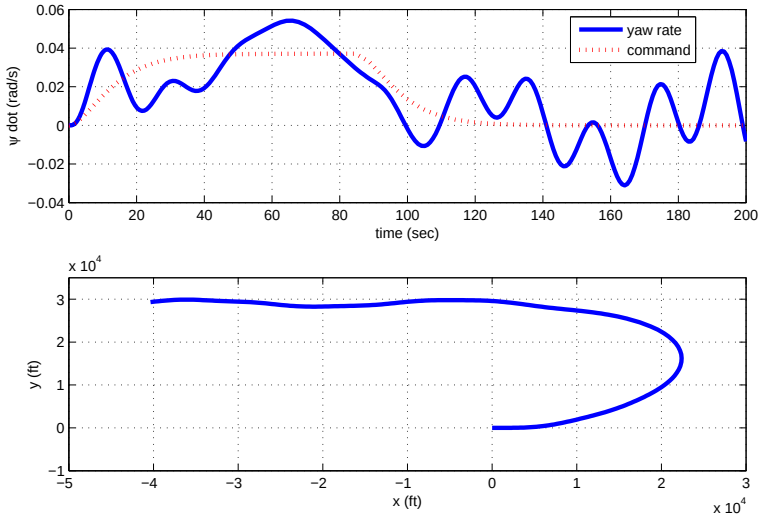

Figure 5.17: Performance under rolling and pitching moment uncertainties.

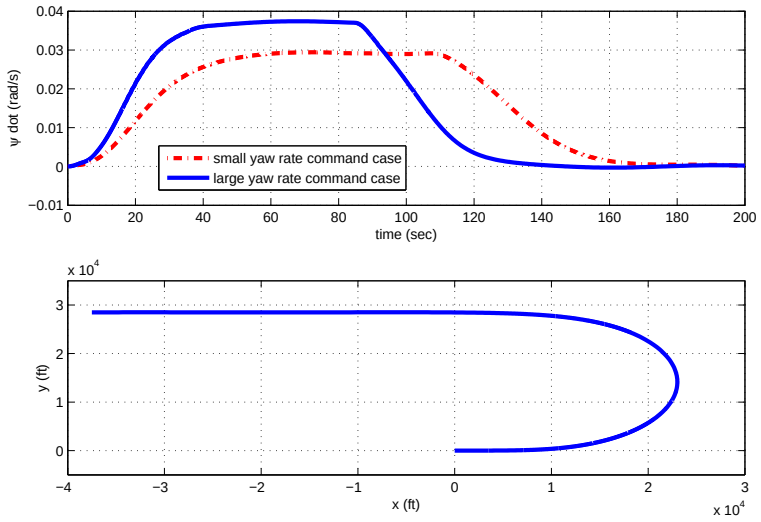

Figure 5.18: Output performance of $\mathcal{L}_1$ - rolling and pitching moment uncertainties.

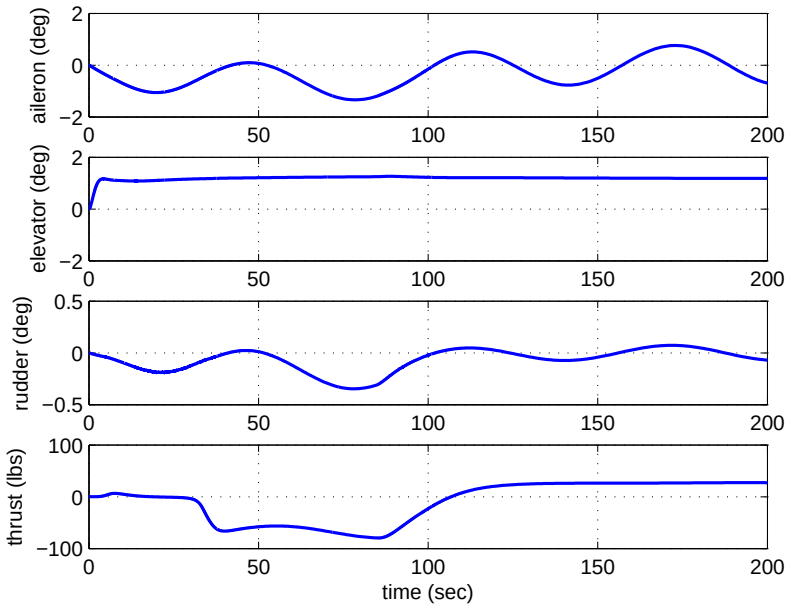

Figure 5.19: Adaptive control signal - rolling and pitching moment uncertainties.

The reference system, which is determined by the closed loop system of the plant and the baseline gain-scheduled controller, is time-varying. The benefits of the proposed controller in this paper are: the adaptive controller with time-varying reference system is proved to have guaranteed performance bounds similar to those obtained for the case of linear time-invariant reference systems; the sufficient condition for stability of this new method is not worsening the slow rate of variation condition required by gain-scheduled controller, which means that the combined adaptive and baseline controller do not require more conservative condition on the rate of variation of the scheduling variables. With this result, the aerial refueling application can be extended to a complete scenario, which includes a racetrack maneuver of aircraft.

Chapter 6

Concluding Chapter

6.1 Summary

This dissertation addresses problems of flight control for aerial vehicles and weapons in highly uncertain dynamical environment. The $\mathcal{L}_1$ adaptive controller is extended in this dissertation to time-varying reference systems. Its output feedback variant is elaborated from the design perspective. Various flight control examples are discussed on mid-to-high fidelity simulations.

Adaptive control for uncertain systems usually needs to handle two types of uncertainties: matched and unmatched uncertainties. Both of these uncertainties appear in practical flight control problems. In this dissertation, adaptive approaches which can compensate for these two types of uncertainties are discussed respectively. Different perspectives of $\mathcal{L}_1$ adaptive control method are studied in several chapters.

Chapter 3 presents $\mathcal{L}_1$ state feedback adaptive controller for time-invariant reference systems. The multi-input multi-output extension of this method is discussed. Two benchmark flight control applications are studied. The following advantages of $\mathcal{L}_1$ adaptive controller over conventional adaptive control methods make it suitable for development of theoretically

justified tools for Verification and Validation of adaptive systems: i) it has guaranteed uniformly bounded transient response for system's both signals, input and output; ii) it enables fast adaptation while maintains a bounded away from zero time delay margin. It is shown that the proposed adaptive control approach can recover the nominal performance of the flight systems in the presence of actuator effectiveness reduction and matched uncertainties, even if the uncertainty is a nonlinear, fast time-varying function of system states. In the simulations section, it is demonstrated via numerical examples that the bounded-away-from-zero time-delay margin of this adaptive controller can be improved by systematic choice of the underlying filters.

In Chapter 4, the $\mathcal{L}_1$ output feedback adaptive controller is explored from its design perspective. It can handle unmatched uncertainties. The adaptive output feedback controller can be applied to achieve reference system behavior that does not verify the Strict Positive Real (SPR) condition for its input-output transfer function. In this dissertation, specific design guidelines are presented that render the approach suitable for practical applications. Longitudinal autopilot design for a missile model is performed using $\mathcal{L}_1$ adaptive output feedback controller. The new piece-wise constant adaptive law along with the low-pass filtered control signal ensures uniform performance bounds for system's both input/output signals. The simulation responses of the proposed controller demonstrate the benefits of the $\mathcal{L}_1$ adaptive controller.

Finally, in Chapter 5, the $\mathcal{L}_1$ state feedback adaptive controller is extended to time-varying reference systems. The adaptive controller intends to augment a gain-scheduled baseline controller. The reference system, which is determined by the closed loop system of the plant and the baseline gain-scheduled controller, is time-varying. The benefits of the proposed controller in this chapter are: i) the adaptive controller with time-varying reference system is proved to have guaranteed performance bounds similar to those obtained for the case of time-invariant reference systems; ii) the sufficient condition for stability of this new method "matches" the slow-variation condition required by gain-schedule controller, which means the combined adaptive and baseline controller do not require more conservative condition on the

variation rate of the scheduling variables. With this result, the aerial refueling application can be extended to a complete scenario, which includes a racetrack maneuver of an aircraft.

6.2 Future Work

The time-delay margin analysis is only studied analytically for a simple case. The time-delay margin of systems with more general form of uncertainties in flight control problems are calculated numerically. Although this still can show that the results agree with the theoretical predictions, analytical analysis is desirable. Further analysis and verification is needed for multi-input multi-output systems with general form of uncertainties. The time-delay margin analysis for $\mathcal{L}_1$ adaptive output feedback controller is also needed.

For the output feedback method, the current design guideline can be improved further, with the help of linear design tools, to find satisfactory controller more quickly. This is especially important if the plant is non-minimum phase and unstable.

There are some issues requiring further investigation of $\mathcal{L}_1$ adaptive controller with time-varying reference systems.

First, extension to more general class of uncertainties, e.g. unknown nonlinear function of states and time, can be done.

Second, although rigorous mathematical details and proofs are given, further relaxation of the assumptions and/or more effective methods are needed if we want to apply the proposed adaptive method to practical linear time-varying systems and baseline controllers with verifiable results.

Third, design guidelines need to be elaborated with details. For the time-varying reference system, more mathematical tools are needed for developing the design guidelines. We discuss here some possible tools towards this end.

As indicated in subsection 5.3.3, the reference system in (5.12)-(5.13) has a different response

as compared to (5.33) achieved with (5.32) due to the inclusion of low pass filter $C(s)$. In [3, 7], specific design guidelines are suggested for selection of $C(s)$ to ensure that in case of constant A_m, b, θ and σ the response of $x_{ref}(t)$ and $u_{ref}(t)$ can be made as close as possible to (5.33). However, in the case of time-varying reference system, the mathematical tools used in [3, 7] cannot be applied. With new mathematical tools, it is possible to show that the desired performance of (5.33) can be recovered asymptotically when the bandwidth of the low pass filter $C(s)$ goes to infinity. We can show this for $C(s) = \frac{\omega}{s+\omega}$. Let $f(t, x_{ref}(t)) = \theta(t)^\top x_{ref}(t) + \sigma(t)$. If the signal $\tilde{f}(t, x_{ref}(t))$ is defined as

$$\tilde{f}(s) = \frac{s}{s+\omega} f(s),$$

then the closed loop reference system changes to

$$\begin{aligned} \dot{x}_{ref}(t) &= A_m(t)x_{ref}(t) + b(t)\left(\tilde{f}(t) + k_g(t)r(t)\right) \\ \frac{1}{\omega}\dot{\tilde{f}}(t) &= -\tilde{f}(t, x_{ref}(t)) + \frac{1}{\omega}\dot{f}(t, x_{ref}(t)). \end{aligned} \tag{6.1}$$

Notice that $\dot{f}(t, x_{ref}(t))$ is bounded. The system (6.1) has a structure of singularly perturbed systems. Let $\mathcal{P}_\epsilon$ be the input-output map from $r(t)$ to the output of the linear time-varying system (6.1), and $\mathcal{P}_0$ be the input-output map from $r(t)$ to $y_{ref}(t)$ of the desired linear time-varying system (5.33). Application of tools from singular perturbation theory [112] and robust control [113, 114] can possibly lead to a provable result of the following nature: the system $\mathcal{P}_\epsilon$ "approaches" the system $\mathcal{P}_0$ in an appropriately chosen metric, when the bandwidth ω of the low-pass filter goes to infinity. This can lead to elaborating the details of design guidelines for $\mathcal{L}_1$ adaptive controller with time-varying reference systems.

Bibliography

[1] K. Wise, E. Lavretsky and N. Hovakimyan, Adaptive Control of Flight: Theory, Applications, and Open Problems, *Proceedings of American Control Conference*, 5966-5971, Minneapolis, MN, June 2006.

[2] M. Steinberg, Historical Overview of Research in Reconfigurable Flight Control, *Proceedings of the Institution of Mechanical Engineers, Part G: Journal of Aerospace Engineering*, 219(4):263-275, 2005.

[3] C. Cao and N. Hovakimyan, Design and Analysis of a Novel $\mathcal{L}_1$ Adaptive Control Architecture with Guaranteed Transient Performance, *IEEE Transactions on Automatic Control*, 53(2):586-891, 2008.

[4] C. Cao and N. Hovakimyan, Adaptive Output Feedback Controller for Systems of Unknown Dimension, *IEEE Transactions on Automatic Control*, 53(3):815-821, 2008.

[5] C. Cao and N. Hovakimyan, Novel $\mathcal{L}_1$ Neural Network Adaptive Control Architecture with Guaranteed Transient Performance, Special Issue on Feedback Control of *IEEE Transactions on Neural Networks*, 18(4):1160-1171, 2007.

[6] C. Cao and N. Hovakimyan, Design and Analysis of a Novel $\mathcal{L}_1$ Adaptive Controller, Part I: Control Signal and Asymptotic Stability, *Proceedings of American Control Conference*, 3397-3402, Minneapolis, MN, June 2006.

[7] C. Cao and N. Hovakimyan, Design and Analysis of a Novel $\mathcal{L}_1$ Adaptive Controller, Part II: Guaranteed Transient Performance, *Proceedings of American Control Conference*, 3403-3408, Minneapolis, MN, June 2006.

[8] C. Cao, N. Hovakimyan Guaranteed Transient Performance with $\mathcal{L}_1$ Adaptive Controller for Systems with Unknown Time varying Parameters and Bounded Disturbance: Part I, *Proceedings of American Control Conference*, 3925-3930 New York, NY, July 2007.

[9] C. Cao and N. Hovakimyan, Stability Margins of $\mathcal{L}_1$ Adaptive Controller: Part II, *Proceedings of American Control Conference*, 3931-3936, New York, NY, July 2007.

[10] C. Cao and N. Hovakimyan, $\mathcal{L}_1$ Adaptive Controller for a Class of Systems with Unknown Nonlinearities: Part I, *Proceedings of American Control Conference*, 4093-4098, Seattle, WA, 2008.

[11] C. Cao and N. Hovakimyan, $\mathcal{L}_1$ Adaptive Output Feedback Controller for Systems of Unknown Relative Degree, *Submitted to American Control Conference*, 2009.

[12] J. Wang, C. Cao, N. Hovakimyan, R. Hindman and D. B. Ridgely, $\mathcal{L}_1$ Adaptive Controller for a Missile Longitudinal Autopilot Design, *Proceedings of AIAA Guidance, Navigation, and Control Conference and Exhibit*, AIAA-2008-6282, Honolulu, HI, 2008.

[13] K. S. Narendra and A. M. Annaswamy, *Stable Adaptive Systems*, Prentice Hall, 1989.

[14] J.-J. E. Slotine and W. Li. *Applied Nonlinear Control*. Prentice Hall, Englewood Cliffs, NJ, 1991.

[15] S. Sastry and M. Bodson, *Adaptive Control: Stability, Convergence and Robustness*, Prentice Hall, 1989.

[16] P. Ioannou and J. Sun. *Robust Adaptive Control*. Prentice Hall, New Jersey, 1996.

[17] M. Krstic, I. Kanellakopoulos, and P. Kokotovic. *Nonlinear and Adaptive Control Design*. John Wiley & Sons, New York, 1995.

[18] K. J. Astrom and B. Wittenmark. *Adaptive Control*. Addison Wesley, Massachusetts, 1989.

[19] A. Datta and M.-T. Ho. On modifying model reference adaptive control schemes for performance improvement. *IEEE Transactions on Automatic Control*, 39(9):1977-1980, September 1994.

[20] G. Bartolini, A. Ferrara, and A. A. Stotsky. Robustness and performance of an indirect adaptive control scheme in presence of bounded disturbances. *IEEE Transactions on Automatic Control*, 44(4):789-793, April 1999.

[21] J. Sun. A modified model reference adaptive control scheme for improved transient performance. *IEEE Transactions on Automatic Control*, 38(7):1255-1259, July 1993.

[22] D.E. Miller and E.J. Davison. Adaptive control which provides an arbitrarily good transient and steady-state response. *IEEE Transactions on Automatic Control*, 36(1):68-81, January 1991.

[23] R. Costa. Improving transient behavior of model-reference adaptive control. *Proc. of American Control Conference*, 576-580, 1999.

[24] P. Ioannou and J. Sun. *Robust Adaptive Control*. Prentice Hall, 1996.

[25] B.E. Ydstie. Transient performance and robustness of direct adaptive control. *IEEE Transactions on Automatic Control*, 37(8):1091-1105, August 1992.

[26] M. Krstic, P. V. Kokotovic, and I. Kanellakopoulos. Transient performance improvement with a new class of adaptive controllers. *Systems & Control Letters*, 21:451-461, 1993.

[27] R. Ortega. Morse's new adaptive controller: Parameter convergence and transient performance. *IEEE Transactions on Automatic Control*, 38(8):1191-1202, August 1993.

[28] Z. Zang and R. Bitmead. Transient bounds for adaptive control systems. *Proc. of* 30^{th} *IEEE Conference on Decision and Control*, 2724-2729, December 1990.

[29] A. Datta and P. Ioannou. Performance analysis and improvement in model reference adaptive control. *IEEE Transactions on Automatic Control*, 39(12):2370-2387, December 1994.

[30] A. M. Arteaga and Y. Tang. Adaptive control of robots with an improved transient performance. *IEEE Transactions on Automatic Control*, 47(7):1198-1202, July 2002.

[31] K. S. Narendra and J. Balakrishnan. Improving transient response of adaptive control systems using multiple models and switching. *IEEE Transactions on Automatic Control*, 39(9):1861-1866, September 1994.

[32] K. S. Narendra and J. Balakrishnan. Improving transient response of adaptive control systems using multiple models and switching. *IEEE Transactions on Automatic Control*, 39(9):1861-1866, September 1994.

[33] R. Marino and P. Tomei, An Adaptive Output Feedback Control for A Class of Nonlinear Systems with Time varying Parameters. *IEEE Transactions on Automatic Control*, 44(11):2190-2194, 1999.

[34] K. S. Tsakalis and P. A. Ioannou, Adaptive Control of Linear Time varying Plants. *Automatica*, 23:459-468, 1987.

[35] R. H. Middleton and G. C. Goodwin, Adaptive Control of Time varying Linear Systems. *IEEE Transactions on Automatic Control*, 33(2):150-155, 1988.

[36] Y. Zhang and P. Ioannou. Adaptive Control of Linear Time varying Systems, *Proceedings of IEEE Conference on Decision and Control*, 837-842, Kobe, Japan, December 1996 .

[37] B. D. O. Anderson and R. M. Johnstone, Adaptive Systems and Time varying Plants. *International Journal of Control*, 37:367-377, 1983.

[38] B. D. O. Anderson, Adaptive Systems, Lack of Persistency of Excitation and Bursting Phenomena. *Automatica*, 21(3), 1985.

[39] K. S. Narendra and A. M. Annaswamy, Persistent Excitation and Robust Adaptive Algorithms, *Proceedings of 3rd Yale Workshop on Applied Adaptive Systems Theory*, New Haven, CT, June 15-17, 1983.

[40] A. M. Annaswamy and J. Jang, Adaptive Gain-scheduled Controller in the Presence of Actuator Anomalies, *Proceedings of AIAA Guidance, Navigation, and Control Conference and Exhibit*, AIAA-2008-7285, Honolulu, HI, 2008.

[41] W. D. Morse and K. A. Ossman, Model Following Reconfigurable Flight Control System for the AFTI/F-16, *Journal of Guidance, Control and Dynamics*, 13(6):969-976, 1990.

[42] K. Wise, E. Lavretsky, J. Zimmerman, J. Francis-Jr, D. Dixon and B. Whitehead, Adaptive Flight Control of a Sensor Guided Munitions, *Proceedings of AIAA Guidance, Navigation, and Control Conference and Exhibit*, AIAA-2005-6385, San Francisco, CA, August, 2005.

[43] Self-Repairing Flight Control System, *Final Report*, WL-TR-91-3025, August, 1991.

[44] P. Maybeck, Application of Multiple Model Adaptive Algorithms to Reconfigurable Flight Control, *IEEE Transactions on Aerospace Electric System*, 27(3):470-480, 1991.

[45] F. Ahmed-Zaid, P. Ioannou, K. Gousman and R. Rooney, Accomodation of Failures on the F-16 Aircraft using Adaptive Control, *IEEE Control Systems Magazine*, 11(1):73-78, 1991.

[46] J. Monaco, D. Ward, R. Barron and R. Bird, Implementation and Flight Test Assessment of an Adaptive, Reconfigurable Flight Control System, *Proceedings of AIAA Guidance, Navigation, and Control Conference and Exhibit*, AIAA-1997-3738, New Orleans, LA, August, 1997.

[47] M. L. Steinberg, An Initial Assessment of Neural Network and Fuzzy Logic for Flight Control, *Proceedings of American Control Conference*, 173-177, Baltimore, MD, 1994.

[48] B. S. Kim and A. J. Calise, Nonlinear Flight Control Using Neural Networks, *Journal of Guidance, Control and Dynamics*, 20(1):26-33, 1997.

[49] K. Wise, Reconfigurable Systems for Tailless Fighter Aircraft - RESTORE, *Final Report*, AFRL-VA-WP-TR-99-3067.

[50] M. Sharma, A. J. Calise and J. E. Corban, Application of an Adaptive Autopilot Design to a Family of Guided Munitions, *Proceedings of AIAA Guidance, Navigation, and Control Conference and Exhibit*, AIAA-2000-3969, Denver, CO, August, 2000.

[51] J. E. Corban, V. Burkemper, K. Holt, J. Evers, A. J. Calise and M. Sharma, Flight Test of An Adaptive Autopilot For Precision Guided Munitions, *Proceedings of AIAA Missile Sciences Conference*, 2000.

[52] M. Sharma, K. Wise and E. Lavretsky, Application and Flight Testing of an Adaptive Autopilot on Precision Guided Munitions, *Proceedings of AIAA Guidance, Navigation, and Control Conference and Exhibit*, AIAA-2006-6568, Keystone, CO, August, 2006.

[53] J. Brinker and K. Wise, Reconfigurable Flight Control for a Tailless Advanced Fighter Aircraft, *Proceedings of AIAA Guidance, Navigation, and Control Conference and Exhibit*, AIAA-1998-4107, Boston, MA, August, 1998.

[54] K. Wise, J. Brinker, A. Calise, D. Enns, M. Elgersma and P. Voulgaris, Direct Adaptive Reconfigurable Flight Control For A Tailless Advanced Fighter Aircraft, *Int. Journal of Robust Nonlinear Control, Special Issue on Reconfigurable Flight Control*, 9:999-1012, 1999.

[55] E. Lavretsky and K. Wise, Adaptive Flight Control for Manned/Unmanned Military Aircraft, *Proceedings of American Control Conference*, Portland, OR, June, 2005.

[56] J. P. Nalepka and J. L. Hinchman, Automated Aerial Refueling: Extending the Effectiveness of Unmanned Air Vehicles, *Proceedings of AIAA Modeling and Simulation Technologies Conference and Exhibit*, AIAA-2005-6005, San Francisco, Aug. 2005.

[57] M. A. Abidi and R. C. Gonzalez, The Use of Multisensor Data for Robotic Applications, *IEEE Transactions on Robotics and Automation*, 6(2):159-177, 1990.

[58] C. M. Andersen, Three Degree of Freedom Compliant Motion Control for Robotic Aircraft Refueling, *Air Force Institute of Technology*, Wright Patterson AFB, OH, Dec. 1990.

[59] R. A. Bennett, Brightness Invariant Port Recognition for Robotic Aircraft Refueling, *Air Force Institute of Technology*, Afit/gae/eng/90d-04, Wright Patterson AFB, OH, 13 Dec. 1990.

[60] W.B. Blake, E.G. Dickes and D.R. Gingras, UAV Aerial Refueling - Wind Tunnel Results and Comparison with Analytical Predictions, AIAA-2004-4820, *Proceedings of AIAA Atmospheric Flight Mechanics Conference and Exhibit*, AIAA-2004-4820, Providence, RI, 2004.

[61] A. Dogan, S. Sato and W. Blake, Flight Control and Simulation for Aerial Refueling, AIAA-2005-6264, *Proceedings of AIAA Guidance, Navigation, and Control Conference and Exhibit*, AIAA-2005-6264, San Francisco, CA, 2005.

[62] G. Campa , M. L. Fravolini, A. Ficola, M. R. Napolitano, B. Seanor and M. G. Perhinschi, Autonomous Aerial Refueling for UAVs Using a Combined GPS-Machine Vision Guidance, *Proceedings of AIAA Guidance, Navigation, and Control Conference and Exhibit*, AIAA-2004-5350, Providence, RI, August 2004.

[63] M. L. Fravolini, A. Ficola, M. R. Napolitano, G. Campa and M. G. Perhinschi, Development of Modelling and Control Tools for Aerial Refueling for UAV, AIAA-2003-5798, *Proceedings of AIAA Guidance, Navigation, and Control Conference*, AIAA-2003-5798, Austin, TX, 2003.

[64] G. Lachapelle, H. Sun, M. E. Cannon and G. Lu, Precise Aircraft-to-Aircraft Positioning Using a Multiple Receiver Configuration, *National Technical Meeting, Institute of Navigation*, San Diego, CA, 1994.

[65] M. Pachter, C. Houpis and D. Trosen, Design of an Air-to-air Automatic Refueling Flight Control System using Quantitative Feedback Theory, *International Journal of Robust and Nonlinear Control*, 7(6):561-580, 1997.

[66] R. P. Shipman, Visual Servoing for Autonomous Aircraft Refueling, *Air Force Institute of Technology*, Afit/gae/eng/89d-48, Wright Patterson AFB, OH, 13 Dec. 1989.

[67] V. Stepanyan, E. Lavretsky and N. Hovakimyan, Aerial Refueling Autopilot Design Methodology: Application to F-16 Aircraft Model, AIAA-2004-5321, *Proceedings of AIAA Guidance, Navigation, and Control Conference*, AIAA-2004-5321, Providence, RI, 2004.

[68] J. Valasek, K. Gunnam, J. Kimmett, M. D. Tandale, J. L. Junkins and D. Hughes, Vision-Based Sensor and Navigation System for Autonomous Air Refueling, *Journal of Guidance, Control, and Dynamics*, 28(5):979-988, 2005.

[69] M. D. Tandale, R. Bowers and J. Valasek, Trajectory Tracking Controler for Vision-Based Probe and Drogue Autonomous Aerial Refueling, *Journal of Guidance, Control, and Dynamics*, 29(4):846-857, 2006.

[70] S. Venkataramanan, A. Dogan and W. Blake, Vortex Effect Modelling in Aircraft Formation Flight, AIAA-2003-5385, *Proceedings of AIAA Atmospheric Flight Mechanics Conference and Exhibit*, AIAA-2003-5385, Austin, TX, 2003.

[71] S. M. Ross, M. Pachter, D. R. Jacques, B. A. Kish and D. R. Millman Autonomous Aerial Refueling Based on the Tanker Reference Frame, *Proceedings of IEEE Aerospace Conference*, Big Sky, MT, March 2006.

[72] A. L. Smith and D. L. Kunz Dynamic Coupling of the KC-135 Tanker and Boom for Modeling and Simulation, *Proceedings of AIAA Modeling and Simulation Technologies Conference and Exhibit*, AIAA-2006-6480, Keystone, CO, August 2006.

[73] Y. Ochi and T. Kominami Flight Controlfor Autonomous Aerial Refueling via PNG and LOS Angle Contorl, *Proceedings of AIAA Guidance, Navigation, and Control Conference and Exhibit*, AIAA-2005-6268, San Francisco, CA, August 2005.

[74] M. Herrnberger, G. Sachs, F. Holzapfel, W. Tostmann and E. Weixler Simulation Analysis of Autonomous Aerial Refueling Procedures, *Proceedings of AIAA Guidance, Navigation, and Control Conference and Exhibit*, AIAA-2005-5866, San Francisco, CA, August 2005.

[75] K. Johnson and K. Awni A Roll Autopilot for Autonomous Air Refueling, *Proceedings of AIAA Guidance, Navigation, and Control Conference and Exhibit*, AIAA-2002-4752, Monterey, CA, August 2002.

[76] V. Patel, C. Cao, N. Hovakimyan, K. Wise and E. Lavretsky, $\mathcal{L}_1$ Adaptive Controller for Tailless Unstable Aircraft in the Presence of Unknown Actuator Failures , *Proceedings of AIAA Guidance, navigation and Control Conference*, AIAA-2007-6314, Hilton Head Island, SC, August 2007.

[77] J. Farrell, M. Sharma and M. Polycarpou, Backstepping-Based Flight Control with Adaptive Function Approximation, *Journal of Guidance, Control and Dynamics*, 8(6):1089-1102, 2005.

[78] D. Li, N. Hovakimyan, C. Cao and K. Wise, Filter Design for Feedback-loop Trade-off of $\mathcal{L}_1$ Adaptive Controller: A Linear Matrix Inequality Approach, *Proceedings of AIAA Guidance, navigation and Control Conference*, AIAA-2008-6280, Honolulu, HI, August 2008.

[79] J. Wang, V. Patel, C. Cao, N. Hovakimyan and E. Lavretsky, Novel $\mathcal{L}_1$ Adaptive Control Methodology for Aerial Refueling with Guaranteed Transient Performance, *Journal of Guidance, Control and Dynamics*, 31(1):182-193, 2008.

[80] W. B. Blake, E. G. Dickes and D. R. Gingras, UAV Aerial Refueling - Wind Tunnel Results and Comparison with Analytic Predictions, *Proceedings of AIAA Atmospheric*

Flight Mechanics Conference and Exhibit, AIAA-2004-4820, Providence, RI, AIAA-2004-4820, 2004.

[81] H. K. Khalil. *Nonlinear Systems*. Prentice Hall, Englewood Cliffs, NJ, 2002.

[82] K. Zhou and J. C. Doyle. *Essentials of Robust Control*. Prentice Hall, Englewood Cliffs, NJ, 1998.

[83] J. Wang, C. Cao, N. Hovakimyan and E. Lavretsky Novel $\mathcal{L}_1$ Adaptive Control Approach to Autonomous Aerial Refueling with Guaranteed Transient Performance, *Proceedings of American Control Conference*, 3569-3574, Minneapolis, MN, June 2006.

[84] J. Wang, V. V. Patel, C. Cao, N. Hovakimyan and E. Lavretsky $\mathcal{L}_1$ Adaptive Neural Network Controller for Autonomous Aerial Refueling with Guaranteed Transient Performance, *Proceedings of AIAA Guidance, Navigation and Control Conference*, AIAA-2006-6206, Keystone, CO, August 2006.

[85] C. Cao, V. Patel, C. K. Reddy, N. Hovakimyan and E. Lavretsky, Are the Phase and Time-delay Margins Always Adversely Affected by High-Gain? *AIAA Guidance, Navigation and Control Conference*, AIAA-2006-6347, Keystone, CO, August 2006.

[86] J. Farrell, M. Sharma and M. Polycarpou, Backstepping-Based Flight Control with Adaptive Function Approximation, *Journal of Guidance, Control, and Dynamics*, 28(6):1089-1102, 2005.

[87] S.P. Fears, H.M. Ross and T.M.Moul, Low-Speed Wind-Tunnel Investigation of the Stability and Control Characteristics of a Series of Flying Wings with Sweep Angles of 50° , NASA TM 4640, June 1995

[88] F. Lewis, S. Jagannathan and A. Yesildirek, *Neural Network Control of Robot Manipulators and Nonlinear Systems*. London, Taylor and Francis, 1998.

[89] S. M. Shahruz and S. Behtash. Design of Controllers for Linear Parameter-varying Systems by the Gain Scheduling Technique. *Journal of Mathematical Analysis and Applications.* 168(1), 1992.

[90] D. J. Stilwell and W. J. Rugh. Stability Preserving Interpolatoin Methods for the Synthesis of Gain Scheduled Controllers. *Automatica.* 36(5), 2000.

[91] A. Packard. Gain-scheduling via Linear Fractional Transformations. *Systems and Control Letters.* 22, 1994.

[92] P. Apkarian and P. Gahinet. A Convex Characterization of Gain-Scheduled H_∞ Controllers. *IEEE Transactions on Automatic Control.* 40(5), 1995.

[93] I. Kaminer, A. M. Pascoal, P. P. Khargonekar and E. E. Coleman. A Velocity Algorithm for the Implementation of Gain-scheduled Controllers. *Automatica.* 31(8), 1995.

[94] W. J. Rugh and J. S. Shamma. Research on Gain Scheduling. *Automatica.* 36(10), 2000.

[95] D. J. Leith and W. E. Leithead, Survey of Gain-scheduling Analysis and Design. *International Journal of Control.* 73(11):1001-1025, 2000.

[96] D. A. Lawrence and W. J. Rugh. Gain Scheduling Dynamic Linear Controllers for a Nonlinear Plant. *Automatica.* 31(3), 1995.

[97] J. S. Shamma and M.Athans. Guaranteed Properties of Gain Scheduled Control for Linear Parameter-varying Plants. *Automatica.* 27(3), 1991.

[98] J. S. Shamma and M. Athans. Analysis of Gain Scheduled Control for Nonlinear Plants. *IEEE Trans. on Autom. Contr.* 35(8), 1990.

[99] J. Pomet and L. Praly, Adaptive Nonlinear Regulation: Estimation from the Lyapunov Equation, *IEEE Transactions on Automatic Control*, 37(6):729-740, 1992.

[100] B. Stevens and F. Lewis, *Aircraft Control and Simulation*. NY, John Wiley and Sons, 1992.

[101] V. L. Kharitonov, Asymptotic Stability of an Equilibrium Position of a Family of Systems of Linear Differential Equations, *Differential Uravnen*, 14:2086-2088, 1978.

[102] S. P. Bhattacharyya, H. Chapellat and L. H. Keel, *Robust Control: The Parametric Approach*. NJ, Prentice Hall, 1995.

[103] C. P. Mracek and D. B. Ridgely, Missile Longitudinal Autopilots: Connections Between Optimal Control and Classical Topologies, *Proceedings of AIAA Guidance, Navigation, and Control Conference and Exhibit*, AIAA-2005-6381, San Francisco, CA, 2005.

[104] W. J. Rugh. *Linear System Theory*. Prentice Hall, Upper Saddle River, NJ, 1995.

[105] C. Cao and N. Hovakimyan. Effect of Non-zero Initialization Error on the Performance Bounds in $\mathcal{L}_1$ Adaptive Control Architecture *In Proc. of AIAA Guidance, Navigation and Control Conference*, AIAA-2007-6645, Hilton Head Island, SC, August 2007.

[106] L.M. Silverman. Synthesis of Impulse Response Matrices by Internally Stable and Passive Realizations. *IEEE Transactions on Circuit Theory.* 15, 1968.

[107] L.M. Silverman and H.E. Meadows. Controllability and Observability in Time-Variable Linear Systems. *Journal of SIAM Control.* 5(1), 1967.

[108] L.M. Silverman. Transformation of Time-Variable Systems to Canonical (Phase-Variable) Form. *IEEE Transactions on Automatic Control.* 11, 1966.

[109] L.M. Silverman and B.D.O. Anderson. Controllability, Observability and Stability of Linear Systems. *Journal of SIAM Control.* 6(1), 1968.

[110] K.S. Tsakalis and P.A. Ioannou. *Linear Time-Varing Systems: Control and Adaptation*. Prentice Hall, Englewood Cliffs, NJ, 1993.

[111] A. Dogan, E. Kim and W. Blake, Control and Simulation of Relative Motion for Aerial Refueling in Racetrack Maneuver. *Journal of Guidance, Control and Dynamics.* 30(5), 2007.

[112] P. Kokotovic, H. Khalil and J. O'Reilly. *Singular Perturbations Methods in Control: Analysis and Design.* Academic Press, New York, 1986.

[113] M. Vidyasagar. The Graph Metric for Unstable Plants and Robustness Estimates for Feedback Stability. *IEEE Transactions on Automatic Control.* 29:403-417, 1984.

[114] A. M. Pascoal, P. P. Khargonekar and R. Ravi. Robust Stabilization of Families of Linear Time-varying Plants with Applications to Singularly Perturbed Systems, *Proceedings of IEEE Conference on Decision and Control*, 2401-2406, Tampa, FL, December 1989.

Appendix

Nominal Conditions and System Matrices

Operating point 1:

$$A_1 = \begin{bmatrix} -0.02 & 0.1 & 38 & 0 & -25 & -0.03 & -32 & 0 & -0.0002 & 0 & 0 \\ 0 & -0.02 & 0 & 0.05 & 0 & -1 & 0 & 0.06 & 0 & 0 & 0 \\ -0.0001 & 0 & -1 & 0.0001 & 1 & 0 & -0.003 & -0.0003 & 0 & 0 & 0 \\ 0 & -9.7 & 0.006 & -2.1 & -0.0003 & 0.2 & 0 & 0 & 0 & 0 & 0 \\ -0.001 & 0 & 12 & 0.0003 & -2.7 & 0 & 0 & 0 & 0 & 0 & 0 \\ 0 & -2.6 & 0.0006 & -0.1 & 0 & -0.01 & 0 & 0 & 0 & 0 & 0 \\ 0 & 0 & 0 & 0 & 1 & -0.005 & 0 & -0.0003 & 0 & 0 & 0 \\ 0 & 0 & 0 & 1 & 0.0002 & 0.05 & 0.0003 & 0 & 0 & 0 & 0 \\ -0.05 & 2.3 & 499 & 0 & 0 & 0 & -500 & -0.14 & 0 & 0 & 0 \\ 1 & 0 & 0 & 0 & 0 & 0 & 0 & 0 & 0 & 0 & 0 \\ 0 & 0 & 0 & 0 & 0.005 & 1 & 0 & 0 & 0 & 0 & 0 \end{bmatrix}$$

$$B_1 = \begin{bmatrix} 0 & 0.1710 & 0 & 0.0024 \\ -0.0003 & 0 & 0 & 0 \\ 0 & -0.0029 & 0 & 0 \\ 0.6072 & 0.0000 & -0.0944 & 0 \\ 0 & -0.4005 & 0 & 0 \\ 0.0345 & 0 & -0.1399 & 0 \\ 0 & 0 & 0 & 0 \\ 0 & 0 & 0 & 0 \\ 0 & 0 & 0 & 0 \\ 0 & 0 & 0 & 0 \\ 0 & 0 & 0 & 0 \end{bmatrix}$$

The nominal values of this operating point is:

$$\begin{pmatrix} 499.39 & 0 & 0.0492 & 0 & 0 & 0.0003 & 0.0492 & 0.0046 & -5000 & 0 & 0 \end{pmatrix}$$

Operating point 2:

$$A_2 = \begin{bmatrix} -0.02 & 13 & 36 & 0 & -28 & 0.7 & -32 & 0 & -0.0002 & 0 & 0 \\ -0.0001 & -0.02 & -0.001 & 0.06 & 0 & -1 & -0.001 & 0.06 & 0 & 0 & 0 \\ -0.0001 & 0.001 & -1 & -0.001 & 1 & 0 & -0.002 & -0.03 & 0 & 0 & 0 \\ 0 & -10 & -0.06 & -2 & -0.03 & 0.2 & 0 & 0 & 0 & 0 & 0 \\ -0.001 & 0 & 12 & 0.03 & -3 & -0.001 & 0 & 0 & 0 & 0 & 0 \\ 0 & -3 & -0.009 & -0.1 & -0.0003 & -0.01 & 0 & 0 & 0 & 0 & 0 \\ 0 & 0 & 0 & 0 & 0.9 & -0.4 & 0 & -0.03 & 0 & 0 & 0 \\ 0 & 0 & 0 & 1 & 0.02 & 0.04 & 0.03 & 0 & 0 & 0 & 0 \\ -0.04 & 210 & 453 & 0 & 0 & 0 & -499 & -11 & 0 & 0 & 0 \\ 1 & 0 & 0 & 0 & 0 & 0 & 0 & 0 & 0 & 0 & 0 \\ 0 & 0 & 0 & 0 & 0.4 & 0.9 & 0 & 0 & 0 & 0 & 0 \end{bmatrix}$$

$$B_2 = \begin{bmatrix} 0 & 0.1798 & 0 & 0.0024 \\ -0.0003 & 0 & 0 & 0 \\ 0 & -0.0029 & 0 & 0 \\ 0.6134 & 0.0001 & -0.0970 & 0 \\ 0 & -0.4054 & 0 & 0 \\ 0.0339 & 0 & -0.1399 & 0 \\ 0 & 0 & 0 & 0 \\ 0 & 0 & 0 & 0 \\ 0 & 0 & 0 & 0 \\ 0 & 0 & 0 & 0 \\ 0 & 0 & 0 & 0 \end{bmatrix}$$

The nominal values of this operating point is:

$$\begin{pmatrix} 499.25 & 0.0013 & 0.0547 & -0.0012 & 0.0124 & 0.0269 & 0.0418 & 0.4318 & -5000 & 0 & 0 \end{pmatrix}$$